



Skolkovo Institute of Science and Technology

Skolkovo Institute of Science and Technology

FILMS WITH PATTERN-PLACED DRUG
FOR USE IN PERSONALIZED MEDICINE

Doctoral Thesis

by

PAVEL PROSHIN

DOCTORAL PROGRAM IN MATERIALS SCIENCE
AND ENGINEERING

Supervisor
Professor Gleb Sukhorukov

Co-supervisor
Professor Alexander Korsunsky

Moscow - 2024

© Pavel Proshin 2024

I hereby declare that the work presented in this thesis was carried out by myself at Skolkovo Institute of Science and Technology, Moscow, except where due acknowledgement is made, and has not been submitted for any other degree.

Pavel Proshin (Candidate)

Prof. Gleb Sukhorukov (Supervisor)

Abstract

Drug-eluting films (DEF) made of bioresorbable polymers are a widely utilized tool in modern personalized medicine. However, many current methods of coating production remain largely confined to the laboratory due to low encapsulation efficiency and/or challenges in scaling up.

This work primarily focuses on a technology for DEFs production that is easy to implement in the laboratory and scalable to an industrial level. Named "PLACE" (Printed Layered Adjustable Cargo Encapsulation), the elaborated approach enables the production of large-area DEFs with advanced features, include precisely controlled drug loading with a significant payload of up to 1 mg/cm² and the ability to manufacture multilayered films by incorporating different drugs and biopolymers within layers. This results in programmable multifunctional coatings, expanding the potential applications of these drug-eluting films.

The initial sections comprise an introduction (Chapter 1) and a literature review (Chapter 2). Subsequently, the experimental section is outlined, encompassing materials, methods, and instruments (Chapter 3). In the Chapter 4, the results of the study are presented, focusing on key parameters for creating PLACE coatings and the release of medicinal and model substances from these films. Methods for achieving accelerated release, such as laser microperforation and the utilization of PVP as a porogen, are discussed. Additionally, the stability of the polymer and the release properties of films irradiated with accelerated electrons are investigated. Chapter 5 delves into practical aspects of utilizing the technology, including approaches to creating patterns and securing coatings on various surfaces.

Publications

Thesis related publications:

- Mordovina, E. A., Plastun, V. O., Abdurashitov, A. S., **Proshin, P. I.**, Raikova, S. V., Bratashov, D. N., Inozemtseva, O. A., Goryacheva, I. Y., Sukhorukov, G. B., and Sindeeva, O. A. (2022). “Smart” Polylactic Acid Films with Ceftriaxone Loaded Microchamber Arrays for Personalized Antibiotic Therapy. *Pharmaceutics*, 14(1), 42.
- **Proshin, P. I.**, Abdurashitov, A. S., Sindeeva, O. A., Ivanova, A. A., and Sukhorukov, G. B. (2022). Additive Manufacturing of Drug-Eluting Multilayer Biodegradable Films. *Polymers* 2022, Vol. 14, Page 4318, 14(20), 4318.
- Abdurashitov, A. S., **Proshin, P. I.**, Sindeeva, O. A., and Sukhorukov, G. B. (2022). Laser Microperforation Assisted Drug-Elution from Biodegradable Films. *Pharmaceutics* 2022, Vol. 14, Page 2144, 14(10), 2144.
- Patent, RU, 2807080, Obtaining and application of films that elute medicinal substances. Abdurashitov A. S., **Proshin P. I.**, Sukhorukov G. B., 2023.

Other articles and publications for the period of study:

- Sindeeva, O. A., Abdurashitov, A. S., **Proshin, P. I.**, Kadrev, A. V., Kulikov, O. A., Shaparov, B. M., Sorokin, N. I., Ageev, V. P., Pyataev, N. A., Kritskiy, A., Tishin, A., Kamalov, A. A., and Sukhorukov, G. B. (2022). Ultrasound-Triggerable Coatings for Foley Catheter Balloons for Local Release of Anti-Inflammatory Drugs during Bladder Neck Dilation. *Pharmaceutics*, 14(10).

- Abdurashitov, A. S., **Proshin, P. I.**, Tuchin, V. V., and Sukhorukov, G. B. (2022). Integrated binary hologram to monitor cargo release from a drug-eluting film. *Light: Advanced Manufacturing*, 3(3), 1–10.
- Abdurashitov, A. S., **Proshin, P. I.**, and Sukhorukov, G. B. (2023). Template-Free Manufacturing of Defined Structure and Size Polymeric Microparticles. *Nanomaterials*, 13(22).
- Ivanova, A. A., Kozyreva, Z. V., Chekalov, A. Y., **Proshin, P. I.**, Abdurashitov, A. S., Bello, A. S., Markovic, S., Sukhorukov, G. B., and Cheremisin, A. N. (2024). Development and characterization of nanostructured surfactant compositions with prolonged action and stimuli-responsive physicochemical properties. *Colloids and Surfaces A: Physicochemical and Engineering Aspects*, 133396.

Acknowledgements

The author thanks the following people for their valuable contributions to this work:

- Prof. Gleb Sukhorukov, Prof. Alexander Korsynsky, and Prof. Dmitry Gorin for the valuable mentorship and support.
- Dr. Arkady Abdurashitov for assistance, technical advice and his involvement to this work.
- Dr. Olga Sindeeva and Olga Gusliakova for consultations on issues of biology and physiology.
- Dr. Alexander Akkuratov for help with GPC measurements.
- Dr. Ivanova Anastasiya for help with viscosity measurements.
- Alexander Kritsky for assistance in carrying out E-beam sterilization in Corad company.
- VS3D team and especially Vadim Ibragimov and Alexander Morozov for invaluable assistance in the development and production of the 3D printer used in the work.
- Viktoria Mikhaylova for the LaTeX template provided.

Contents

Abstract	1
Publications	2
Acknowledgements	4
Contents	5
List of Symbols, Abbreviations	7
List of Figures	10
List of Tables	15
Chapter 1. Actuality and problem statement	16
Chapter 2. Review of the Literature	21
2.1 Personalized medicine and drug delivery	21
2.1.1 Introduction to Personalized Medicine	21
2.1.2 The idea of targeted drug delivery	24
2.1.3 Summarizing	25
2.2 Drug-eluting systems based on biodegradable polymers	26
2.2.1 Biodegradable Polymers	26
2.2.2 Formulation and Drug Incorporation. Mechanisms of Drug release . . .	33
2.2.3 Conclusions and Findings	69
2.2.4 Sterilization methods for polymeric DDS	71
2.3 Drug type, dosage and stability issue	74
Chapter 3. Materials and methods	80
3.1 Chemical Materials	80
3.2 Methods	80
3.2.1 Three-Dimensional (3D) Printing Software and Hardware	80
3.2.2 Film casting	82
3.2.3 SEM	82
3.2.4 Cross-sections	83
3.2.5 GPC measurements	84
3.2.6 Laser microperforation process	85
3.2.7 Viscosity measurements	85
3.2.8 Prolonged drug release investigation	86
Chapter 4. Results	90
4.1 Introduction to PLACE Technology	90
4.2 Film fabrication and parameter optimization	94
4.2.1 PVA matrix optimization	94
4.2.2 Drug loading studies	98

4.2.3	Base and cover films forming	101
4.3	Drug release characterization	107
4.3.1	Quantification of the vancomycin elution from PLACE films	107
4.3.2	Impact of laser microperforation	113
4.3.3	Influence of porogen agents	126
4.4	E-beam sterilization and film stability	140
4.4.1	Impact on PLGA films	140
4.4.2	Impact on release properties	144
4.5	Multilayered film development	147
Chapter 5.	PLACE Technology: application and adhesion Studies	151
5.1	Description of methods and research objects	151
5.1.1	Materials used	153
5.1.2	Surface investigation of titanium Samples	153
5.1.3	Fixation procedure	155
5.1.4	Evaluation of the reliability of polymer film fixation on the surface of a prosthesis with variable surface roughness and relief	155
5.2	Evaluation of the effectiveness of methods for coating complex-shaped products with polymer films containing drugs	158
5.2.1	Description of methods and research objects	158
5.2.2	Patch method of application	158
5.2.3	Template method of application	160
5.2.4	Conclusive remarks on applicability.	165
Chapter 6.	Economic feasibility, future outlook, and final conclusions	167
6.1	Cost-effectiveness and production feasibility of biodegradable PLACE films for medical applications	167
6.2	Future directions and perspectives	169
6.3	Conclusion	170
Bibliography	176

List of Symbols, Abbreviations

Term: definition

3D: Three-Dimensional

ABS: Acrylonitrile Butadiene Styrene

AG: Applicator Gap

AIC: Akaike Information Criterion

CAD: Computer-Aided Design

CDs: Carbon Dots

Cef: Cefazolin

CNC: Computer Numerical Controlled

CPOP: Controlled Porosity Osmotic Pump

CS: Coater Speed

DDS: Drug Delivery Systems

DECs: Drug-Eluting Coatings

DEFs: Drug-Eluting Films

DOX: Doxorubicin

E-beam: Electron Beam

ENG: Etonogestrel

EOP: Elementary Osmotic Pump

FESEM: Field Emission Scanning Electron Microscopy

FG: Fully Hydrolyzed

5-FU: 5-Fluorouracil

GPC: Gel-Permeation Chromatography

GOF: Goodness of Fit

GS: Gentamicin Sulfate

HIFU: High-Intensity Focused Ultrasound

ID: Inner Diameter

IMC: Indomethacin

IMDs: Implantable Medical Devices

KET: Ketoprofen

LNG: Levonorgestrel

LS: Linear Speed

MB: Methylene Blue

MCA: Microchamber Arrays

MIC: Minimum Inhibitory Concentration

MID: Medical Implantable Device

MN: Microneedle

MSE: Mean Squared Error

MSC: Model Selection Criterion

MW: Molecular Weight

NPs: Nanoparticles

NTs: Nanotubes

NIR: Near Infrared

PBAT: Polybutylene Adipate Terephthalate

PBS: Phosphate-Buffered Saline

PCL: Polycaprolactone

PDMS: Polydimethylsiloxane

PEG: Polyethylene Glycol

PEO: Polyethylene Oxide

PG: Partially Hydrolyzed

PGA: Polyglycolic Acid

PHB: Polyhydroxybutyrate

PLACE: Printed Layered Adjustable Cargo Encapsulation

PLA: Polylactic Acid

PLGA: Poly(lactide-co-glycolide)
PP: Polypropylene
PVA: Polyvinyl Alcohol
PVP: Polyvinylpyrrolidone
RhB: Rhodamine B
SamSMU: Samara State Medical University
SEM: Scanning Electron Microscopy
TCH: Tetracycline Hydrochloride
TCM: Trichloromethane
TEM: Transmission Electron Microscopy
TNT: Titanium Nitride
TrA: Tranexamic Acid
UV: Ultraviolet
Vanc: Vancomycin
ZO: Z-offset

List of Figures

Figure 2.1	Basic biopolymers and their degradation products	29
Figure 2.2	PCL chemical structure.	31
Figure 2.3	PHB chemical structure.	31
Figure 2.4	PVA chemical structure.	32
Figure 2.5	Common use DDS and their pharmacokinetics [77].	35
Figure 2.6	Diffusion-controlled (a), swelling-controlled (b), and erosion-controlled release (c).	38
Figure 2.7	(a) PLA:PCL/TCH electrospun fibre mats SEM microphotograph; (b) Drug release profiles for PLA:PCL fiber mats containing TCH, IMC, and halloysite nanotubes modified with 3-aminopropyltriethoxysilane [80].	39
Figure 2.8	DECs with barrier diffusion layer (a) and "diffusion bridge" clusters (b)	41
Figure 2.9	(a) Emulsification process; (b) Electrospray coatings and (c) Cumulative release profiles of ReoPro-loaded stents[86].	42
Figure 2.10	Kinetics of drug release and polymer absorption with the Synergy stent [98].	43
Figure 2.11	(a) PLA sutures coated with a 50/50 mix of PCL/PGA degraded over a period of 13 weeks. (b) The total drug release rate for sutures with different PCL/PGA ratios [99].	44
Figure 2.12	(a) Elementary osmotic pump; (b) controlled porosity osmotic pump (CPOP).	46
Figure 2.13	The <i>in vitro</i> release rate of KCl from EOP in water [101].	47
Figure 2.14	Reservoir formation methods. (a) Formation of film on the template; (b) Formation of layer of core-shell structures on a MID surface; (c) Drug loading and sealing of reservoirs created on the surface of MID.	48
Figure 2.15	(a) Schematic illustrations of the fabrication process of PLGA-based microstructures, optical micrographs of microcapsules (b) on PVA and in water (c). Scale bar=50 μm [107]	49
Figure 2.16	Process of manufacturing of MCA film.	51
Figure 2.17	(a) Free-standing printed PLLA microchamber arrays (1 wt. %); (b) Closed cobalt-chromium endovascular stent covered with free-standing PLLA microchamber arrays; (c) In vitro cumulative RhB release in PBS at 37 °C during 14 days. [114]	52
Figure 2.18	(a) Extended release profiles of ceftriaxone from microchamber arrays made with different PLA concentrations in a patterned film (ranging from 1% to 2.5%); (b) The antibacterial efficacy of microchamber arrays containing ceftriaxone [115].	53
Figure 2.19	Simplified scheme of particles (a) and fibers (b) electrodeposition.	55
Figure 2.20	(a) Setup scheme and (b) release profile for Heparine-loaded microspheres [123].	57
Figure 2.21	(a) Triaxial needle and spinning process; (b) TEM of trilayer fiber; (c) KET-containing fiber release profile [124].	57
Figure 2.22	Release profiles for hormone etonogestrel released from PLA microparticles [126].	59

Figure 2.23	(a) Polymer films applied to TNT via dip coating. (b) Overall drug release profiles from uncoated TNT/Ti and TNT/Ti coated with thin and thick PLGA layers [127].	60
Figure 2.24	(a) FESEM image showing the top view of the sample after anodization, sonication, and annealing; (b) FESEM image of the NTs loaded with vancomycin; (c) Overall drug release from the devices [128].	61
Figure 2.25	Cumulative percentage of the drug release from the scaffolds [129]. . . .	62
Figure 2.26	Schematic diagram showing the design of an MN patch with an effervescent backing and the process of applying the MN patch to the skin. The effervescent backing rapidly dissolves, allowing the MNs to quickly penetrate the skin [54].	63
Figure 2.27	Rat plasma concentrations of LNG after applying LNG-loaded effervescent microneedle (MN) patches. The therapeutic level for LNG in humans is shown by the blue dashed line. Data points show the mean \pm SD ($n = 10$). (E) Cumulative LNG absorption <i>in vivo</i> over time from the LNG-loaded effervescent MN patches, based on pharmacokinetic modeling of the data presented in (D). Each point represents the mean \pm SD ($n = 10$). [54]	64
Figure 2.28	Profiles of release of LNG from core-only and core-shell MNs [131]. . . .	65
Figure 2.29	(a) Release profiles of TrA from microneedles with 3% and 10% TrA concentrations; (b) Total amount of TrA (μg) that permeated through rat skin from microneedles with 10% TrA and from a cream with 10% TrA over 72 hours [132].	66
Figure 2.30	(a) 3D-printed orthopedic screws, pins, and plates made from PLA; (b) 3D-printed standard 4 mm screws using regular PLA and PLA-GS mix. . . .	67
Figure 2.31	(a) Top: Horizontal cross-sections of C40 with infill percentages of 100%, 50%, and 25%. Bottom: P6-100 before (left) and after (right) the dissolution test. (b) Dissolution profiles of core-only tablets (C40) compared to core-shell formulations P6-100 and P8-100.	69
Figure 2.32	Biofilm formation process[177]	78
Figure 3.1	Custom 3D printer (a). Structure of a syringe extruder (b). Vacuum table for holding substrates (c). Web-based printer control interface with webcam window (e).	81
Figure 3.2	Laboratory-made Dr. Blade machine	82
Figure 3.3	Sample in cryoslicing process (a) and sliced samples on SEM stub (b). . .	84
Figure 3.4	Absorption spectra and calibration curves for a) Vancomycin, b) Methylene Blue dye, c) Cefazolin, d) Eosin Y.	87
Figure 4.1	The design of the PLACE approach. (a) Mixing of the drug-containing matrix, (b) film fabrication pathway, and freestanding ready-to-use film (c).	91
Figure 4.2	Structure of a syringe extruder.	92
Figure 4.3	Maximum flow test results for water and 9% PVA solution	94
Figure 4.4	Selection of parameters for PVA solution preparation. (a) Print defects when using 6 wt.% PVA solution; line width on a straight section (b) and on turns (c) using 9 wt.% PVA solution; the dependence of the dynamic viscosity of PVA on the concentration (d).	98

Figure 4.5	SEM image for the surface of uncoated drug tracks for Cef100, Cef200 and Cef400 samples, (a), (b) and (c) respectively.	100
Figure 4.6	SEM image for the surface of uncoated drug tracks for Cef400 sample printed on heated bed.	100
Figure 4.7	(a-b) imprinted PLGA film squares onto the PVA surface before (a-b) and after (b-c) exposure to chloroform vapor.	102
Figure 4.8	Empirical testing of the concentration of the covering solution graph . .	103
Figure 4.9	SEM image of PLAGE film's edge	104
Figure 4.10	(a) Film holder made of acid-resistant stainless steel. (b) Diffusion cell	105
Figure 4.11	Test of permeability of PLGA film	106
Figure 4.12	Chemical structure of vancomycin	107
Figure 4.13	PLAGE film on PP substrate (a) and microimages of drug-filled stripes (b-c).	108
Figure 4.14	Daily and cumulative release profiles for the Vancomycin-loaded samples with 100 and 200 mg/ml of PVA matrix Vancomycin added.	109
Figure 4.15	SEM images of films after release in PBS.	112
Figure 4.16	Chemical structure of Methylene Blue dye.	113
Figure 4.17	(a) Optical image showing microperforations created at various laser energies. Scale bar is 50 μm . (b) Relationship between laser energy and hole diameter for MB-loaded PLGA films. The average diameter of ten holes produced at each energy level is shown.	114
Figure 4.18	(a) Initial view of an MB-loaded film placed in a flow cell. (b) Appearance of the MB-loaded film after 24 hours in a high-flow environment. (c) Pseudo-colored map showing the amount of MB released from films with microperforations of various diameters after 24 hours in a high-flow setting. (d) Pseudo-colored map displaying the maximum elution rate observed for different hole diameters and their surrounding areas.(e) Graph showing how the diameter of the holes affects the width of the elution zone where over 90% of the substance is released.	116
Figure 4.19	(a) MB elution data over one week, based on the number of laser-created holes.(b) Positions of the holes in different sample groups (0, 1, 2, and 4 holes) are indicated by green circles. (c) SEM image of a laser-induced hole, with an average diameter of 10 μm	117
Figure 4.20	The linear dependence between the elution rate and the number of holes.	118
Figure 4.21	Two-week MB elution data for 4H sample.	119
Figure 4.22	(a) Series of perforations were created with varying repetition rates, hole made with repetition rate of 3 pulses	121
Figure 4.23	Spectra of Cefazolin (in green), it's residue (in red) and variations of it's degradation products in differernt days (in blue).	122
Figure 4.24	Samples photo (a) and SEM images of laser-perforated film (b-c). . . .	123
Figure 4.25	One-week MB elution data depending on the number of laser-made holes for Vanc200LP samples	124
Figure 4.26	SEM images for 4-hole after release samples.	126
Figure 4.27	Optical images of PLGA films with 10% of PEG 8000 (a) and partly immersed in water PEG 4000 (b).	129
Figure 4.28	SEM micrographs of sample with 10% PEG 400.	129
Figure 4.29	Emulsification of PLGA solutions with the addition of 10% PVP 55k (a) and K90 (b), clear mixture with PVP K17 (c).	130

Figure 4.30	PVP-rich regions were observed for samples with 10% additive (a), while complete phase separation occurred at 20% PVP (b) in non-heated samples. The most homogeneous films were achieved using a heated table with 10% PVP K17 (c and d). The cluster size distribution histogram for these samples is shown in image (e).	131
Figure 4.31	The SEM image of the edge of the PLGA film containing 10 wt.% of PVP K17	132
Figure 4.32	Microphotographs of samples surface.	133
Figure 4.33	Daily and cumulative release profiles for the MB-loaded samples with 10% and 20% PVP added.	134
Figure 4.34	SEM microphotographs of samples with loaded MB and containing 20% PVP (a-c) and 10% PVP (d-f).	136
Figure 4.35	SEM microphotographs of sample with loaded Vancomycin and containing 10% PVP	137
Figure 4.36	Daily and cumulative release profiles for the Vancomycin-loaded samples with 10% PVP added.	138
Figure 4.37	SEM microphotographs of samples with loaded Vancomycin and containing 10% PVP (a-c) after 5 days of incubation in PBS, and after all 2 week period (d-f).	140
Figure 4.38	Irradiated PLGA films and control (non-irradiated) sample after 1-4 week incubation in PBS.	141
Figure 4.39	SEM microphotographs of Irradiated PLGA films after 1-4 week incubation in PBS.	142
Figure 4.40	Up-scaled photo of 3-week incubated sample	142
Figure 4.41	Surface of Irradiated PLGA film (a) and control (non-irradiated) sample (b) after 4 week incubation in PBS.	143
Figure 4.42	Daily and cumulative release profiles for the MB-loaded samples. Irradiated (in green) and non-irradiated (in orange).	145
Figure 4.43	(a) Control sample surface before release; (b-c) Sample surface after incubation for 19 days in PBS.	146
Figure 4.44	(a) Irradiated sample surface before release; (b-c) Sample surface after incubation for 15 days in PBS.	146
Figure 4.45	Large-area multilayered film under UV light (a), its optical image (b) and SEM image of cross-section (c).	148
Figure 4.46	Formula of Eosine Y dye.	148
Figure 4.47	Perforation scheme (a) and resulting multi-drug films (b).	149
Figure 4.48	Absorption spectra of release solutions, day 1-7 (a). Daily and cumulative release curves for multi-drug films (b).	149
Figure 5.1	A - General view of the samples, from left to right: sample with a polished surface, sample with a rough surface, sample with a trabecular structure. B - Microphotograph of the polished sample surface, C - Microphotograph of the rough surface sample, D - Microphotograph of the sample surface with trabecular structure.	154
Figure 5.2	Microphotograph of the sample surface with trabecular structure.	155
Figure 5.3	Samples with fixed films under a layer of physiological solution after 7 days of incubation. 1 - films fixed on Sulfacrylate, 2 - thermally fixed films. A - sample with a polished surface, B - sample with a rough surface, C - sample with a trabecular structure.	156

Figure 5.4	Samples with fixed films after qualitative assessment of polymer film adhesion using the shear method. 1 - films fixed on Sulfacrylate, 2 - thermally fixed films. A - sample with a polished surface, B - sample with a rough surface, C - sample with a trabecular structure.	157
Figure 5.5	A - Procedure for applying a drug-containing polymer coating to the surface of an individual endoprosthesis using the patch method. B - Final view of the endoprosthesis with the drug coating.	159
Figure 5.6	A - main control elements of the Instant Meshes program; 1 - model loading button, 2 - type of polygons used for mesh construction, 3 - number of polygons used for mesh construction, 4 - "comb" tool for manual local mesh orientation in areas of complex model geometry, 5,6 - buttons for building the orientation field of the mesh and the mesh itself, respectively. B - initial model loaded into the program, C - result of the program's work - a uniform square mesh formed on the surface of the 3D model.	162
Figure 5.7	A - initial representation of the surface area of an individual prosthesis in *.stl format in the form of a triangular mesh of varying density. B - the same surface area, presented in the form of a uniform square mesh after semi-automatic retopology of the surface in the Instant Meshes program.	162
Figure 5.8	A - model of an individual implant after retopology with seams applied to it, along which the model will be cut. 1,2 - areas of the model with curvilinear geometry requiring a greater number of seams for cutting them into flat shapes. B - cutting of the prosthesis model along seams used to create individual drug-containing coatings.	164
Figure 5.9	A - the process of applying drug-containing polymer coatings to the surface of a complex-shaped individual prosthesis using the die-cut method. B - the final appearance of the prosthesis with modified polymer film surfaces.	165

List of Tables

Table 2.1	Mechanical and thermal properties of widely used biodegradable polymers in medical applications. [47]	30
Table 3.1	Absorption spectra range and characteristic wavelength of used cargo. .	86
Table 4.1	Kinetic drug release study of Vanc100 group from DDSolver. Goodness of fit parameters.	109
Table 4.2	Kinetic drug release study of Vanc100 group from DDSolver. Best fit values.	110
Table 4.3	Kinetic drug release study of Vanc200 group from DDSolver. Goodness of fit parameters.	111
Table 4.4	Kinetic drug release study of Vanc200 group from DDSolver. Best fit values.	111
Table 4.5	GOF parameters for the Zero order model fitting	118
Table 4.6	Best fit values for the Zero order model fitting	118
Table 4.7	GOF parameters for the 8-14 day range for samples with four microperforations.	120
Table 4.8	Best fit values for the 8-14 day range for samples with four microperforations.	120
Table 4.9	GOF parameters for the 1-14 day range for samples with four microperforations.	124
Table 4.10	Best fit values for the 1-7 day range for samples with four microperforations.	125
Table 4.11	Porogens tested in presented work.	128
Table 4.12	GOF parameters for the samples with 10% PVP K17	134
Table 4.13	Best fit values for the 8-14 day range for samples with four microperforations.	134
Table 4.14	GOF parameters for the samples with 10% PVP K17	137
Table 4.15	Best fit values for the 5-14 day range for samples with four microperforations.	138
Table 4.16	Data from GPC analysis for PLGA polymer before and after irradiation. .	144
Table 4.17	The best GOF parameters for the multi-drug samples	149
Table 4.18	Best fit values for the 5-14 day range for samples with multiple drugs. .	150
Table 6.1	Base parameters for PLACE film for manufacturing	173

Chapter 1. Actuality and problem statement

In the modern landscape of medicine, there has been a paradigm shift towards personalized healthcare, aimed at tailoring treatments to meet the individual needs of patients. This personalized approach recognizes the unique genetic makeup, lifestyle factors, and specific health conditions of each patient, offering the potential for more effective and targeted therapies. Within the context of modern medicine, targeted drug delivery systems (DDS) have emerged as a crucial tool in addressing the complexities of disease treatment. These systems offer a localized approach to drug administration, allowing for the precise delivery of therapeutic agents to exact sites within the human body. The targeting capabilities of DDS are valuable in the treatment of localized diseases or conditions, such as tumors, infections, and inflammatory disorders. In these cases, conventional systemic drug administration may result in suboptimal drug concentrations at the target site or unnecessary exposure of healthy tissues to the drug. Moreover, DDS can enable the use of potent therapeutic agents that may otherwise be too toxic for systemic administration. By delivering drugs directly to the site of action, DDS can achieve therapeutic concentrations while minimizing exposure to healthy tissues, thereby reducing the risk of adverse effects [1]. This targeted approach improves drug safety and tolerability while enabling the use of lower doses., potentially reducing treatment costs and improving patient compliance [1].

Over the past two decades, the use of bioresorbable polymer drug-eluting films (DEFs) for site-specific drug delivery has become prevalent across various medical device applications [2, 3]. These films, composed of biocompatible polymers like polycaprolactone (PCL), polylactic acid (PLA), polyglycolic acid (PGA), and their copolymers, frequently function as drug-eluting coatings (DECs) for implantable medical devices (IMDs), providing sustained and prolonged release of therapeutic agents over extended durations. IMDs play a crucial role in managing chronic conditions such as cardiovascular disease, diabetes, and cancer. For

instance, drug-eluting stents (DES) are commonly used to treat coronary artery disease are coated with a polymer matrix containing an anti-proliferative drug, which is gradually released to prevent restenosis. DES have significantly improved patient survival rates during cardiac stenting procedures, reducing adverse cardiac events compared to bare-metal stents (BMS). Research published in the New England Journal of Medicine indicates that drug-eluting stents (DES) decrease the risk of vessel revascularization by 50% compared to bare-metal stents, leading to improved long-term outcomes [4]. Over time, overall complication rates for procedures like stent implantation have decreased, reflecting advancements in procedural safety and outcomes [5]. This widespread adoption has made cardiac stenting procedures safer and more accessible. Additionally, the latest generation of drug-eluting stents featuring biocompatible polymers, have further minimized stent-related complications, thereby improving the overall safety of the procedure. [6, 7, 8].

Developing antimicrobial DEC and coatings with anti-inflammatory properties is also crucial for mitigating complications and improving the long-term performance of implantable medical devices [9, 10, 11]. For example, catheter-associated urinary tract infections (CAUTIs) are a major contributor to hospital-acquired infections, affecting up to 70–80% of hospitalized patients, with reported cases exceeding 380,000 annually and resulting in 9,000–13,000 deaths per year [12, 13, 14]. They begin with microbe adhesion and colonization on catheter surfaces, followed by biofilm formation. Orthopedic implant-associated infections (OIAs) also pose significant challenges post-orthopedic surgeries, resulting in increased morbidity, prolonged hospitalization, and substantial healthcare expenses. The infection rate varies among patients, with primary joint replacements experiencing rates of less than 1–2% within the first two years post-surgery, while revision surgeries can see rates as high as 40% [15, 16]. Bacterial pathogens like *Staphylococcus aureus* and coagulase-negative staphylococci commonly cause these infections by forming biofilms on implant surfaces, rendering them resistant to antibiotic treatment alone [10]. Developing antimicrobial DEC capable of preventing bacterial colo-

nization and infection at implant sites is crucial for improving patient outcomes and reducing healthcare costs [14].

Despite their potential, the availability of drug delivery systems on the market remains limited, with many existing systems tailored for specific drugs or diseases, leaving a gap in universal applicability [17, 18]. The limitations stem from the challenges of adapting and scaling existing methods to accommodate a broader range of therapeutic agents, release profiles, and medical devices. Creating diffusion-controlled composites offers a straightforward method for producing large-area drug-eluting films (DEFs) on an industrial scale and enables the fabrication of multilayer coatings capable of releasing different drugs at distinct time intervals. However, this method is limited for long-term prevention and treatment because composite layers have a low drug load capacity and insufficient non-linear drug release kinetic [19]. On the contrary, reservoir-based systems exhibit the capability to retain a substantial amount of substance with various molecular weights and release it in a desired gradual manner. Recent studies have demonstrated the effectiveness of such coatings for encapsulating low molecular weight drugs and dyes. However, the challenge lies in the complexity of transitioning from laboratory techniques to real production. The template process involved in reservoir-based systems limits manufacturing flexibility, requiring a new template for every new product type. Additionally, creating microcavities and containers on the surface of implantable devices must consider surface roughness, strength and biocompatibility characteristics of surface materials, making this approach less universally applicable [20, 21]. Additionally, semi-manual laboratory methods for drug loading add further complications to scaling up the production of reservoir-based DEFs, making their practical application challenging. While efforts are underway to address these challenges, developing versatile and scalable manufacturing methods for DEC remains a priority in biomedical research [22]. The complexities inherent in designing DEFs capable of accommodating diverse drugs with substantial payloads, programmable release profiles, and serving as coatings for medical devices underscore the need for innovative approaches to fully realize their potential in

advancing patient care and personalized medicine.

Aim: The aim of this work is to establish methodological foundations for producing drug-eluting films (DEFs) using additive technologies, enabling the controlled release of active substances with different dosage regimens. These films can be applicable for both surface modification of medical devices and the use them as free-standing films for drug elution, advancing personalized medicine.

Tasks:

1. Implement additive manufacturing methods to enhance scalability and robustness of manufacturing processes of reservoir-based delivery systems for drug-eluting coatings (DECs) .
2. Evaluate and optimize the loading capacity per unit area of drug-eluting coatings to ensure controllable and effective drug delivery.
3. Develop methods to program drug elution kinetics within drug-eluting coatings, allowing for predictable release rates of therapeutic agents.
4. Explore the feasibility and benefits of creating multi-drug/multi-layer drug-eluting coatings for enhanced therapeutic outcomes.
5. Investigate techniques for applying drug-eluting coatings to both simple and complex shapes of medical implantable devices, aiming to maximize versatility and applicability.

Novelty: The novelty of PLACE (Printed Layered Adjustable Cargo Encapsulation) technology lies in its innovative approach to drug delivery coatings. Unlike traditional methods, PLACE offers precise control over drug release profiles through additive manufacturing techniques. By sequentially depositing drug-containing layers onto a base film using 3D printing, this method eliminates the need for templates, resulting in more efficient and customizable coating fabrication. Additionally, the incorporation of techniques such as laser microperforation and porogen utilization further enhances the flexibility and control over drug release

kinetics. Overall, PLACE represents a significant advancement in the development of drug-eluting coatings, with potential applications across various medical devices and therapeutic interventions.

Practical significance and testing: The practical significance of PLACE technology lies in its ability to improve drug delivery systems, offering tailored and efficient solutions for medical applications. By enabling precise control over drug release profiles, PLACE coatings can enhance treatment efficacy while minimizing adverse effects. Moreover, the scalability and versatility of this technology make it suitable for a wide range of medical devices and therapies. Moreover, the ease of changing the shape of the coating facilitates adaptation to different implant designs and anatomical structures. This flexibility streamlines the manufacturing process and reduces the time and resources required to develop custom coatings for individual implants. Additionally, it enables rapid prototyping and iteration, allowing researchers and clinicians to quickly test and refine coating designs based on feedback from preclinical and clinical studies.

Testing of PLACE technology involves comprehensive evaluations to ensure its efficacy and safety in real-world applications. This includes assessing the stability and release properties of the coatings under various conditions, such as sterilization process. Additionally, practical issues like coating adhesion and compatibility with different surfaces were thoroughly investigated. Through rigorous testing and validation, PLACE technology can be optimized for clinical use, providing clinicians with reliable tools for personalized and effective patient care.

Chapter 2. Review of the Literature

2.1 Personalized medicine and drug delivery

2.1.1 Introduction to Personalized Medicine

The term "personalized medicine" was first mentioned in the literature in a 1971 paper by Gibson [23]. In this paper, Gibson explored how the role of family doctors was changing within a healthcare system that was becoming more focused on specialized experts. He highlighted the need for a personalized approach, cautioning against viewing patients as just medical cases rather than individuals. Gibson believed that future doctors should continue to uphold the traditional values of service and trust, while also embracing modern scientific and technological advancements.

Thirty years after its initial introduction, the term "personalized medicine" resurfaced, primarily associated with pharmacogenomics—tailoring medical treatments based on individual genetic profiles [24]. Since then, the concept of "personalized medicine" has expanded to encompass a broad array of ideas and approaches. However, many researchers connect it to the breakthroughs that followed the decoding of the human genome, which greatly enhanced our knowledge of diseases and treatment options [25]. In 2005, the establishment of the Personalized Medicine Coalition in the USA marked the inception of a definition for personalized medicine as an advancing field wherein physicians utilize diagnostic tests to ascertain the most effective medical treatments for each patient [26]. A different group of commentators has engaged in discussions about personalized medicine within a broader context, transcending technologies and genetic diversity. This viewpoint considers aspects such as data management, societal effects, and practical difficulties [27, 28]. Fierz's model of personalized medicine covers six key aspects. It begins by examining the distinct characteristics of diseases and individual risk factors. It also looks at how variations in the environment and

genetics influence health. The model emphasizes the importance of developing drugs tailored to genetic profiles and considers how personalized medicine affects the overall healthcare process, including patient education and privacy. Additionally, it highlights the need for proper regulation and patient empowerment, along with effective management of health information. [29]. Some experts highlighted the role of scientific advancements and molecular insights in improving the accuracy of disease prediction, while others saw personalized medicine as influenced more by current sociopolitical ideas of personalization. This shift represents a move toward a healthcare model that prioritizes individual needs, evolving into what is now called personalized healthcare.

Next the concept of "personalized healthcare" began appearing again in literature around the early 2000s, particularly with the advent of new information technologies and platforms. Zhang et al. referred to a comprehensive system that links healthcare providers with a person's unique environment and personal data [30]. Jang et al. highlighted how smart technologies, like wearables and flexible platforms, can tailor healthcare to individual needs. Additionally, some people use the term "personalized healthcare" to describe methods involving genetic testing and genomics, which help customize patient care within the framework of global systems biology.[31, 32].

Simmons et al. outlined personalized healthcare as a systematic approach to patient care that includes P4 medicine, which stands for predictive, personalized, preventive, and participatory [33, 34]. This method moves from reactive to proactive care by using technology to improve health promotion, prevent diseases, detect issues early, and provide targeted treatments. They highlighted the necessity of building supportive infrastructure, validation processes, regulations, and reimbursement systems to make personalized healthcare effective.

Now the personalized healthcare approach focuses on customizing medical decisions, practices, interventions, and treatments to fit each individual based on their unique traits. Key concepts related to personalized healthcare and medicine include:

1. **Environment and social aspects**

Patient Empowerment and Informed Decision-Making: Encouraging collaboration between healthcare providers and patients in making treatment decisions based on the patient's values, preferences, and individual circumstances.

- **Patient Education:** Empowering individuals with information about their health, genetic predispositions, and treatment options to make informed choices.
- **Integration with Healthcare Systems:** Integrating personalized medicine into routine clinical practice, including training healthcare professionals and updating medical guidelines.
- **Collaborative Research and Consortia:** Fostering collaboration among researchers, clinicians, and industry globally to advance the field of personalized medicine.

2. **Diagnostics, Data Integration and Analysis:**

- **Big Data in Healthcare:** Integrating vast amounts of data, including genomics, electronic health records, lifestyle data, and other relevant information to identify patterns and correlations.
- **Bioinformatics:** Applying computational tools and methods to analyze and interpret biological data, especially in genomics and proteomics.
- **Wearable Devices** for monitoring and collecting real-time data on individual health metrics, such as heart rate and activity levels.
- **Identification of Biomarkers:** Biomarkers are measurable indicators of biological processes or responses. They can be used for disease diagnosis, prognosis, and prediction of treatment response.
- **Molecular Diagnostics:** Utilizing techniques like PCR and sequencing to analyze molecular and genetic information for diagnostic purposes.

- Risk Prediction: Determining who is more likely to develop specific diseases by analyzing genetic and environmental factors.
- Preventive Interventions: Implementing personalized preventive strategies and interventions to reduce the risk of disease development.

3. Targeted Therapies and Treatment Tailoring:

- Targeted Drug Development: Designing drugs that specifically target the molecular and genetic characteristics of a patient's disease.
- Precision Treatment Plans: Developing treatment plans based on the specific genetic and molecular profile of the individual to enhance treatment efficacy and minimize side effects.

These ideas represent a change in healthcare from a standard, uniform approach to one that is personalized for each individual patient. In the context of this dissertation, the focal point shifts from the broader context of personalized healthcare and medicine to the specific focus on concept targeted therapy and drug delivery devices.

2.1.2 The idea of targeted drug delivery

Drug delivery refers to the method or process by which drugs, medications, or therapeutic agents are transported to their intended target within the body. Its role is enhancing the effectiveness of medical treatments by ensuring that drugs are administered to the right place, in the right amount, and at the right time.

The evolution of drug delivery systems has undergone a long journey. In the early stages, conventional methods like oral administration or intravenous injections were predominant, but their limitations in precision and potential for systemic side effects prompted the exploration of more sophisticated approaches, so controlled release systems approach were suggested, aimed at improving patient compliance and minimizing the frequency of administration [35, 36].

In the present day, the need for Targeted Drug Delivery (TDD) over conventional drug systems is addressing limitations of drugs in terms of pharmacokinetic, pharmaceutical, and therapeutic features with conventional delivery [37]. In other words, the goal is to optimize the drug’s therapeutic effects while decreasing side effects resulting from multitarget interactions, higher doses, and non-target concentrations. Three main instruments can be employed for this purpose - coordinated drug administration, the targeting site, and the pharmaceutical carrier. The target can be a specific organ, group of cells, or be an area of the body with condition requiring treatment that the drug will interact with. The carrier is a specially designed molecule, particle or implantable device that required to efficiently transport the loaded drug to target. It’s crucial to note that when referring to a pharmaceutical carrier, we are discussing the engineering system itself—the delivery vehicles—rather than the compounds being delivered [38]. Ideally, a drug targeting complex should be safe, non-allergenic, chemically stable, biodegradable, compatible with biological tissues, and stable in both the body and lab conditions [35, 39, 40].

Implantable devices, such as drug-eluting stents and intratumoral implants, provided localized and sustained drug release, particularly beneficial for chronic conditions requiring continuous and controlled drug supply [3, 41, 42, 43],].

2.1.3 Summarizing

1. Personalized healthcare means adjusting medical decisions, methods, interventions, and treatments to fit each patient’s individual characteristics. The main ideas in personalized healthcare have been outlined.
2. The shift from personalized healthcare to targeted therapies emphasizes precision interventions tailored to patients’ individual needs. Drug delivery devices, including implantable and injectable devices, play a pivotal role in targeted therapies.
3. Targeted drug delivery addresses the shortcomings of traditional drug sys-

tems, aiming to optimize therapeutic effects and minimize side effects. Key elements of TDD include coordinated drug administration, precise targeting of sites, and specialized carriers. Pharmaceutical carriers for TDD should be atoxic, non-immunogenic, biochemically inert, biodegradable, and biocompatible.

In summary, the integration of personalized medicine and advanced drug delivery systems represents a transformative approach in healthcare, aiming for more effective, efficient, and patient-centered care.

2.2 Drug-eluting systems based on biodegradable polymers

The choice of polymer, drug, and coating characteristics is intricately tied to the unique demands of medical applications, mirroring the nature of surgical procedures and the specific implantable medical devices (IMDs) in use. These drug-eluting systems exhibit versatility in applications, ranging from cardiovascular interventions employing drug-eluting stents to nanoparticle formulations designed for targeted and prolonged drug delivery. This chapter aims to provide a comprehensive overview of the theoretical aspects, advancements, challenges, and future prospects in the realm of drug-eluting systems based on biodegradable polymers.

2.2.1 Biodegradable Polymers

The drug delivery system landscape has changed significantly, and within targeted drug delivery systems, drug eluting coatings have become a dynamic frontier. These coatings serve as pharmaceutical carriers directly applied to implantable medical devices, including a range of devices such as stents, catheters, balloons, and bone implants. The primary goal of DEC is to enhance the biocompatibility of IMDs while reducing the risks associated with surgery, including inflammation, thrombosis, and implant-associated infection (IAI) [2, 3].

In this paradigm, DEC leverages the properties of various polymers with both biodegradable and non-biodegradable variants playing pivotal roles in shaping the

future of medical devices. Non-biodegradable polymers, distinguished by their enduring structural integrity, are prominently employed in the fabrication of medical devices themselves, forming the robust foundations of devices that demand long-lasting and stable structures. However, the focus of this work extends predominantly to the realm of biobased biodegradable polymers, illuminating their significance as agents of IMDs functionalization and drug delivery within the intricate tapestry of medical advancements.

"Biobased" refers to a polymer made entirely or partially from renewable organic materials, including biological substances and organic waste [44]. These plastics break down in composting conditions into water, carbon dioxide, biomass, and inorganic materials at a rate typical for compostable substances, without leaving harmful residues [45]. This is important for "biocompatibility," meaning a material should safely interact with biological systems. It should not release toxins, cause inflammation, or provoke an immune response. It needs to be stable chemically, compatible with surrounding tissues, and, for implants, degrade in a controlled way.

It should be noted that the terms "biodegradable" and "biocompostable" are related but have distinct meanings when referring to polymers. Biodegradable polymers and biocompostable polymers are both types of materials designed to break down into natural harmless elements during a certain period of time. Biodegradable polymers are materials that can be decomposed by natural processes into simpler substances. This breakdown occurs under normal conditions when exposed to light, water, or with the help of microbes or enzymes. However, the time frame for such a transformation is not defined, and as a rule, it is a long process. On the other hand, biocompostable polymers specifically break down only in composting conditions - at elevated temperatures, a certain level of acidity, and enzyme activity. The degradation time of such polymers is standardized and does not exceed several weeks or months.

In the context of biocompatible DEC, the prevalent choice revolves around the utilization of biobased biocompostable polymers. Notably, polymers such

as polylactic acid (PLA), polyhydroxyalkanoates (PHAs), and starch stand out as the go-to options, representing the forefront of commonly employed biobased biodegradable materials. Furthermore, synthetic polymers like Polybutylene Adipate Terephthalate (PBAT), Polyvinyl Alcohol (PVA), poly(lactide-co-glycolide) (PLGA), and polycaprolactone (PCL) also find application in this domain. The upcoming sections of this text will delve into a comprehensive exploration of polymers central to the research at hand and closely related studies.

Polylactic Acid (PLA), polyglycolic acid (PGA) and their copolymers (PLGA). PLA, an aliphatic polyester, is a biodegradable thermoplastic synthesized through the condensation polymerization of lactic acid. The lactic acid used in its production comes from renewable sources like corn and tapioca. PLA is primarily used in the food industry for making disposable products like cutlery, and packaging for food [19, 44].

The permeability of PLA to oxygen and water enhances its susceptibility to biodegradation compared to other synthetic biomedical polymers. As one of the most biodegradable polymers, PLA primarily undergoes degradation through hydrolysis, a process influenced by the chirality of the monomer. PLA can be produced using either the D or L stereoisomers of lactic acid, yielding different types of polymers: crystalline (PLLA), semicrystalline (PDLA), and amorphous (PDA). The D and D/L forms degrade more rapidly due to their lower crystallinity compared to the L form. The degradation process can be further accelerated by increasing the polymer's surface area or porosity. This degradation primarily occurs through the hydrolysis of ester bonds, which generates lactic acid or its oligomers, speeding up the breakdown. [46, 47]. Temperature and pH significantly influence degradability, with higher rates observed at physiological temperatures compared to 25°C [48]. Moreover, lower pH levels slow down PLA degradation compared to physiological pH [49]. PLA can also break down through enzymatic biodegradation. After implantation, immune cells release enzymes such as lactate dehydrogenase and acid phosphatase at the site, which help degrade PLA [50].

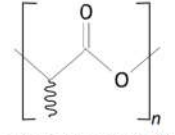
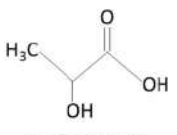
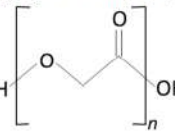
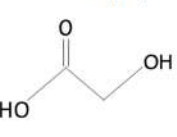
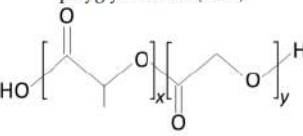

Structure	Products of Degradation
 <p>poly(lactic acid) (PLA)</p>	 <p>lactic acid (LA)</p>
 <p>poly(glycolic acid) (PGA)</p>	 <p>glycolic acid (GA)</p>
 <p>poly(lactic-co-glycolic acid) (PLGA)</p>	 <p>lactic acid (LA) glycolic acid (GA)</p>

Figure 2.1: Basic biopolymers and their degradation products

PLA's high thermal processability enables a diverse range of processing techniques [51]. At room temperature, PLA appears as a white powder with a melting temperature around 175°C and a glass transition temperature of about 55°C [52]. This characteristic makes PLA suitable for extrusion, film casting, blow molding, fiber-spinning, and other processing methods [53]. Being soluble in various organic solvents, PLAs find applications in the medical field for biocompatible devices, including sutures for wound closure, drug delivery systems such as microspheres and nanoparticles, and scaffolds for tissue engineering [54]. PLAs are insoluble in ethanol, methanol, and aliphatic hydrocarbons [55]. In orthopedics, PLA-based materials are being explored for implants like screws, pins, and plates, providing temporary support during healing and gradually degrading as bones recover [56].

Polyglycolic Acid (PGA), a homopolymer derived from glycolic acid, stands out for its remarkable mechanical strength and rapid degradation profile [57]. Existing solely in a highly crystalline form, PGA surpasses PLA in mechanical properties, featuring a melting point greater than 200°C [51]. Its notable tensile strength, combined with heightened sensitivity to hydrolysis, positions PGA for applications in medical devices such as resorbable sutures and meshes, appreciated for their effectiveness in wound closure as they gradually degrade during tissue

Material	$E(GPa)$	$\sigma(MPa)$	$\epsilon(\%)$	$T_g(^{\circ}C)$	$T_{melt}(^{\circ}C)$	Loss of Mech. Prop (months)	Total Degradation (months)
PLA	3.4-4.8	10-100	2-6	60-65	170-180	6	12-67
PGA	6.8-12.5	70-647	Min	35-40	180-230	0.25-1	2-12
PLGA	2	20-50	3-10	45-55	-	1-4	2-6
PCL	0.3-0.4	16-23	300-700	-60	59-64	2	>30

Table 2.1: Mechanical and thermal properties of widely used biodegradable polymers in medical applications. [47]

healing [58].

In many cases, a copolymer of PLA and PGA proves preferable. The adjustable ratio of these monomers allows for fine-tuning the polymer’s degradation rate, melting point, and mechanical properties, presenting a versatile option for various biomedical applications [59]. The crystallinity of PLGA significantly affects its mechanical properties and how quickly it degrades. Increasing the PGA content in PLGA reduces its crystallinity, resulting in a faster degradation rate. The 50:50 ratio of PLA to PGA in PLGA is known to degrade the most rapidly. PLGA copolymers also have a glass transition temperature above 37°C, making them rigid and suitable for implants [58]. High-molecular-weight PLA and PLGA are usually made by Ring-Opening Polymerization (ROP) of lactide or glycolide, and cyclic diesters of lactic and glycolic acids, using tin-based catalysts [60]. However, it’s crucial to note that impurities generated during the reaction process may persist in the body, leading to potential complications in medical applications. Consequently, further purification becomes imperative, complicating the synthesis process and substantially elevating the cost of medical-grade polymer production.

Polycaprolactone (PCL). Polycaprolactone (PCL) is a biodegradable polyester that has gained prominence in the field of medical devices due to its unique combination of properties. PCL possesses notable toughness and flexibility as a semicrystalline polymer, characterized by a glass transition temperature of -60°C and a melting point approximately at 60°C [61, 51]. In comparison to other

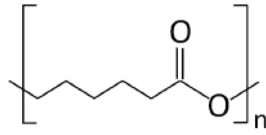


Figure 2.2: PCL chemical structure.

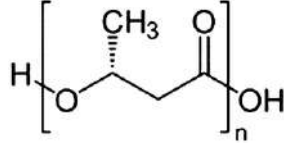


Figure 2.3: PHB chemical structure.

biodegradable polymers, PCL offers distinct advantages. One notable feature is its prolonged degradation profile. PCL degrades more slowly than PLA and PLGA, making it ideal for situations where a longer-lasting support structure is needed. Its unstable aliphatic ester bonds allow PCL to degrade through both hydrolysis of ester bonds and bulk degradation processes [49, 62]. The hydrophobic nature of PCL, hindering water molecule penetration, contributes to slow degradation. This property is particularly advantageous in the development of medical devices such as implants, spacers, removable drug delivery systems, and tissue engineering constructs. Its compatibility with various processing techniques, including 3D printing and electrospinning, further enhances its versatility in creating complex medical devices [63, 64].

Polyhydroxyalkanoates (PHA). Polyhydroxyalkanoates (PHAs) are a subset of polyhydroxesters, encompassing 3-, 4-, 5-, and 6-hydroxy alkanoic acids. Illustrated in Fig., the general chemical structure of PHAs characterizes these biocompatible, biodegradable polyesters, synthesized by bacteria from renewable sources [65]. Among the marketed PHA structures, medium chain length PHA, polyhydroxybutyrate (PHB), and poly(hydroxybutyrate-co-valerate) (PHBV) are prominent, with PHB (Fig. 2.3) being an extensively researched short-chain length PHA polymer [44]. The synthesis of PHB involves the fermentation of microorganisms, such as bacteria (e.g., *Cupriavidus necator*), utilizing carbon sources like

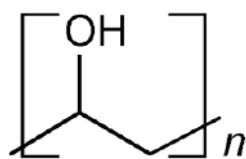


Figure 2.4: PVA chemical structure.

sugars or lipids. Microorganisms accumulate PHB as intracellular granules during fermentation, and subsequent extraction and purification from microbial cells yield PHB that can be processed into diverse forms like films, fibers, or molded articles for medical device applications [65]. PHB exhibits *in vivo* enzymatic hydrolysis-driven degradation, producing non-toxic byproducts, aligning with applications where controlled degradation is a key consideration [66]. However, limitations such as brittleness, slow crystallization, poor thermal stability, and suboptimal processability in melt and solution contexts constrain its application scope. Ongoing scientific efforts primarily focus on enhancing PHB functionalities, notably through copolymerization with hydroxyvalerate (HV) [51]. Despite these advancements, these polymers have yet to find widespread industrial use in medicine and are not employed in the present work.

Polyvinyl Alcohol (PVA). Polyvinyl Alcohol (PVA), a water-soluble synthetic polymer derived from the hydrolysis of polyvinyl acetate, exhibits significant potential in drug delivery system applications. PVA’s intrinsic biocompatibility and film-forming properties render it a valuable material across diverse medical applications.

In the medical arena, PVA showcases versatility, particularly in drug delivery systems, wound dressings, and contact lenses[67, 68, 69, 70]. PVA-based nanoparticles and hydrogels find utility in drug delivery, benefiting from their water solubility and facilitating controlled and sustained drug release. Furthermore, PVA-based hydrogel films exhibit promise in wound healing applications, creating an environment conducive to the healing process[71]. Additionally, owing

to its water solubility and hydrophilic characteristics, PVA is commonly blended with other polymer compounds for various industrial applications, enhancing the mechanical properties of films [72, 73, 74].

Currently, a diverse array of polymers is employed in the research and development of DDSs, spanning both early scientific investigations and formulations already approved by the FDA. To address specific challenges and meet application requirements, researchers often turn to combinations of different polymer classes, leveraging various formulations to enhance the effectiveness of DDSs.

2.2.2 Formulation and Drug Incorporation. Mechanisms of Drug release

A fundamental aspect of DDS design lies in comprehending the mechanisms governing drug elution, as it directly impacts the release kinetics and overall performance of the system. The following provides an overview of key mechanisms involved in drug elution from DDS.

Mathematical models

The power law equation serves as a comprehensive semi-empirical model designed to elucidate drug release from polymeric systems. Originating from the works of Korsmeyer, Gurny, Doelker, Buri, and Peppas [75], and later refined by Ritger and Peppas [76], this model establishes an exponential correlation between drug release and time, expressed as:

$$\frac{M_t}{M_\infty} = Kt^n; \quad (1)$$

M_∞ denotes the equilibrium drug amount, which often closely approximates the initial drug quantity present in the dosage form at the onset of release. M_t represents the cumulative drug release at time t , K symbolizes the constant incorporating structural modifications and system geometrical attributes—also referred

to as the release velocity constant. Meanwhile, n serves as the release exponent, capturing the temporal dependence of drug release mechanisms.

In the context of the Ritger-Peppas model, when the release exponent n equals 0.5, the system is characterized as Fickian. This implies that drug release predominantly occurs through diffusion. Such diffusion-controlled release adheres to first-order kinetics, where the rate of drug release is directly proportional to the residual drug content within the carrier matrix. As time progresses, the drug release rate diminishes due to a declining concentration gradient of the drug within the carrier material.

The Korsmeyer-Peppas model is based on the power-law relationship between drug release and time, and it is characterized by an exponent of release, n , which can range from 0.5 to 1.0, depending on the release mechanism. When $n > 0.5$, the model is non-Fickian, and drug release is influenced by factors such as swelling or relaxation of polymer chains. If the exponent of release, n , in the Korsmeyer-Peppas model is equal to 1, it indicates that the drug release follows zero-order kinetics:

$$\frac{M_t}{M_\infty} = Kt; \quad (2)$$

In zero-order release, the rate of drug release is constant over time, independent of the concentration of the drug within the carrier material (Fig. 2.5). This means that the system releases a consistent amount of drug per unit time, resulting in a linear release profile. Achieving zero-order release kinetics is desirable in drug delivery systems because it can lead to stable drug plasma concentrations within the therapeutic window without the need for frequent redosing. This can minimize adverse effects and improve patient compliance. Additionally, zero-order release can reduce the overall cumulative dose within the body compared to immediate-release and first-order release systems, ultimately reducing the risk of chronic toxicity.

There are also another models, suitable for the determination of drug elution kinetic, but used for more specified cases. The Higuchi model is frequently used

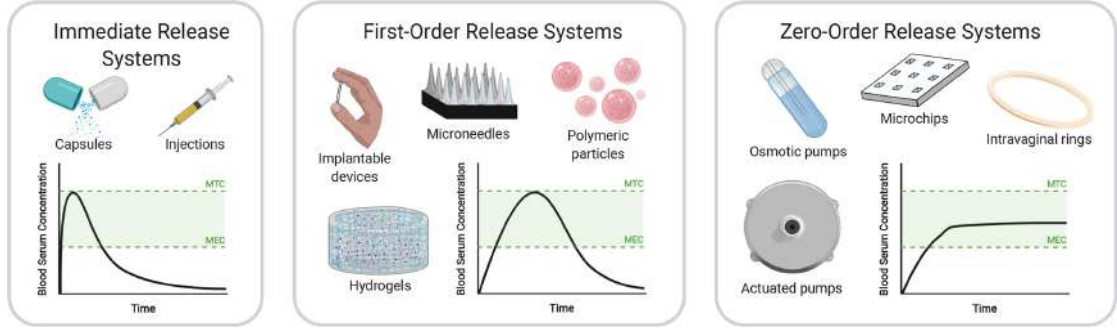


Figure 2.5: Common use DDS and their pharmacokinetics [77].

to explain how drugs are released from polymeric matrices and gels when the drug is evenly dispersed. If drug release from the composite is governed by diffusion, Higuchi's model, which relates drug release to the square root of time, can be used:

$$\frac{M_t}{M_\infty} = K\sqrt{t}; \quad (3)$$

Another approach - The Hixson–Crowell model is used when the surface area and size of drug particles change over time. It explains drug release in systems where particles decrease in size due to dissolution or erosion.

$$\sqrt[3]{1 - \frac{M_t}{M_\infty}} = -Kt; \quad (4)$$

Since the Hixson–Crowell model focuses more on changes in particle size and surface area over time due to erosion or dissolution, the Korsmeyer–Peppas model is more versatile and can accommodate various release mechanisms, including diffusion, swelling, and erosion, making it suitable for a broader range of polymeric systems.

The Peppas–Sahlin model is a release kinetics model that provides insights into drug release mechanisms from polymeric systems. Developed by Nikolaos Peppas and Jennifer Sahlin in 1989 [78], this model combines both diffusional and relaxational mechanisms to describe the drug release process, particularly in anomalous transport scenarios.

The model is described by the equation:

$$\frac{M_t}{M_\infty} = K_1 t^m + K_2 t^{2m}; \quad (5)$$

The first term $K_1 t^m$ represents the Fickian (F) diffusional contribution, indicating how the drug diffuses through the polymer matrix. The second term $K_2 t^{2m}$ represents the Case II relaxational contribution (R), describing the relaxation or deformation of the polymer matrix as the drug is released.

The coefficient m is the diffusional exponent, which is related to the power law coefficient n . Coefficient m typically ranges between 0.5 and 1.0, with values closer to 0.5 indicating more Fickian (or Case I) diffusion, and values closer to 1.0 indicating more non-Fickian (or Case II) release mechanisms.

The Peppas–Sahlin model has been widely used to analyze drug release data from various polymeric delivery systems, providing valuable insights into the underlying release mechanisms and aiding in the design and optimization of drug delivery systems.

To assess the relative contributions of two mechanisms to the release, the ratio of the relaxational contribution (R) to the Fickian contribution (R/F) are calculated as follows:

$$R/F = \frac{k_2 t^m}{k_1}; \quad (6)$$

The Hopfenberg model is a mathematical model used to describe drug release from erodible polymers in various geometrical forms such as planar films, spheres, and cylinders. Proposed by Hopfenberg, this model incorporates equations to account for heterogeneous erosion in drug delivery systems.

The basic equation describing drug release according to the Hopfenberg model is:

$$\frac{M_t}{M_\infty} = 1 - \left[1 - \frac{k_0 t}{C_0 a_0} \right]^n; \quad (7)$$

In this context, M_t represents the amount of drug released at time t , and M_∞ denotes the total amount of drug available for release. The erosion rate constant

is k_0 , and C_0 stands for the initial drug concentration in the matrix. The initial radius for spheres or cylinders is a_0 , or half the initial thickness for films. The value of n in the equation depends on the geometry of the drug delivery system: it is 1 for films, 2 for cylinders, and 3 for spheres.

The Hopfenberg model is particularly valuable for understanding drug release mechanisms in erodible polymers, where erosion significantly influences release kinetics. By considering initial conditions, erosion rates, and system geometry, this model provides insights into drug release profiles, aiding in the optimization and prediction of drug delivery systems under varying conditions.

Release mechanisms and forming methods

The kinetics of drug release from a drug delivery system are governed by a mass of factors, reflecting the complex interplay between the composition of the DDS, the method used to integrate the drug and the polymer, as well as the inherent properties of both the drug and the polymer. The specific properties of the drug, such as its solubility and molecular weight, alongside those of the polymer, including its degradation rate, solubility, and swelling behavior, further modulate the release kinetics. The release of incorporated drug from DDS usually presume sustained or prolonged, and controlled release mechanisms. The main aim of prolonged release is to maintain the drug's effect over a long time. Controlled drug release, on the other hand, focuses on achieving a specific release rate based on the drug delivery system, which can include sustained, burst, or triggered release [79].

A widely adopted method in coating production involves the use of composite films, where drug powder is dispersed within a coating polymer layer. This approach streamlines the coating process, offering versatility and simplicity. The release mechanism in composite films is intricately influenced by several factors, including drug solubility, volume fraction of the drug, molecular weight, the permeability and degradation characteristics of the carrier matrix. Therefore corre-

sponding release mechanisms could be diffusion- (Fig. 2.6 a), swelling- (Fig. 2.6 b), and erosion-driven release (Fig. 2.6 c).

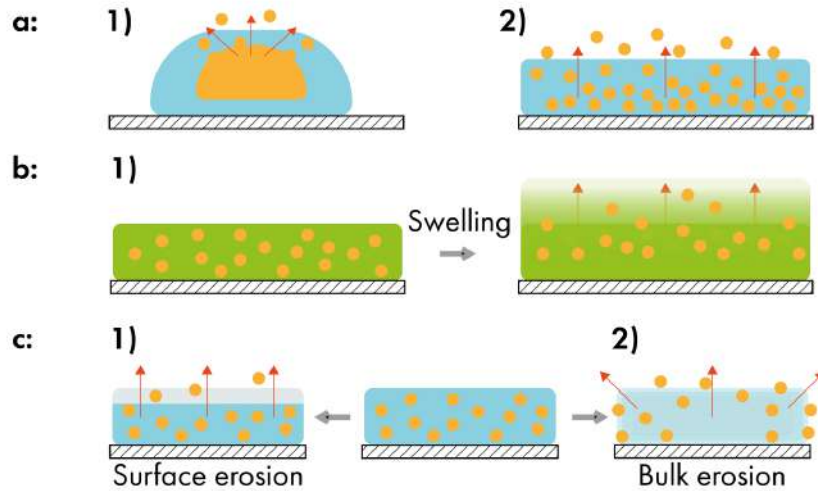


Figure 2.6: Diffusion-controlled (a), swelling-controlled (b), and erosion-controlled release (c).

Diffusion-controlled release. The majority of polymer DEC's can be considered as simple matrix system, where the drug is uniformly dispersed within a non-erodible matrix (Fig. 2.6 a2). In this system, drug release involves dissolving the drug in the matrix, diffusing it through the polymer, and then removing it from the surface of the composite. For non-swelling polymers, the slowest step in this process is usually the diffusion of the drug through the polymer matrix.

In view of in-demand DDSs, several remarks for such system can be drawn. At first, since using of biodegradable polymers like PLA, PLGA, PCL, and their copolymers is most beneficial for implantable DDSs, it is important to take into account the mechanisms of their interaction with water. Water is absorbed by the biopolymer instantly upon immersion in water or contact with body fluids during administration *in vivo*. Water inside the polymer matrix creates pores, making water absorption a pore-forming process. Initially, the membrane may be too dense for drug molecules to pass through. But as more water-filled pores develop and grow, they form a network that enables drug release. During this period, in

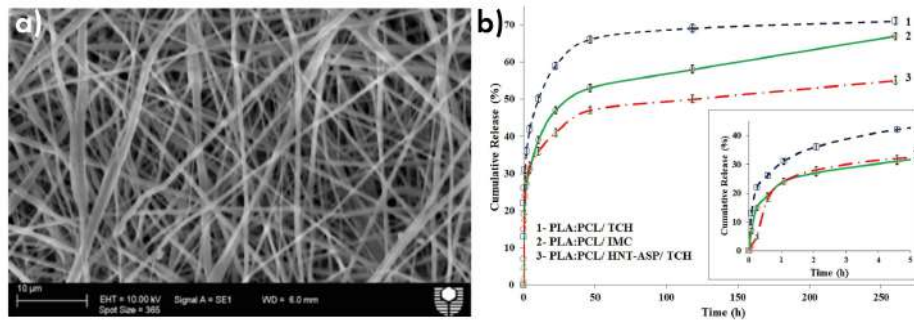


Figure 2.7: (a) PLA:PCL/TCH electrospun fibre mats SEM microphotograph; (b) Drug release profiles for PLA:PCL fiber mats containing TCH, IMC, and halloysite nanotubes modified with 3-aminopropyltriethoxysilane [80].

the absence of a protective layer, the matrix system typically exhibits an initial burst release, releasing approximately 20-60% of its cargo. Subsequently, the drug release rate decelerates due to diminishing drug concentration gradients and drug elimination. This sustained slow release persists until polymer degradation occurs via hydrolysis, often exhibiting an avalanche-like pattern. Following this phase, there is a secondary delayed burst release. To avoid this erratic release profile, nano-sized matrix formulations with reduced diffusion path and surface to volume ratio, such as nanoparticles and nanofibers, can be employed.

Haroosh and coworkers investigated electrospun composite nanofibers composed of PLA and PCL to achieve sustained release of the hydrophilic drug tetracycline hydrochloride (TCH) and the hydrophobic drug indomethacin (IMC) [80]. All composites exhibited an initial burst release of more than 30% within the first 5 hours (Fig. 2.7). The highest elution rate was observed for the hydrophilic TCH, while the hydrophobic IMC demonstrated a slower release rate due to stronger interactions with the hydrophobic polymers. Loading the hydrophilic drug TCH into halloysite nanotubes modified with 3-aminopropyltriethoxysilane (HNT-ASP) and mixing them with hydrophobic PLA:PCL blends slowed the drug release rate and improved the interaction between TCH and the PLA:PCL blends.

Therefore, while monolithic matrix systems represent a straightforward approach, they are not ideal for achieving sustained release due to their initial burst

and ineffective subsequent release. Attaining ideal zero-order release for water-soluble drugs proves challenging with this system. However, strategies such as leveraging polymer erosion or swelling and incorporating hydrophobic drugs can enhance the efficacy of these drug-eluting constructs (DECs). These approaches will be discussed in more detail below.

Swelling-controlled release. The next strategy in drug delivery systems involves the incorporation of swelling agents or layers (Fig. 2.6 b1). A swelling agent typically has a three-dimensional network of hydrophilic polymer chains that are cross-linked either chemically or physically. These agents, often referred to as hydrogels, can absorb substantial amounts of moisture or liquid water due to their hydrophilic nature. As the polymer network swells and its free volume increases, the drug can diffuse through this expanded network to reach the target area. Due to this property, hydrogels are often used as dressing materials, capable of absorbing blood and other body liquids and/or releasing drug into the wound quickly [81, 82]. Rapid release of the incorporated drug is also widely in demand in the cosmetology industry, where hydrogels are used for manufacturing of masks and patches [83]. In the other hand, release of medications in hours is not suitable for long term drug delivery, when drugs should be administrated for weeks and months. Therefore, water-swelling polymers are not used as independent DECs, but can be a part of complex multilayered DDS, acting both as a diffusion barrier, smoothing burst release from polymer matrix (Fig. 2.8a), or as a porogen additive or a "diffusion bridge", enhancing cargo diffusion through dense base polymer (Fig. 2.8b).

A notable application of this approach is demonstrated in the work of Liu et al., where they designed a drug-eluting stent using multiple techniques. They applied N-nitrosomelatonin-loaded PLGA nanoparticles to SS 316L stainless steel stents using electrophoretic deposition and then added a collagen diffusion barrier with dip coating. This innovative design showcased controlled release profiles for both hydrophobic and hydrophilic drugs. The stent with a collagen top layer exhibited

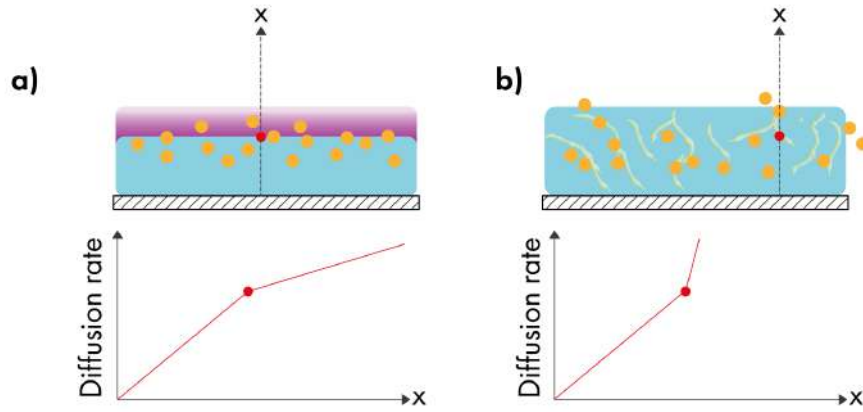


Figure 2.8: DEC with barrier diffusion layer (a) and "diffusion bridge" clusters (b)

the 30% lower burst release followed by sustained release over a specified period, exemplifying the efficacy of this approach [84]. Thakkar et al. also addressed these challenges by designing stents coated with a bilayer composed of sirolimus, polyvinyl pyrrolidone additive, and 50/50 PLGA as base layer with a PVP top layer serving to protect inner drug layer from light and moisture[85]. This bilayered design demonstrated a biphasic release profile, with the PVP additive enhancing the overall drug elution rate in initial stage. In another study, researchers sprayed a blend of PLGA, ReoPro (abciximab), and polyvinyl alcohol (PVA) onto 316L stainless steel disks to test its effectiveness as a drug release platform for drug-eluting stents (DES) [86]. This research highlighted the correlation between the weight percentage of PVA and the release rate of drug, resulting in a controlled burst release over a specific timeframe.

Erosion-controlled release. When considering prolonged release more than 1 month, the effect of polymer hydrolysis should be taken into account. Majority of the biodegradable polymers contain prone to hydrolysis or enzymatic degradation bonds such as ester or amide. Degradation processes could undergo in two typical modes, surface and bulk degradation. In a surface-degrading polymer, only the outer surface in contact with liquids breaks down. Meanwhile, in a bulk-degrading

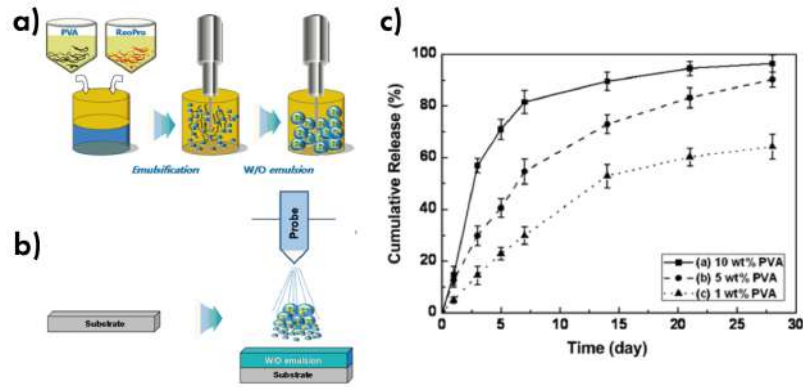


Figure 2.9: (a) Emulsification process; (b) Electrospray coatings and (c) Cumulative release profiles of ReoPro-loaded stents[86].

polymer, the degradation occurs uniformly throughout the entire material [87].

PLGA typically undergoes bulk erosion, as opposed to surface erosion, due to its relatively rapid hydration [88]. Surface erosion has been reported for polylactic acid (PLA) in alkaline media, whereas in neutral or acidic environments, bulk erosion appears to be predominant [89, 90]. PCL breaks down more slowly compared to other biodegradable polymers because of its hydrophobic properties and high crystallinity. The slow erosion rate of PCL allows it to stay several months *in vivo* without significant degradation [91]. The dissolution of polymer degradation by-products and erosion results in the formation of pores. Initially, small pores form through water absorption or polymer erosion, which then enlarge as water contact triggers hydrolysis. Locally produced acids speed up the degradation process, causing the polymer to dissolve and erode within the pores. As this happens, the small pores grow and combine into fewer, larger pores. The degradation-controlled approach is especially well-suited for drugs with low solubility, making it a preferred method in the manufacturing of Drug-Eluting Stents (DES). As the polymer gradually degrades, it exposes more of the load to the surrounding environment, facilitating a controlled release.

Notable examples include the commercially available Nobori Stent, which incorporates Biolimus A9 and a biodegradable PLA polymer, ensuring a controlled release and subsequent degradation of the polymer matrix [92, 93, 94]. Similarly,

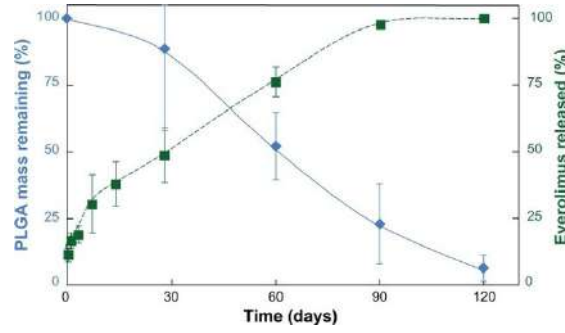


Figure 2.10: Kinetics of drug release and polymer absorption with the Synergy stent [98]

the BioMatrix Flex Stent utilizes a PLA-based biodegradable polymer to release Biolimus A9, allowing for a gradual drug release profile while facilitating polymer degradation over time [95, 96]. Additionally, the Synergy Stent employs a bioabsorbable polymer composed of PLGA for sustained drug release of everolimus for 4 months (Fig. 2.10) [97, 98]. These advancements in drug-eluting stents have significantly propelled cardiovascular interventions, providing substantial benefits in interventional cardiology over the last decade.

Liu et al. adopted a similar strategy to coat sutures [99], aiming to achieve sustained release of Ciprofloxacin (CPFX). Their study introduced a novel approach to drug delivery by coating PLA sutures with a mixture of PGA, PCL, and CPFX (Fig. 2.11a), resulting in prolonged drug release lasting over a month. The research demonstrated improved control over the rate of drug release by manipulating the PCL-PLGA ratio (Fig. 2.11b). Initially, all sutures exhibited rapid drug release within the first 100 hours of degradation, followed by a gradual slowing of the drug release rate thereafter. With more polycaprolactone in the drug carrier, the drug release rate decreased. The study proposed that for CPFX-PCL/PGA, drug release happens through a combination of drug diffusion and the dissolution of the polymeric carrier.

Despite the advantages offered by matrix disusion-, swelling-, and erosion-controlled release systems, they are not without their limitations. Achieving zero-order kinetics, where the rate of drug release remains constant over time, can

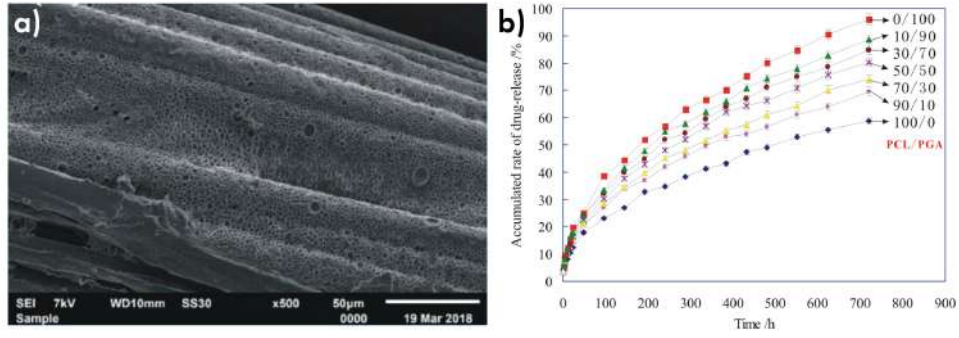


Figure 2.11: (a) PLA sutures coated with a 50/50 mix of PCL/PGA degraded over a period of 13 weeks. (b) The total drug release rate for sutures with different PCL/PGA ratios [99].

be challenging with these systems. Additionally, even in improved formulations, the occurrence of burst release, where a large amount of drug is rapidly released upon administration, remains a concern. These drawbacks underscore the need for alternative drug delivery approaches that offer enhanced control and consistency in drug release profiles. Reservoir systems, with their structured design and precise control over drug release kinetics, present a promising solution to address these challenges and advance the field of drug delivery.

Reservoir system.

Diffusion-controlled reservoir system. In this system, the drug is contained within a reservoir or compartment that is surrounded by a membrane (Fig. 2.61a). Reservoir can be filled with pure drug, or drug-containing active layer. The drug is released from the reservoir through diffusion or osmotic pressure. The rate at which the active ingredient diffuses is influenced by the barrier layer's thickness, surface area, and permeability. Typically, the release rate is primarily controlled by this diffusion. When there is enough drug in the compartment, the diffusion follows zero-order kinetics.

In a simplified model, the release rate of the active ingredient at time t , represented by $\frac{dM}{dt}$, can be described using Fick's first law of diffusion (Eq. 8). In this

equation, A denotes the surface area, l is the thickness of the layers, D is the diffusion coefficient through the matrix, B is the distribution coefficient between the film and the environment, and S represents the solubility of the active ingredient.

$$\frac{dM}{dt} = \frac{A}{l}DBS; \quad (8)$$

When parameters like D , l , B , and S are kept constant, $\frac{dM}{dt}$ stays stable, leading to a consistent release rate of the active ingredient. However, as the ingredient is released, the material's surface area or permeability can change, disrupting the expected zero-order release kinetics and making the release rate unpredictable. Therefore, choosing the right barrier materials is crucial for ensuring controlled release. It's important that the properties of the membrane film remain stable throughout the treatment. Maintaining long-term stability is particularly challenging with biopolymers, making biopolymer-based systems for zero-order release both rare and difficult to produce.

Osmotically-controlled reservoir system. Osmotic devices are a leading approach for controlled drug delivery. They work on the principle of osmosis, where water moves through a selectively permeable membrane due to differences in osmotic pressure. This principle is used to create effective controlled drug delivery systems, where the osmotic pressure produced by osmogens drives the controlled release of the drug [100, 101, 102].

Typically, osmotic drug-delivery pumps consist of a reservoir core coated with a semipermeable membrane. The core formulation includes a drug, an osmotic agent, and/or a water-swelling polymer. Osmogens, essential components of osmotic formulations, dissolve in biological fluid upon penetration into the pump, creating osmotic pressure buildup inside the pump and facilitating drug release through delivery ports. Common osmogens include inorganic salts and carbohydrates, such as potassium chloride, sodium chloride, mannitol, and highly water-soluble drugs. Swellable polymers may also be incorporated to increase hydrostatic pressure inside the pump, particularly for moderately water-soluble drugs,

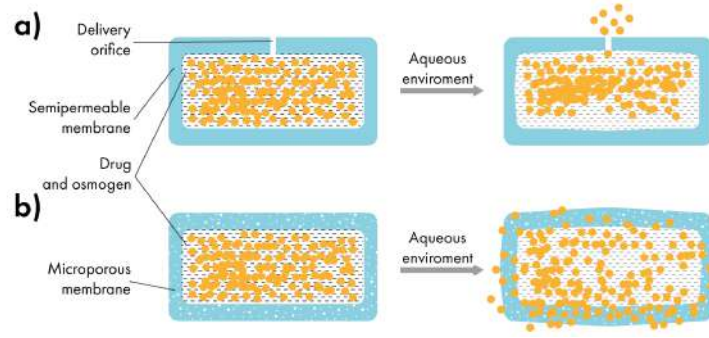


Figure 2.12: (a) Elementary osmotic pump; (b) controlled porosity osmotic pump (CPOP).

while non-swellable polymers are preferred for highly water-soluble drugs [103]. A semipermeable membrane, crafted from materials like PLA, PLGA, or other biopolymers, includes one or more delivery ports. These ports enable the gradual release of the drug solution over time.

Delivery orifices in the membrane are critical for controlling drug release from osmotic systems. Optimal orifice size is essential to maintain control over drug release rates while preventing solute diffusion or system deformation [104]. Laser drilling is a commonly used technique to create delivery orifices, allowing for precise control over orifice size by adjusting laser parameters such as power, beam dimensions and number of repetitions [105]. In some oral osmotic systems, pore-forming agents are added to the membrane coating solution to create delivery orifices on-site. These agents dissolve when they come into contact with water, leading to the formation of openings through which the drug can be released [106].

The elementary osmotic pump (EOP), introduced by Theeuwes in 1974 and shown in Figure 2.12a, consists of a tablet containing an active agent that generates osmotic pressure. A small orifice in the membrane allows the drug to be released, with the release rate initially described by the following equation:

$$\frac{dM_t}{dt} = \frac{dV}{dt} \cdot S; \quad (9)$$

where $\frac{dV}{dt}$ denotes the rate at which water flows into the tablet, and S represents the solubility of the agent within the tablet.

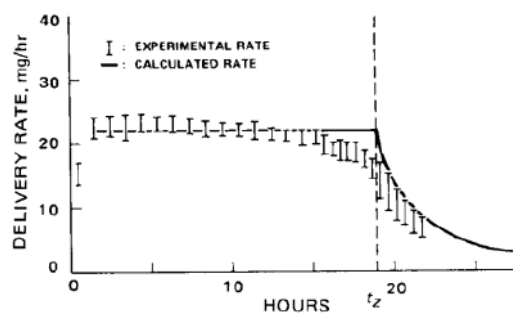


Figure 2.13: The *in vitro* release rate of KCl from EOP in water [101].

When exposed to water, the core of the device absorbs it at a controlled rate determined by the membrane's permeability and the osmotic pressure of the core. It releases a saturated solution equal to the volume of water absorbed during each time period. The solute release rate remains constant while there is still excess solid inside the device. However, once the concentration of the solute falls below saturation, the release rate gradually decreases to zero. The typical release rate obtained from this system is illustrated in Figure 2.13. The controlled porosity osmotic pump (CPOP), depicted in Figure 2.12b, features delivery orifices that are formed *in situ*. This process involves using water-soluble porogens within the semi-permeable membrane, which are dissolved out to create the orifices [77]. The CPOP system reduces local overdose risks by releasing drugs from the entire surface, not just a single hole. It also simplifies manufacturing by eliminating the need for laser drilling, as the orifices form *in situ*. Unlike more complex pumps with multiple parts and compartments, CPOPs can be easily used in drug-eluting coatings.

Fabrication methods of reservoir systems. When considering reservoir systems within the context of drug delivery system films and coatings, fabrication methods focus on creating thin films with reservoir-like structures or forming reservoirs directly on the MID itself.

Thin film reservoir-like structures are achieved through various fabrication techniques. These methods involve using special microarray templates created

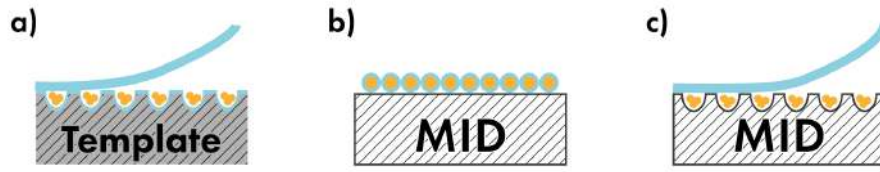


Figure 2.14: Reservoir formation methods. (a) Formation of film on the template; (b) Formation of layer of core-shell structures on a MID surface; (c) Drug loading and sealing of reservoirs created on the surface of MID.

by microfabrication processes like photolithography. Techniques such as layer-by-layer assembly, solvent casting, or electrospinning can be employed to deposit alternating layers of polymers and drugs, creating reservoirs within the film (Fig. 2.14 a). Also a thin film of polymeric reservoir-like capsules can be formed directly on MID using core-shell electrodeposition techniques or deposition of layer of microfluidic-made capsules (Fig. 2.14 b).

Alternatively, reservoir systems can be directly integrated onto the surface of the MID, forming discrete reservoirs as a part of the MID during device manufacturing. Fabrication methods may involve microfabrication techniques such as micromachining, laser perforation, etching, and anodization to create microscale reservoirs or channels on the surface of the MID. The drug can be loaded into these reservoirs or channels, and then sealed by a biopolymer film. The release is controlled by diffusion through this membrane (see Fig. 2.14c).

Microchamber array films. Microneedle patches One of the pioneering works in the fabrication of reservoir-like polymer microstructures was conducted by Guan et al. Their study demonstrated the production of polymer particles through soft lithography techniques, using materials such as PLGA and PCL [107].

Figure 2.15 depicts (a) schematic illustrations detailing the fabrication process of PLGA-based microstructures, alongside optical micrographs showcasing microcapsules (b) on PVA and (c) in water. It's noteworthy that the released microcapsules exhibited significant swelling in water, potentially due to osmotic pressure from the encapsulated sucrose, as well as finite water diffusion through

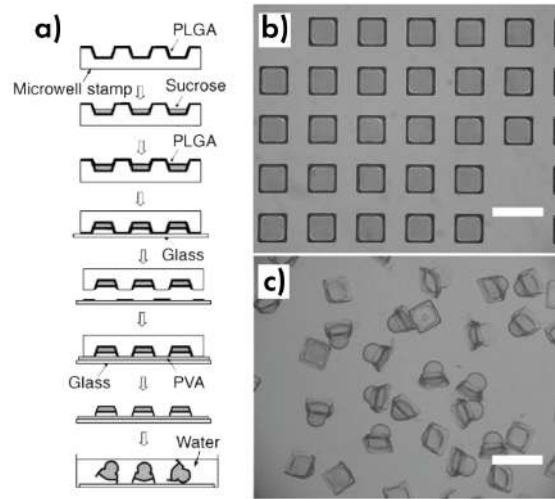


Figure 2.15: (a) Schematic illustrations of the fabrication process of PLGA-based microstructures, optical micrographs of microcapsules (b) on PVA and in water (c). Scale bar=50 μm [107]

the thin PLGA shell of the microcapsule. A similar procedure involves imprinting micro-wells on sacrificial poly(methyl methacrylate) (PMMA) film, followed by layer-by-layer assembly of oppositely charged polyelectrolytes (PAH and PSS) on the patterned substrate. This method was utilized by Kiryukhin et al. in 2011 [108], resulting in the creation of highly ordered arrays of hollow microchamber arrays (MCA) with controlled geometry and mechanical properties, suitable for various applications such as solid-state delivery systems. Subsequently, this method was adapted to fabricate PLA and PLGA-based microchambers using a reusable PDMS template by Meiyu Gai in 2017 [109].

Methods for automating and scaling the production of such films have been extensively studied in our laboratory for a long time. Today, classical template-based MCA films represent an array of microcontainers filled with drugs and sealed between two polymer films, which can be conceptualized in the context of three main steps: formation of the containers on the base polymer film, loading of the medicinal substance, and application of the cover film.

In the first step, a base polymer film is typically formed on a stamp made of polydimethylsiloxane (PDMS) using the dip-coating method (see Figure 2.16 step

1). Subsequently, the drug is loaded into the isolated containers in the form of a dry powder, and then, the filled containers are sealed by a second polymer film (see Figure 2.16 steps 2 and 3).

The first two steps represent the most challenging and innovative procedures in the fabrication process. However, due to the mechanical properties of the soft PDMS stamp, it can deform during its removal from the template, which limits the resolution of the pattern and can reduce reproducibility. Roof collapse of PDMS wells may occur in the case of a low aspect ratio of features, while buckling and lateral collapse may occur when the aspect ratio is high and the ink concentration in the stamp is low [110]. To address this issue, modifications to the PDMS stamp can be implemented. For example, hard PDMS can be used to transfer sub-micron features. Another potential issue is PDMS swelling in organic solvents, which can lead to changes in shape and dimensions. To overcome this problem, several approaches can be utilized. One method is to reduce the polymer dipping time, which can help mitigate the extent of PDMS swelling. Additionally, using solvents with minimal swelling effects, such as acetonitrile, acetone, and alcohols, can be effective [111, 112]. These solvents are less likely to cause significant changes in the shape and dimensions of the PDMS stamp during the fabrication process. Microchamber structures are typically no larger than 100 microns, requiring precise manufacturing of templates to ensure high-quality surfaces. For instance, small PDMS stamps (1 to 5 cm²) work well, but larger stamps (over 8 cm²) often suffer from defects due to surface curvature and bending from solvent swelling [112]. Increasing the template size raises manufacturing costs, whether using lithographic methods or direct PDMS pyrolysis [113]. Scaling up the DEFs production also faces challenges with powder loading. This process is hard to automate due to variations in powder properties like granule size, hygroscopicity, and compressibility, making it dependent on operator skill. Additionally, expensive drugs and methods like spraying or screen printing can produce significant hazardous waste. Although there have been notable advancements in microchamber array film manufacturing, several challenges still exist. These limitations affect



Figure 2.16: Process of manufacturing of MCA film.

scalability and automation, leading to high defect rates. As a result, MCA films often show significant burst release, where up to 50% of the drug may be released within the first day. Even small defects in sealing or porosity caused by water can greatly increase the rate at which the drug diffuses.

Zykova et al. determined that using PLLA is optimal for fabricating microchamber arrays, each capable of holding 2.88×10^{-9} μg of cargo, successfully loaded with Rhodamine B (Fig. 2.17a). Their in vitro experiments in PBS at 37°C showed that Rhodamine B was completely released over 13 days through diffusion. Their investigation unveiled that low-frequency ultrasound (LFUS, 20 kHz) could initiate Rhodamine B release by causing damage to the microchambers and subsequent detachment of individual PLLA microchambers over time. Moreover, they demonstrated the versatility of the free-standing printed PLLA microchamber arrays, showcasing their potential application as endovascular stent covers, capable of offering additional pharmacological effects such as triggered local delivery of anticoagulants (Fig. 2.17b).

It is noteworthy, however, that despite the successful release of Rhodamine B over almost a two-week period, more than 40% of the substance was released within the first few hours (Fig. 2.17c). This rapid release, especially in a reservoir system composed of hydrophobic PLA, may indicate the presence of defects through which Rhodamine B diffused away. Nonetheless, the remaining non-defective microchambers exhibited controlled release of the substance, highlighting the potential of the microchamber array system when functioning ideally.

In a study by Mordovina Ekaterina in our lab, microchambers were loaded

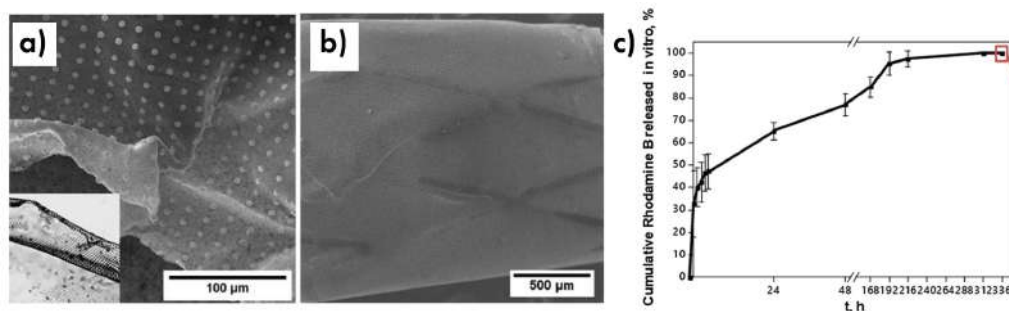


Figure 2.17: (a) Free-standing printed PLLA microchamber arrays (1 wt. %); (b) Closed cobalt-chromium endovascular stent covered with free-standing PLLA microchamber arrays; (c) In vitro cumulative RhB release in PBS at 37 °C during 14 days. [114]

with ceftriaxone at concentrations ranging from 12 to 38 $\mu\text{g}/\text{cm}^2$, depending on the thickness of the patterned film made with varying PLA concentrations in chloroform. Results showed that microchambers with the thinnest film of 1 μm had a low holding capacity, with approximately 50% of the loaded ceftriaxone released after 15 minutes (Fig. 2.18a). Subsequently, another 40% was released after 6 hours, leaving less than 5% of the drug after 24 hours, resulting in over 95% release within the first 24 hours.

Increasing the PLA concentration from 1.5% to 2.5% slowed the release of ceftriaxone. Initially, 10–15% of the drug was released within the first 15 minutes, followed by an additional 60% over the next 6 hours. After 24 hours, about 10% of the drug remained, with 80–85% having been released. The remaining drug continued to be released over the next 48 and 72 hours, with roughly 5% released during each of these periods. Although increasing the PLA film thickness threefold did not significantly improve the release profile, the best results were achieved with a 72-hour release period.

The study found that increasing the thickness of the patterned film enhanced efficiency by minimizing nano- and microdefects from the printing process. Although the efficiency was relatively low, the released ceftriaxone successfully in-

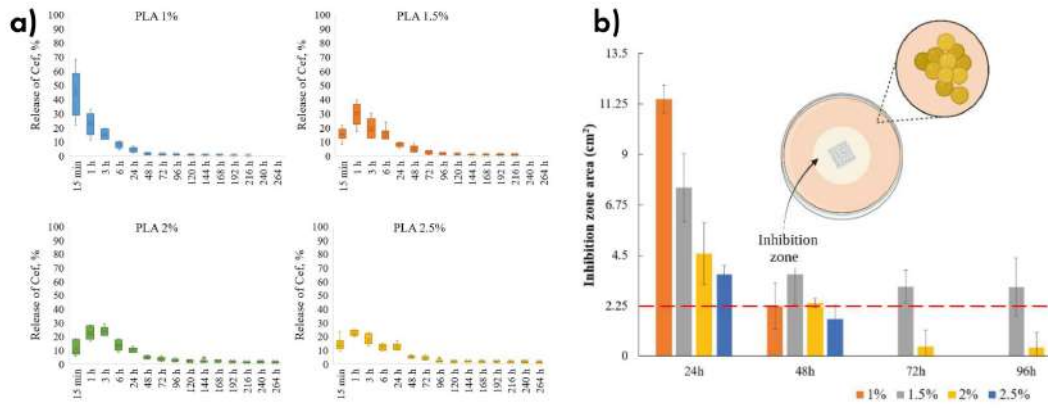


Figure 2.18: (a) Extended release profiles of ceftriaxone from microchamber arrays made with different PLA concentrations in a patterned film (ranging from 1% to 2.5%); (b) The antibacterial efficacy of microchamber arrays containing ceftriaxone [115].

hibited the growth of *Staphylococcus aureus* for up to 96 hours in *in vitro* tests (Fig. 2.18b). This demonstrates the potential of microchamber films for developing personalized and adjustable antibacterial treatments.

Thus, *in vitro* studies indicate a significant contribution of defects in films to the release of drugs from them, reducing their effectiveness due to the burst effect. While this property makes them promising for short-term drug release applications such as antibacterial therapy and as anticoagulant coatings, they are still far from being ideal reservoir-like systems. On the other hand, the fabrication technology of MCA presents a high level of tunability, allowing for easy modification of any part of the microchamber - including the base layer, cargo, and covering polymer film. Leveraging this manufacturing diversity enables the creation of triggerable drug delivery systems. For instance, Liu et al. found that the degradation rate of PLA microchambers is highly dependent on the surrounding pH and follows first-order kinetics [99]. This pH sensitivity can be leveraged to control the release rate of the encapsulated substances. Additionally, Gai et al. in 2017 demonstrated that high-intensity focused ultrasound (HIFU) can be used to trigger the release of cargo from microchamber arrays that contain trapped air bubbles [109]. In the same

year, they successfully developed and applied biocompatible microchamber arrays for precise and controlled delivery of bioactive substances to single cells using NIR-laser technology [116]. By incorporating gold nanoparticles (AuNPs) into the microchamber walls, the researchers achieved efficient cargo release through photothermal effects triggered by laser stimulation. Their research also demonstrated cell growth on PLA microchamber arrays' surfaces, indicating potential applications in cell analysis, regenerative medicine, and other fields requiring targeted and controlled drug delivery to individual cells. Similarly, Kurochkin et al. utilized the same approach to induce drug release from gold nanoparticles-doped microchamber array films using optical fibers [117]. They encapsulated Rhodamine B inside the chambers of the polymeric film and employed a continuous-wave NIR diode laser for photothermal unsealing of the chambers. Sindeeva also found that carbon nanodots (CDs) can perform as well as gold nanoparticles in PLA microchambers for controlling the opening and release of substances when exposed to laser light [118]. The author also showed that PLGA-based microchamber array films can be sensitive to low-intensity therapeutic ultrasound [119]. In live animal studies using a laser imaging system, researchers found that blood flow was reduced when epinephrine hydrochloride (EH) was released from PLGA microchamber arrays implanted under the skin of a mouse after ultrasound exposure.

In conclusion, microchamber array (MCA) films offer a rich and tunable platform for drug delivery, showing promise for various medical applications. However, the lack of methods to produce large-area films with good repeatability presents a significant obstacle to their widespread adoption as DEC's in medicine. While laboratory-scale methods demonstrate the potential of MCA technology, continued research and innovation are needed to overcome scalability and repeatability challenges.

Core-shell structures. Electrodeposition Electrospraying represents a powerful technique for the fabrication of core-shell structures with precise control over structures characteristics. Despite some limitations and challenges, its

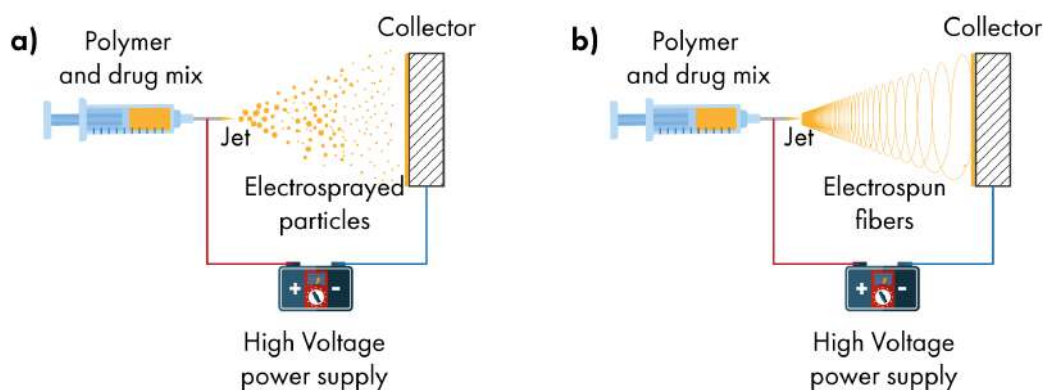


Figure 2.19: Simplified scheme of particles (a) and fibers (b) electrodeposition.

versatility and scalability make it an attractive option for various applications in drug delivery. The principle behind electro spraying involves the use of an electric field to disperse a liquid into droplets or fibers, which are then solidified on collector surface to form coating. A schemes of the Electrospray setups are shown in Figure 2.19 . An electric field is first applied between a nozzle and a collector. This electric field charges the liquid at the nozzle tip. When the electric field gets strong enough, it makes the droplet at the tip stretch into a cone shape, known as the Taylor cone. This concentrated electric field then causes the liquid to be expelled as either a continuous stream or separate droplets. The final form of the expelled liquid depends on the voltage applied and the properties of the liquid. The size and shape of structures produced through electro spraying can be controlled by adjusting various factors. These include the properties of the polymer solutions—such as concentration, viscosity, molecular weight, and solvent type—as well as the settings of the electro spraying process, including the flow rate, voltage, and distance between the nozzle and the collector. Further insights into the configuration of electro spraying apparatus and its underlying physical parameters are available in other comprehensive reviews [120, 121]. Once ejected from the nozzle, the droplets undergo rapid solvent evaporation, leading to the solidification of the polymer, either in-flight or upon deposition onto the collector surface, depending on the processing conditions. To create core-shell structures, a coaxial

nozzle setup can be used, where one polymer solution forms the core, and another surrounds it to create the shell [120, 122]. The solidified particles are collected on a substrate or collector surface, where they can undergo further processing steps such as drying, crosslinking, or additional coating to enhance their properties or stability

Many works employing electrospray deposition focus on manufacturing composite micro- and nano-sized particles and fibers, primarily suited for long-term delivery applications. This emphasis on long-term delivery is due to the high optimization requirements for parameters such as solution properties, processing conditions, and equipment setup. Material compatibility poses a significant challenge, as not all substances are suitable for electrospraying, necessitating the identification of compatible materials and settings for each system. The use of a core-shell approach further complicates the system, limiting the number of drug delivery systems suitable for sustainable release and long-term applications.

One notable example of successful work in this area is by Li et al. [123]. The researchers employed coaxial electrospraying coating as a novel technique to create an anti-acute thrombogenic surface on vascular grafts. The release study conducted in the research involved monitoring the release profile of heparin from the PCL-PEG encapsulated microspheres over a 15-day period. Initially, a burst release of approximately 50% of the total heparin content occurred during the first 2 days, attributed to heparin molecules distributed on the microspheres' surface. Following this burst release phase, a relatively steady release of heparin was observed until day 6, with only 10% of the total heparin content released, indicating controlled and sustained release (see Fig. 2.20). From day 6 onwards, heparin released from the core part of the microspheres exhibited sustained release behavior until the end of the study period. This sustained release profile is crucial for maintaining the anticoagulant properties of the coating over an extended period. The authors indicated that the coaxial electrospraying coating approach provided a more controlled and sustained release of heparin compared to other methods such as blending systems or static electricity adsorption.

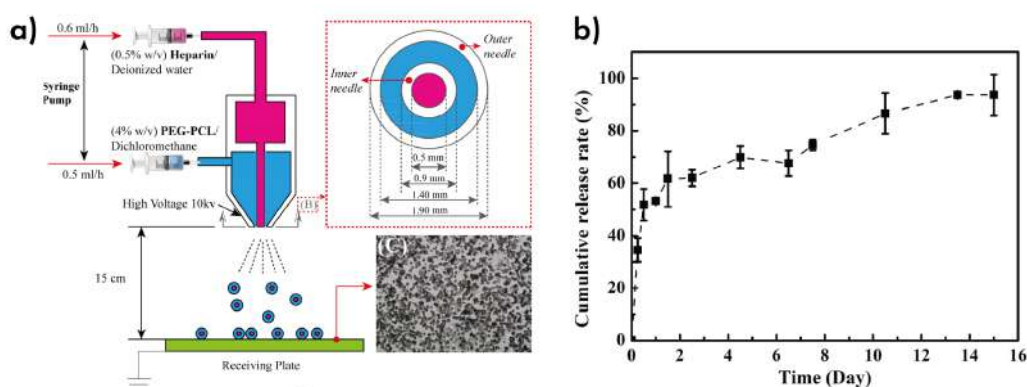


Figure 2.20: (a) Setup scheme and (b) release profile for Heparine-loaded microspheres [123].

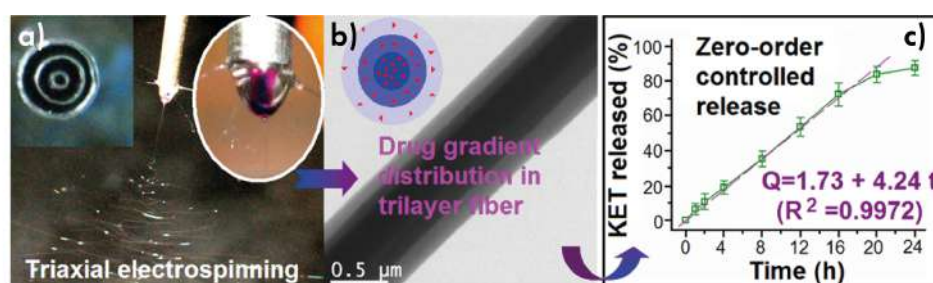


Figure 2.21: (a) Triaxial needle and spinning process; (b) TEM of trilayer fiber; (c) KET-containing fiber release profile [124].

The group of Deng-Guang Yu demonstrated interesting results regarding the *in vitro* dissolution tests on trilayer nanofibers fabricated using triaxial electrospinning [124]. These tests revealed that the nanofibers exhibited a zero-order release of the active ingredient ketoprofen for over 20 hours (see Fig. 2.21). This zero-order release profile indicates sustained and controlled release of the drug without the initial burst release commonly observed in monolithic drug-loaded nanofibers. Despite the relatively short release time, these results are significant for nano-sized systems and could be implemented for the manufacturing of safe narcotic pain relief drug delivery systems. Another example of electrospun fibers is the work of the Jouybari group [125]. The study aimed to produce tri-layer nanofibers using a triaxial electrospinning method to control the release of 5-Fluorouracil (5-FU), Doxorubicin (DOX), and Paclitaxel (PTX) for breast cancer therapy. The release

of 5-FU from these nanofibers followed a zero-order kinetic pattern, while the Korsmeyer-Peppas model was used to describe the release behavior of all three drugs from both single-layer and tri-layer nanofibers. The tri-layer nanofibers exhibited higher stability and enhanced cell killing efficacy against MCF-7 breast cancer cells compared to single-layer nanofibers, with a maximum cell killing of 94.2% achieved after 14 days of incubation.

Despite the significant advancements in capsule- and fiber-based coatings, the progress in this area lags behind that of free floating microparticles obtained by electrodeposition. This disparity may be attributed to the greater emphasis on injectable drug delivery systems. However, core-shell capsules, acting as medicinal reservoirs and capable of being placed on the surface of implanted devices, hold substantial potential and cannot be overlooked. A recent noteworthy example of core-shell capsules suitable for prolonged drug release is the work conducted by Tang et al. [126]. A one-step coaxial electrospray method was used to create injectable PLA microparticles for the sustained release of the hormone etonogestrel (ENG). The method produced uniform core-shell PLA microparticles for controlled release of ENG. By adjusting voltage, polymer concentration, and flow rate during coaxial electrospraying, the microparticles maintained an average diameter of 14 μm and a shell thickness of 2.5 μm . They achieved a drug loading of 54% and an encapsulation efficiency of 99%. Initially, only 10% of the drug was released on the first day. Over 3 months, the microparticles steadily released ENG, with their shell structure remaining unchanged, as confirmed by pharmacokinetic studies (see Fig. 2.22).

In conclusion, electrospraying emerges as a promising technique for the fabrication of DECAs, offering precise control over particle size and morphology, and also possibility of technical scaling. Despite its potential, challenges such as material compatibility and reproducibility need to be addressed for widespread implementation.

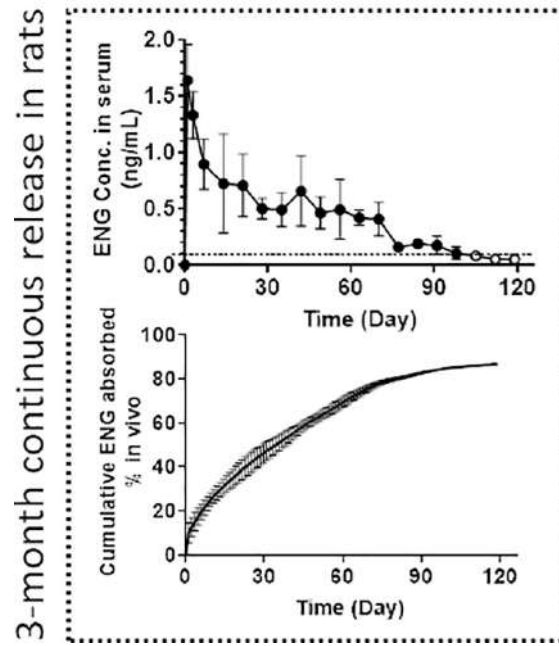


Figure 2.22: Release profiles for hormone etonogestrel released from PLA microparticles [126].

Integrated reservoir systems In addition to applying functional coatings made entirely of polymer, integrated reservoir systems refer to reservoirs that are seamlessly incorporated into a medical device, often through microtexturing or surface material modification techniques. Alternatively, they themselves can constitute a medical device, such as a microneedle patch or spacer. These reservoirs are designed to store and release therapeutic agents in a controlled manner, directly from the surface of the device.

As a rule integrated reservoir systems represent porous or reservoir-structured coatings made on the surface of implants. For instance, Gulati and his team developed a biodegradable drug-coated titanium implant using chitosan and PLA. The coating, which covered drug reservoirs made from titania nanotubes (TNT), served as a barrier to control drug release. By varying the coating thickness, they could adjust the coating's diffusion resistance and its degradation rate. Their approach significantly improved drug release performance, reducing initial burst release from 77% to under 20% and extending the total release period from 4 days

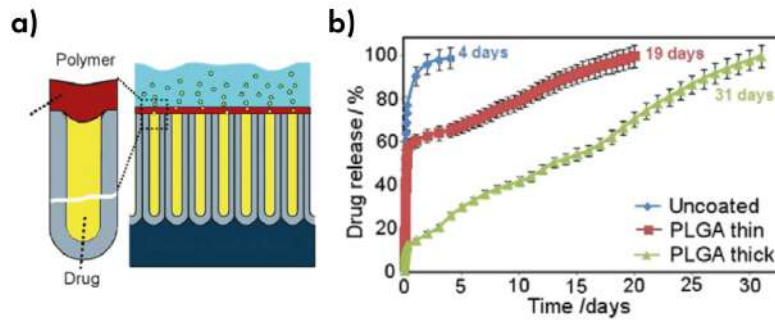


Figure 2.23: (a) Polymer films applied to TNT via dip coating. (b) Overall drug release profiles from uncoated TNT/Ti and TNT/Ti coated with thin and thick PLGA layers [127].

to over 30 days (see Fig. 2.23) [127]. The similar approach was adopted in the study by Davoodian et al. [128]. The research aimed to explore the utilization of nanotubes grown on nitinol surfaces for localized drug delivery by loading them with vancomycin and covering them with PLA. Characterization revealed that ultrasonication for 5 minutes effectively developed open-top nanotubes by desorbing debris, thus optimizing their formation (Fig. 2.24a). Vancomycin loading into the nanotubes was achieved through a vacuum technique, resulting in increased drug-loading levels and homogeneous distribution. The PLGA membrane coating on the nanotubes appeared uniform, with depressions indicating the underlying nanotube structure (Fig. 2.24b). The drug release kinetics displayed biphasic behavior, with an initial burst release attributed to the concentration gradient and sustained 1-week release from drug reservoirs within the nanotubes (Fig. 2.24c). Cytocompatibility assessment using dental pulp stem cells demonstrated viability over 1, 3, and 7 days, confirming the biocompatibility of the system. Overall, the study successfully showcased the potential of PLGA-coated drug-loaded nanotubes based reservoirs on nitinol for controlled drug delivery, with optimized formation, drug release kinetics, and biocompatibility.

Another type of scaffold was used by Jadidi in 2020[129]. The study aimed to investigate the impact of PLA encapsulation on the release of vancomycin from

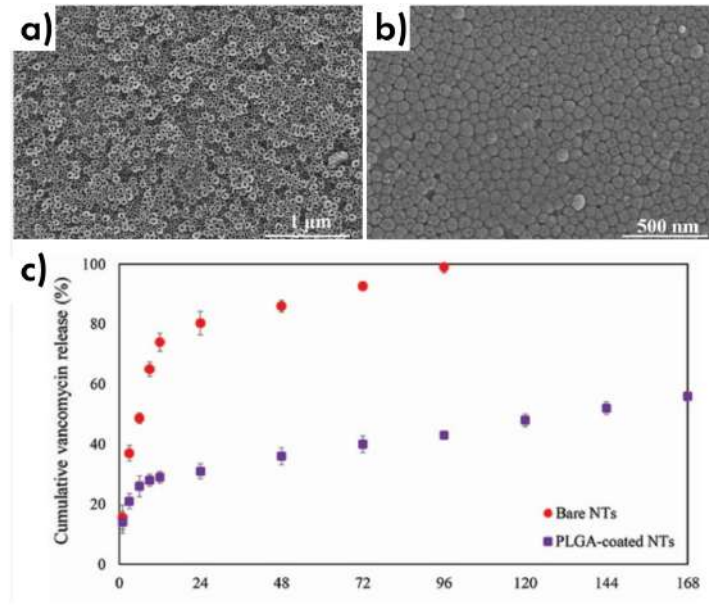


Figure 2.24: (a) FESEM image showing the top view of the sample after anodization, sonication, and annealing; (b) FESEM image of the NTs loaded with vancomycin; (c) Overall drug release from the devices [128].

calcium-magnesium silicate (bredigite) scaffolds for potential bone tissue engineering applications. By fabricating interconnected porous bredigite scaffolds loaded with vancomycin hydrochloride and encapsulating them with PLGA coatings of varying thicknesses, the researchers analyzed the drug release data using various kinetics models and characterized the morphological and chemical changes in the scaffolds. The experimental data fitting revealed that vancomycin release from the bare scaffold followed a dissolution-controlled kinetics mechanism, while the PLGA-coated scaffolds exhibited a combination of diffusion- and dissolution-controlled mechanisms for drug release. The 5% PLGA-coated scaffold transformed the release kinetics to a slower, single-stage anomalous transport with a more prominent diffusion contribution, whereas the 10% PLGA-coated scaffold displayed a two-stage release profile with the first stage showing a combined action of dissolution and diffusion, dominated by diffusion in the second stage, releasing only 40% of encapsulated drug after 7 days of incubation (Fig. 2.25).

In summary, integrated reservoir systems represent a powerful approach for

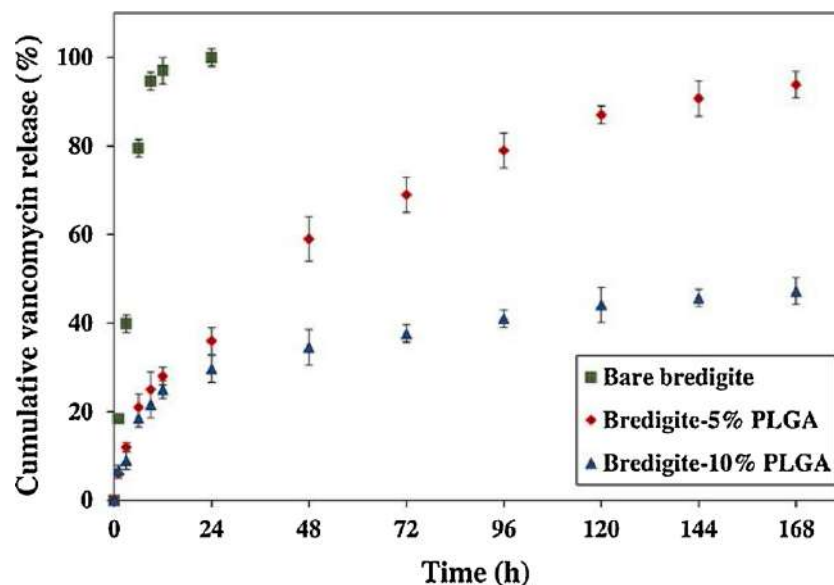


Figure 2.25: Cumulative percentage of the drug release from the scaffolds [129].

controlled drug delivery, offering sustain release kinetics. While these systems can be utilized in select specialized devices, their limited applicability stems from the need for tailored adaptation of devices and materials. This lack of universality hinders widespread acceptance and utilization of integrated reservoir systems in mainstream drug delivery applications. Moving forward, efforts to develop more versatile and adaptable reservoir systems are essential to overcome these limitations and unlock their full potential.

Microneedle Additional example of integrated reservoir systems is microneedle patches. These patches consist of arrays of tiny needles made from biocompatible materials such as polymers or metals. The needles are designed to penetrate the outer layer of the skin, creating microchannels that allow for the delivery of therapeutic agents stored within the patch. While microneedle patches share similarities with microchambers arrays in their structural design, they serve as autonomous devices with distinct applications and functionalities. Unlike microchambers, which are typically integrated into larger systems or devices for specific purposes such as drug delivery or sensing, microneedle patches operate independently. Their design includes an array of tiny needles arranged on a patch-like substrate, allowing for

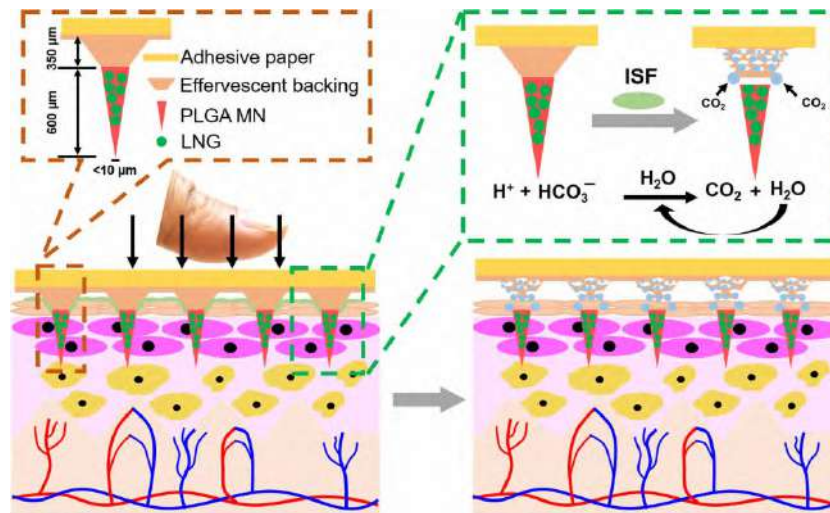


Figure 2.26: Schematic diagram showing the design of an MN patch with an effervescent backing and the process of applying the MN patch to the skin. The effervescent backing rapidly dissolves, allowing the MNs to quickly penetrate the skin [54].

efficient and minimally invasive delivery of drugs or vaccines directly into the skin. This standalone functionality enables microneedle patches to be easily applied by individuals without the need for specialized equipment or expertise. Microneedle patches offer several advantages, including painless administration, improved patient compliance, and targeted delivery of drugs or vaccines [130]. One common use of patches is the delivery of hormonal medications, for example for contraception use. In Li work the authors aimed to develop a novel effervescent microneedle patch for long-acting contraception that is simple to administer, environmentally friendly, and well-tolerated [54]. The effervescent microneedle patch was fabricated using polydimethylsiloxane molds. The microneedles were arranged in an array on the patch, which featured pedestals to lift them. When the patch was applied to the skin, the effervescent backing caused it to fizz, causing the microneedles to detach from the patch within a minute. After removal of the patch, the microneedles stayed embedded beneath the skin surface (see Fig. 2.26). The microneedles were fabricated from a biodegradable PLA, which facilitated the slow release of levonorgestrel (LNG) for over a month, both *in vitro* and *in vivo* in rats. LNG was

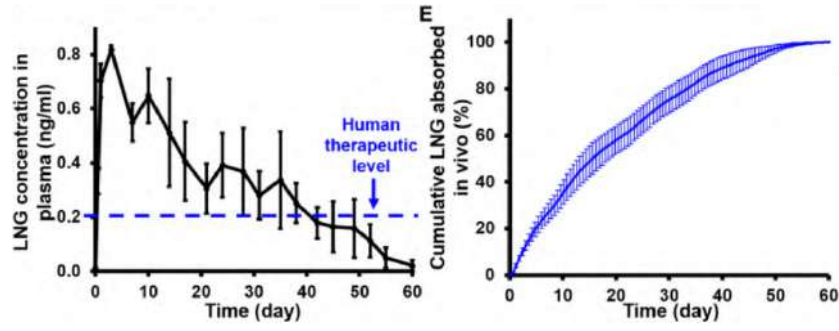


Figure 2.27: Rat plasma concentrations of LNG after applying LNG-loaded effervescent microneedle (MN) patches. The therapeutic level for LNG in humans is shown by the blue dashed line. Data points show the mean \pm SD ($n = 10$). (E) Cumulative LNG absorption *in vivo* over time from the LNG-loaded effervescent MN patches, based on pharmacokinetic modeling of the data presented in (D). Each point represents the mean \pm SD ($n = 10$). [54]

released into phosphate-buffered saline with minimal initial burst, at an average rate of about 1.5% per day over at least two months. In pharmacokinetic studies, rats were given LNG-loaded effervescent MN patches applied to the skin for less than a minute. Plasma LNG levels peaked at approximately 0.8 ng/ml, then gradually decreased. The concentration remained above the therapeutic threshold for over a month before falling to near zero after 60 days (Fig. 2.27).

Two years ago, a more intricate approach was employed to achieve zero-order release, wherein the authors devised a novel core-shell microneedle patch [131]. In this design, a shell controlled the release of the ENG hormone for up to 6 months. ENG was encapsulated in a core made from PLGA, PLLA and PDLA. These layers were created by casting into a microneedle mold. When applied to the skin, the microneedles separated from the patch in under a minute due to an effervescent layer. This design limited the initial release to about 6% in the first 24 hours and provided a steady release of ENG for around 6 months *in vitro* (see Fig. 2.28). In contrast, a single-material microneedle patch with the same ENG core but without the shell and cap released about 23% of the drug initially and lasted only about 2 months. Microneedle patches are frequently utilized in cosmetology, as demon-

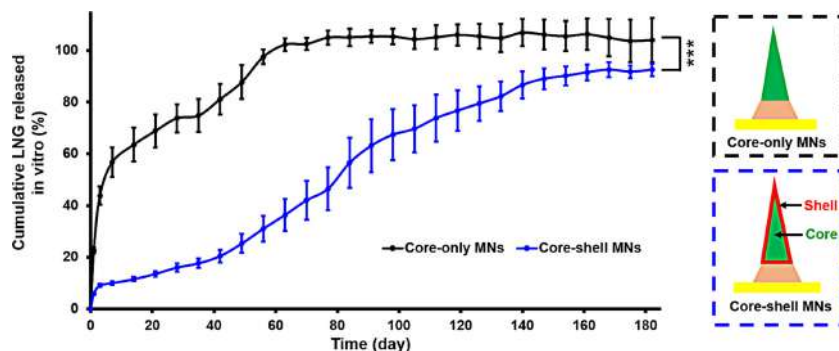


Figure 2.28: Profiles of release of LNG from core-only and core-shell MNs [131].

strated by the study conducted by Chamgordani's group, which aimed to develop a long-lasting MN patch loaded with triamcinolone acetonide (TrA) for prolonged dermal delivery [132]. The researchers investigated various parameters including drug content, uniformity, in-vitro release kinetics, ex-vivo skin permeation, and statistical significance of the MN patch compared to a conventional cream formulation containing TrA. The total TrA released from microneedles with 3% and 10% TrA formulations was measured. For the 10% formulation, the cumulative release was about 30 μg , or 9% of the initial amount. For the 3% formulation, it was about 20 μg , or 22%. Both formulations followed a zero-order release model (Fig. 2.29a). The MN patch with a 10% TrA formulation demonstrated superior skin delivery compared to a conventional cream with an equivalent drug concentration. This was evidenced by a significantly higher cumulative amount of TrA that permeated through rat skin with the MN patch, highlighting its enhanced permeation efficiency (Fig. 2.29b) .

Although microneedle (MN) patches are commonly employed for transdermal delivery, there has been limited interest in investigating them extensively, primarily because they are mainly utilized for transdermal applications. However, it's worth noting that our review is primarily focused on implantable devices.

3D printed DDS While microneedle patches are primarily utilized for transdermal delivery, our review focuses on implantable devices. One promising option for reservoir-like structures in our review is the utilization of 3D printed devices.

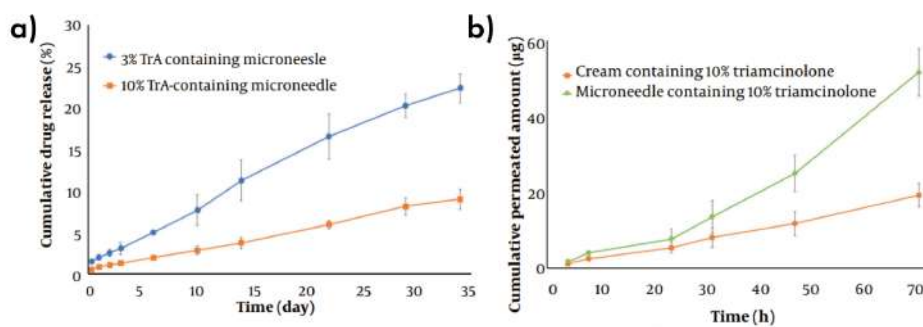


Figure 2.29: (a) Release profiles of TrA from microneedles with 3% and 10% TrA concentrations; (b) Total amount of TrA (μg) that permeated through rat skin from microneedles with 10% TrA and from a cream with 10% TrA over 72 hours [132].

The concept of manufacturing drug formulations using 3D printers is relatively new, but it offers significant potential. Currently, the most common 3D printing technology available is FDM printing, which, although accessible, suffers from limitations such as poor resolution and difficulty in producing dense models without imperfections like pores. Another option is SLA technology, which offers greater accuracy but is hindered by a lack of biocompatible materials [133]. Despite these challenges, additive manufacturing of reservoir-like tablets and implantable pumps holds promise due to its high flexibility. With this approach, there is no need to manufacture specific templates for each formulation; instead, all forms and dimensions are controlled by the operator in the 3D model and can be adjusted at any time. This flexibility enables the production of individualized drug formulations that adhere to the principles of personalized medicine.

As example Boyer et al. achieved a high complexity level by 3D printing vascular Y-stents with internal mesh structures. Using water-soluble PLA filaments, they post-processed the stents and meshes through optional cross-linking and iodization. The iodine served a dual purpose: antimicrobial action and enhanced visibility in CT imaging. The study demonstrated both effects and proposed iodization as a method for precisely locating 3D-printed implants [134]. The

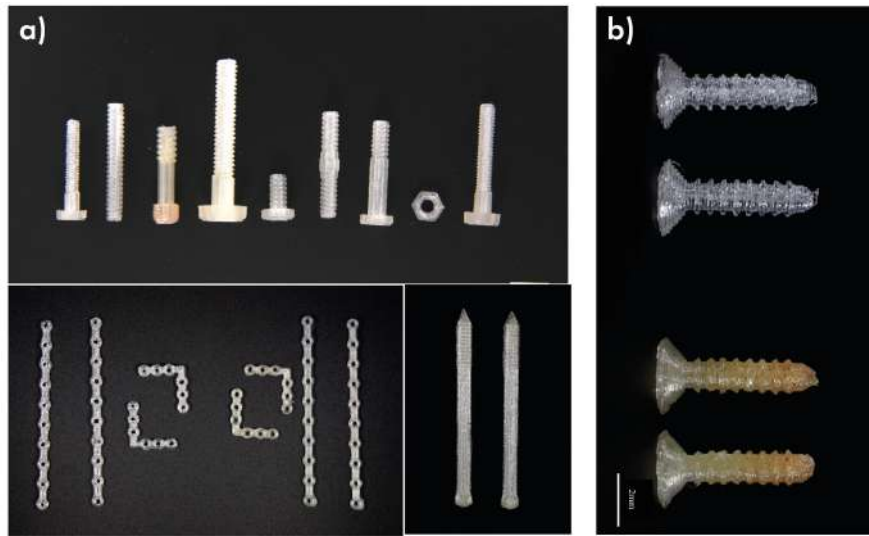


Figure 2.30: (a) 3D-printed orthopedic screws, pins, and plates made from PLA; (b) 3D-printed standard 4 mm screws using regular PLA and PLA-GS mix.

selection of an appropriate printing technique and material allows for the incorporation of various drugs, including those sensitive to high temperatures. This was exemplified by Lee et al., who 3D-printed PCL discs loaded with rifampicin using an extrusion technique at a low temperature of 60°C to preserve the antibacterial activity of the heat-sensitive drug [135]. Utilizing heat-resistant drugs expands the range of polymers that can be employed, including those that are highly processable, without compromising efficacy. Tappa et al. employed 3D printing to produce a diverse range of fixation implants, including screws, pins, and plates, as depicted in Figure 2.30a-b [136]. They utilized gentamicin (GS) and methotrexate-loaded PLA filaments for these constructs. The incorporation of these drugs led to a reduction in both flexural and compression strength of the printed implants. Specifically, the compression strength decreased by 48% for gentamicin-loaded samples and 42% for methotrexate-loaded samples compared to drug-free controls. The tunable mechanical properties of 3D-printed fixations offer the potential to tailor implants to the specific requirements of various bone types. Additionally, the use of degradable biomaterials could eliminate the need for implant removal during revision surgeries.

A lot of articles in the literature have focused on printlets, which are printable tablets designed for oral drug administration. Printlets represent a significant advancement in pharmaceutical manufacturing, as they offer several advantages over traditional tablet formulations. One key benefit is the ability to precisely control the composition, shape, and size of the tablets, allowing for tailored drug release profiles and improved patient adherence. Additionally, 3D printing technologies enable the incorporation of multiple drugs or therapeutic agents into a single printlet, facilitating combination therapy and personalized medicine approaches [137, 138]. Moreover, printlets can be customized to meet the specific needs of patients, such as pediatric or geriatric populations who may have difficulty swallowing conventional tablets. The versatility of 3D printing also extends to the production of printlets with complex geometries or surface textures, which can enhance drug dissolution rates or provide controlled release mechanisms. As example Fina et al. produced 3D printed oral paracetamol formulation using paracetamol-loaded filaments. The filament used for 3D printing contained hydroxypropyl cellulose (HPC) as the main thermoplastic polymer (Fig. 2.31a). To achieve prolonged drug release, Klucel EF polymer was added, while polyethylene oxide (PEO) with a high molecular weight of 7,000,000 Da helped extend the release time and form a swellable hydrogel for drug suspension. Hydroxy ethylcellulose, at 5% w/w, was used to keep the drug suspended. Mannitol, a water-soluble sugar, served as a pore former and plasticizer. Together with the ABS shell, this complex core enabled the drug to be released steadily and completely over 50 hours (Fig. 2.31b).

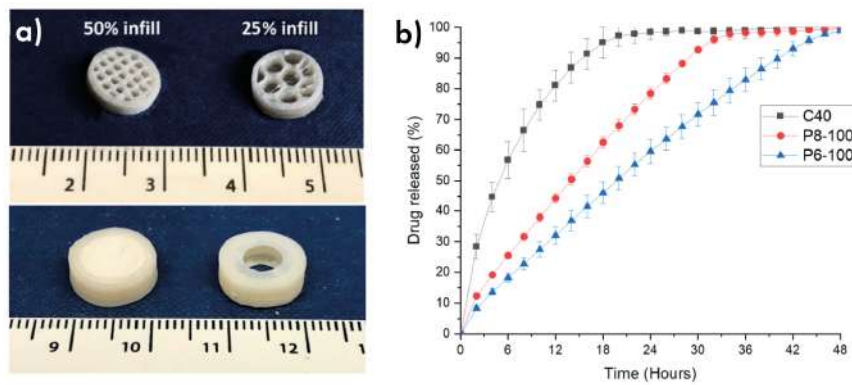


Figure 2.31: (a) Top: Horizontal cross-sections of C40 with infill percentages of 100%, 50%, and 25%. Bottom: P6-100 before (left) and after (right) the dissolution test. (b) Dissolution profiles of core-only tablets (C40) compared to core-shell formulations P6-100 and P8-100.

2.2.3 Conclusions and Findings

1. **Polymers in DEC Development:** Both biodegradable and non-biodegradable polymers play pivotal roles in shaping the future of medical devices. Biobased biodegradable polymers like PLA, PHAs, and starch, along with synthetic polymers such as PBAT, PVA, PLGA, and PCL, are extensively utilized for their biocompatibility and controlled degradation properties.
2. **Mathematical Models for Drug Release:** The chapter introduces mathematical models like the Ritger-Peppas and Korsmeyer-Peppas models, which describe drug release from DDS. These models classify release profiles as first-order or zero-order based on factors like diffusion and polymer swelling. Achieving zero-order release kinetics is emphasized for DDS as it maintains constant drug release over time, leading to stable plasma concentrations within the therapeutic window. This can enhance patient compliance and minimize adverse effects, ultimately reducing the risk of chronic toxicity.
3. **Influential Factors and Release Mechanisms:** Drug release kinetics in DDS are influenced by factors such as the composition of the DDS,

drug integration method, and properties of the drug and polymer. Release mechanisms are categorized as diffusion-controlled, swelling-controlled, and erosion-controlled release mechanisms, highlighting the use of biodegradable polymers like PLA, PLGA, and PCL in drug delivery systems.

- **Diffusion-Controlled Release:** Involves a simple matrix system where the drug is dispersed within a non-erodible polymer matrix. Release occurs through dissolution, diffusion, and elimination from the composite surface. Biodegradable polymers like PLA, PLGA, and PCL are commonly used, with drug release influenced by polymer-water interaction and hydrolysis.
- **Swelling-Controlled Release:** Utilizes swelling agents or layers, often hydrogels, to absorb moisture and facilitate drug diffusion. While hydrogels enable rapid drug release, they are typically incorporated into multilayered DDS to control burst release and enhance drug diffusion.
- **Erosion-Controlled Release:** Involves degradation of the polymer matrix through hydrolysis or enzymatic action, leading to the formation of pores and gradual drug release. This approach is suitable for drugs with low solubility and is commonly used in drug-eluting stents (DES) to achieve sustained release profiles over several months. Notable examples include stents incorporating biodegradable polymers like PLA and PLGA, ensuring controlled drug release and polymer degradation over time.

4. **Reservoir Systems as Advanced Diffusion-Controlled Systems:** Reservoir systems can be considered separately, as more advanced diffusion-controlled systems. They store the drug formulation in a compartment and control its release rate through a membrane, often achieving zero-order release kinetics. These systems offer versatility, accommodating various types of drugs, and hold promise for improving drug delivery efficacy.

5. **Fabrication Methods for Reservoir Systems:** The chapter elucidates various types of reservoir systems employed in controlled drug delivery and discusses several fabrication methods, such as electrodeposition, electro-spraying, and microfabrication. These techniques enable the creation of precise reservoir structures with controlled drug release kinetics.
6. **Exploration of Additive Manufacturing:** Another significant finding is the exploration of additive manufacturing, particularly 3D printing, for the production of reservoir-like structures in drug delivery systems. Despite challenges in resolution and material compatibility, 3D printing holds promise for personalized medicine by allowing the fabrication of customized drug formulations tailored to individual patient needs. This approach could revolutionize the field of controlled drug delivery by offering greater flexibility and precision in drug release kinetics.

In conclusion, the review of various DEC systems underscores the challenges in achieving optimal drug delivery efficacy. While several systems have been reviewed, many fall short of providing a universal solution. Reservoir systems emerge as the most advanced, offering precise control over drug release kinetics. However, challenges remain in manufacturing coatings using this system. To address these challenges and advance DEC technology, the development of an innovative approach coupling additive manufacturing technologies with reservoir-based systems can be proposed. This methodological foundation aims to offer universality, scalability, and precise control over drug release profiles, benefiting both surface modification of medical devices and the creation of free-standing films for drug elution. This approach has the potential to contribute to drug delivery systems and enhance therapeutic outcomes.

2.2.4 Sterilization methods for polymeric DDS

Sterilization is a critical step in the production and deployment of medical implantable devices, primarily aimed at ensuring patient safety. When these devices

are implanted into the body, they come into direct contact with bodily tissues and fluids. Any microbial contamination present on these devices can lead to infections, which can range from mild to severe and even life-threatening [139]. The primary objective of sterilization is to eliminate or significantly reduce the microbial load on the device's surface. This includes bacteria, viruses, fungi, and spores that could potentially cause infections. By removing these pathogens, the risk of post-surgical infections is minimized, maintaining devices effectiveness and extending its lifespan.

From a regulatory standpoint, sterilization is a mandatory requirement for medical devices. Regulatory bodies, such as the Food and Drug Administration (FDA), have stringent guidelines in place that mandate medical devices to be sterile before they can be used in clinical settings. Adhering to these regulations is essential not only for obtaining regulatory approval but also for ensuring that the devices meet the highest standards of safety and efficacy. Lastly, it's essential to consider the biocompatibility of the implant material during the sterilization process. The chosen sterilization method should effectively kill or remove microorganisms without compromising the physical and chemical properties of the implant [140, 141]. This ensures that the implant remains biocompatible, meaning it is safe for implantation and does not induce adverse reactions or complications within the body.

Dry heat sterilization and steam sterilization, or autoclaving, offers an environmentally friendly and cost-effective sterilization method. It effectively eliminates a broad spectrum of microorganisms without leaving any toxic residues, ensuring safety for most materials. However, its application is restricted to materials capable of withstanding high temperatures or moisture. There's also a potential risk of degradation or alteration, particularly for sensitive materials. Consequently, this method is not suitable for drug-containing biomaterials [142].

Biomedical devices made from biodegradable polyesters typically undergo sterilization using ethylene oxide (ETO). The literature indicates that approximately fifty percent of all sterile medical devices in the U.S. undergo sterilization using

ethylene oxide. These devices span a broad range, from general healthcare products like wound dressings to specialized equipment designed for specific medical applications, such as stents used for treating particular areas of the body. This method is preferred over other sterilization techniques, such as irradiation, heat, steam, or acid, as these alternative methods can lead to significant deformation of the devices and hasten the degradation of the polymer material. ETO sterilization does have its drawbacks. These include the accelerated degradation of the polymer, morphological disturbances, possible interactions with drug, and the presence of residual ethylene oxide gas within the sterilized device, that can be toxic when implanted [143, 144].

Gamma radiation sterilization is known for its effectiveness in microbial inactivation and its ability to penetrate dense materials thoroughly. However, it can induce cross-linking and degradation of biopolymers, affecting their mechanical properties. For biopolymers the effect can be significant, gamma-radiations induce chain scission and consequential decrease of 30-50% of molecular weight [145, 146].

Electron beam (E-beam) sterilization is a rapid and effective method that provides uniform dose distribution and moderate penetration. For electron beams of 10 MeV, the penetration depth in water is approximately 4 cm [147]. Although it induces fewer material degradations compared to gamma radiation, it can still cause chain scission and alter the molecular structure of biopolymers [148]. The use of specialized equipment and regulatory approval is necessary for its application. Therefore, when considering sterilization using accelerated electrons for Drug Eluting Coatings (DECs), understanding the radiation stability of biopolymers is crucial.

Biopolymers such as poly(lactic-co-glycolic acid) (PLGA) and other natural polymers are generally sensitive to radiation and may undergo various chemical and physical changes upon exposure to high-energy radiation [149, 150]. These changes can potentially affect the mechanical properties, stability, and functionality of the materials. Hence, it is essential to carefully evaluate the radiation

dose and its impact on the properties of the polymer when sterilizing DEC made from biopolymers using accelerated electrons. Optimizing the radiation dose is necessary to achieve microbial sterilization while minimizing adverse effects on the biopolymer's integrity and the drug release mechanism.

Furthermore, E-beam sterilization can also affect drug molecules and materials used for packaging in medical devices. For instance, studies have shown that high doses of irradiation can lead to the oxidation of sensitive proteins and even the syringe material, potentially inducing further protein oxidation through by-products [151]. However, other research indicates that selecting the optimal irradiation dosage can preserve the functionality of Drug Delivery Systems [152, 153, 154].

In conclusion, while accelerated electrons offer an efficient sterilization method for DEC, careful optimization of radiation parameters is necessary to preserve the stability and functionality of the biopolymer matrix. Sterilization of biopolymers is a critical step to ensure the safety and efficacy of medical devices, implants, and other biomedical applications.

2.3 Drug type, dosage and stability issue

Water-soluble drugs are preferred in pharmaceutical development due to their inherent advantages in absorption, bioavailability, and patient safety. A drug's ability to dissolve in water is crucial for effective absorption into the bloodstream, which directly impacts its therapeutic efficacy. Poorly soluble drugs, while common, present challenges that modern formulation technologies have sought to overcome [155, 156, 157].

One major advantage of water-soluble drugs is higher bioavailability. These drugs dissolve easily in gastrointestinal fluids after oral administration, leading to faster absorption, quicker onset of action, and more predictable therapeutic effects. In contrast, poorly soluble drugs often exhibit erratic absorption, complicating the prediction of their effects [158]. For intravenous administration, water solubility is even more critical, as it ensures the drug can directly enter the bloodstream with-

out causing precipitation or requiring complex solubilization strategies [159, 160]. Poorly soluble drugs administered intravenously risk precipitation, which can lead to complications such as tissue irritation or embolism [159, 161]. Water-soluble drugs also pose a lower risk of tissue accumulation, reducing long-term toxicity. Poorly soluble drugs may precipitate in tissues, forming aggregates that can cause irritation or damage. Studies have shown that poorly soluble drugs are more likely to form deposits in non-target tissues, which increases the risk of adverse effects. Another advantage of water-soluble drugs is their ease of formulation into various dosage forms, including syrups, injections, and suspensions, facilitating both oral and intravenous routes of administration. Poorly soluble drugs, however, require complex formulation strategies such as nanoparticles or lipid-based systems to enhance solubility, which increases production costs and regulatory hurdles [162]. Despite these issues, poorly soluble drugs remain prevalent, and their solubility challenges lead to variable bioavailability. Inconsistent absorption can result in subtherapeutic levels, requiring higher doses that increase toxicity risks. For example, poorly soluble drugs are often associated with a narrow therapeutic window, where the effective and toxic doses are close together. Modern approaches like nanoparticles and solid dispersions have been developed to enhance the solubility and bioavailability of these drugs. By reducing particle size or using solubilizing agents, these strategies increase dissolution rates, improving the therapeutic outcomes of poorly soluble drugs and reducing the risks of dose-dependent toxicity [163, 164]. In my dissertation, I will develop a system specifically designed for water-soluble drugs due to their inherent advantages in pharmaceutical applications. By focusing on soluble drugs, the system can ensure consistent absorption, avoid the complexities associated with poorly soluble drugs, and simplify formulation, making it more effective and reliable for practical use.

Dosage and stability issues are also paramount considerations in drug delivery, particularly when designing therapeutic regimens for specific drugs. Tailoring doses and administration schedules to individual drugs is crucial for minimizing side effects and optimizing therapeutic outcomes. This is especially crucial for

antibiotics. Choosing the best antibiotic approach for treating infections related to orthopedic implants is a complex task. The ideal antibiotic should have demonstrated success in treating these infections in real-world settings, showing effective bone penetration as well as robust antibacterial and antibiofilm properties [165, 166]. Additionally, since these infections often need extended treatment periods, the antibiotic should also be safe, well-tolerated, and suitable for outpatient use.

The first limitation arises from the fact that most of drugs are initially tested for intravenous or other systemic administration, with well-studied dosage regimens and pharmacokinetics for this administration type. However, there are no established dosage recommendations for drugs incorporated into MID. Furthermore, in the current state-of-the-art in the field of antibiotic-loaded implants, there exists a significant discrepancy among different studies employing the same antibiotic. This variation could stem from differences in study designs, experimental conditions, and variable sample sizes. Consequently, this observed inconsistency undermines the reliability of these studies, casting doubt on the efficacy of the described approach. Moreover, many studies on antibiotic-loaded coatings tend to focus solely on short-term antibacterial efficacy, neglecting systematic assessments of their biocompatibility, antibacterial effects, or long-term toxicity. According to a review by Souza et al. [167], no human data were available up to 2016 to substantiate the efficacy of antibiotic-loaded implants in limiting microbial adhesion. Another challenge lies in ensuring the long-term stability and effectiveness of antibiotics. As previously mentioned, most of drugs available are manufactured for short-term systemic administration, such as lyophilized powders that should be dissolved immediately prior the administration, tablets, and injection solutions. These forms are typically intended to be stored dry or undiluted under clearly defined conditions. However, it remains unstudied what happens when they are stored within drug delivery systems in the organism for extended periods, in contact with body fluids.

Considering these factors, it is essential to approach this issue with the utmost

technical precision. The dosage of an antibiotic should consistently fall within the therapeutic window to prevent bacteria from developing resistance and to avoid causing harm to the body due to toxicity. Additionally, maintaining the stability and effectiveness of the antibiotic throughout the entire duration of therapy is imperative. While much attention has been given to the activity of antibiotics and some mechanisms of bacterial resistance have been well studied, it is important to recognize the diverse effects antibiotics have on microorganisms depending on the administered dose.

Traditionally, antibiotics were viewed solely as molecular weapons with inhibitory properties exploited clinically. However, it is now understood that antibiotics exhibit diverse effects on microorganisms, particularly at doses lower than the minimal inhibitory concentration [168]. At these sub-inhibitory doses, antibiotics can modulate the expression of a significant portion of the bacterial genome, exerting stimulatory effects rather than inhibitory ones [169]. This phenomenon suggests that antibiotics function as signaling agents, with their production tightly regulated during specific growth stages and under certain physiological conditions [170, 171]. Accumulation of antibiotics triggers a coordinated response once a certain population threshold is reached, indicating a sophisticated regulatory mechanism. The precise regulation of antibiotic delivery ensures that they are administered at concentrations often much lower than therapeutically prescribed levels, yet still effective in influencing bacterial behavior. This phenomenon, termed 'sub-inhibitory,' plays a crucial role in regulating interspecies nutrient utilization strategies and reducing niche overlap in mixed microbial populations [172]. Understanding the multifaceted effects of antibiotics, particularly at sub-inhibitory doses, is essential for optimizing therapeutic strategies and combating antibiotic resistance effectively.

Recent studies investigating natural populations of *Streptomyces* spp. have shed light on the pivotal role played by sub-inhibitory antibiotics in regulating interspecies nutrient utilization strategies and reducing niche overlap within mixed microbial populations. These findings underscore the significance of antibiotics

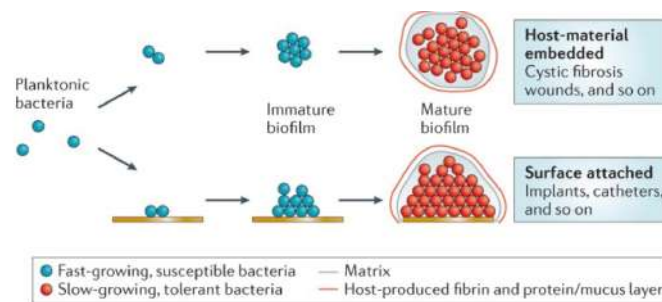


Figure 2.32: Biofilm formation process[177]

beyond their traditional role as antimicrobial agents. Moreover, other antimicrobial agents exhibit similar effects, albeit with variations. These agents not only influence microbial behavior but also upregulate the expression of secretion system genes. This heightened expression results in increased cytotoxicity when these agents are tested against macrophage cell lines and in competitive interactions with other organisms in the environment. Notable examples for tobramycin, tetracycline, and norfloxacin—widely used antibiotics—were demonstrated by Linares et al. At low concentrations, these antibiotics can even be beneficial for the behavior of susceptible bacteria in natural environments [173].

Additionally, various antibiotics, regardless of bacterial resistance, can prompt a hyper-adhesive state characterized by increased production of surface adhesins[174, 175, 165]. This heightened adherence to tissues and medical surfaces is particularly concerning as it can exacerbate the formation of biofilms that are tolerant to antibiotics. Biofilms represent a mode of bacterial growth where organisms live in communities, secreting a gel-like matrix composed of sugars (Fig. 2.32). This matrix acts as a barrier, reducing the effectiveness of antimicrobial agents by limiting their access to bacteria. Consequently, addressing biofilm-related infections may require significantly higher concentrations of antimicrobials compared to treating individual bacterial cells [176, 175].

Therefore, it becomes crucial to optimize the delivery of antimicrobial agents to target biofilm sites effectively. Following antibiotic exposure, Kaplan et al. observed that antibiotic-resistant strains displayed a greater increase in biofilm

formation compared to susceptible strains [178]. Furthermore, heightened adherence to surfaces can enhance the ability of certain organisms, including multidrug-resistant *Salmonella enterica* serovar Typhimurium, to invade host cells [179].

The impact of changes caused by antibiotics on patients is substantial. Recognizing how antibiotics behave in real-world conditions necessitates a reevaluation of their clinical use. This highlights the need for extensive, long-term research into each drug and its delivery method. Such studies should encompass the kinetics of substance release, its stability over time, and comprehensive *in vivo* investigations to grasp the true pharmacodynamics and effectiveness.

Furthermore, these experiments should be conducted in collaboration with attending physicians who can aid in selecting the most suitable antibiotic for the patient's condition. It's essential to note that this work doesn't assess the actual effectiveness of a particular antibiotic but rather delineates approaches for the controlled release of water-soluble low-molecular drugs from coatings.

Chapter 3. Materials and methods

3.1 Chemical Materials

Polyglycolic-*co*-lactic acid (PLGA) granules (PURASORB® PDLG 5010) were acquired from Corbion N.V. (Amsterdam, Netherlands). Acetone, ethyl acetate, and sodium chloride were procured from Sigma-Aldrich (Darmstadt, Germany). Polyvinyl alcohol (PVA) powder with a molecular weight (MW) of 72,000 g/mol and a degree of hydrolysis of 85–89% was supplied by AppliChem GmbH (Darmstadt, Germany). All reagents were utilized as received. For the preparation of solutions, deionized (DI) water (with an electrical conductivity of approximately $18.2 \text{ M}\Omega \cdot \text{m}^{-1}$ at 25 °C) generated by the Milli-Q Plus185 water purification system from Millipore (Darmstadt, Germany) was utilized. Vancomycin sodium salt (Vankorus) was sourced from the pharmaceutical company LEKKO (Volginsky, Russia). Novaprint PP-GF polypropylene filament (Moscow, Russia) was employed for printing upgrade parts. Methylene blue dye (Sigma-Aldrich), PP substrate (Komus, Russia), Cefazolin sodium salt (Pharmstandard, Russia), Eosin Y (Lenreactiv, Russia).

3.2 Methods

3.2.1 Three-Dimensional (3D) Printing Software and Hardware

All 3D models for the 3D printer upgrade and experiments were prepared in the Fusion360 CAD program (Autodesk, USA). They were printed using a VS3D mini 160 3D printer (VS3D, Russia) with ABS CF-15 filament (FDPlast, Russia).

The printer body was manufactured by VS3D company (Moscow, Russia), assembled by author and utilizes the Klipper open-source software without any modifications to the code (Fig. 3.1a, c). The machine features standard 3D printer Core-XY kinematics. Its distinctive elements include a vacuum printer heated

bed (Fig. 3.1c) and an extruder designed for dispensing liquids from disposable syringes (Fig. 3.1b). The printing head and vacuum table were designed by the author of this research and manufactured by VS3D.

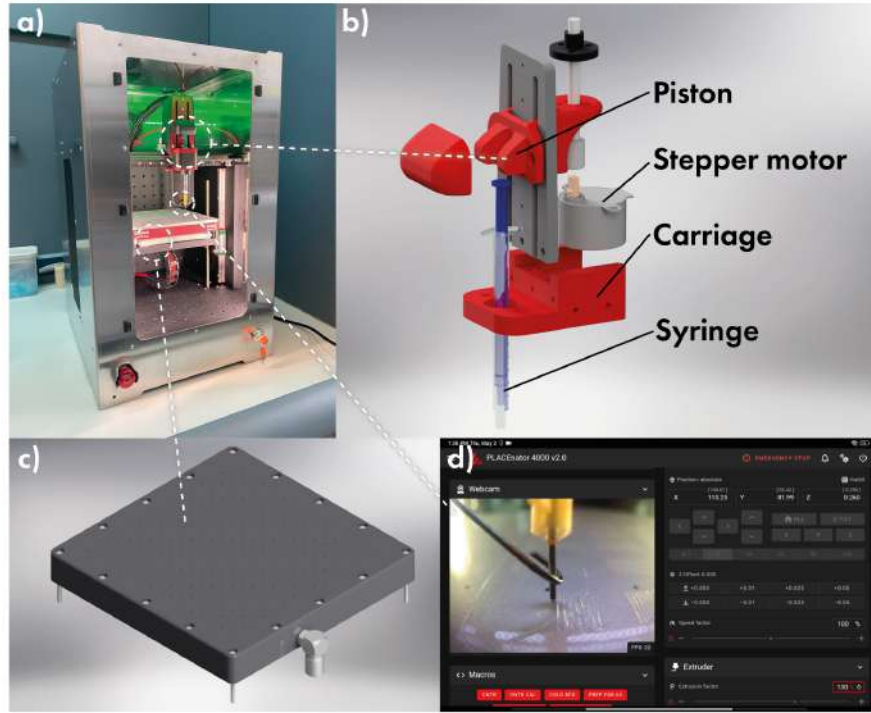


Figure 3.1: Custom 3D printer (a). Structure of a syringe extruder (b). Vacuum table for holding substrates (c). Web-based printer control interface with webcam window (e).

The sample models were designed in Fusion360 CAD software as solid blocks measuring $10 \times 5 \times 0.01$ mm and saved as *.stl* files. These models were then processed in PrusaSlicer (Prusa, Poland) with the following settings: extrusion width of 0.3 mm, no solid fill layers at the bottom and top, 50% infill density, printing speed ranging from 5 to 20 mm/s, travel speed of 100 mm/s, and a "Rectilinear" infill pattern. The resulting g-code was used without any modifications.

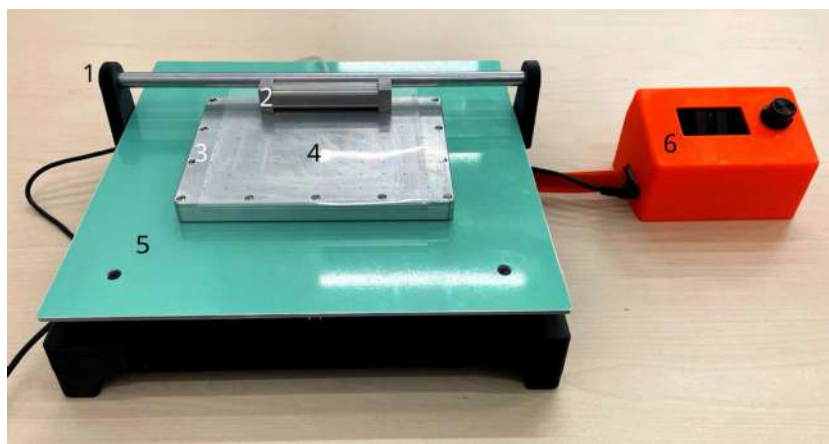


Figure 3.2: Laboratory-made Dr. Blade machine

3.2.2 *Film casting*

Polymer films were fabricated using the Dr. Blade coating technique. This method is known for its reliability and scalability in producing homogeneous polymer films with minimal solution wastage [180, 181]. Films were cast on a laboratory-made machine (Fig. 3.2) equipped with a heated table (5) and a digital speed controller (6) for the pusher (1), all based on an Arduino microcontroller. The process involves spreading the polymer solution onto a substrate (4) secured on a vacuum table (3) using a specialized applicator bar (2). The applicator bar moves across the surface at a consistent distance, referred to as the Applicator Gap (AG), to create a wet film.

3.2.3 *SEM*

Scanning electron microscopy (SEM) measurements were conducted using a VEGA III microscope (TESCAN, Czech Republic) and a Quattro ESEM (Thermo Fisher Scientific, USA).

The samples for SEM analysis were carefully selected and handled to prevent contamination. They were mounted to SEM sample stubs using conductive carbon adhesive tape, ensuring the samples lay flat and were securely positioned to prevent any movement during imaging. For larger samples, they were sectioned into

smaller pieces using a scalpel to fit onto the sample stubs. When required, samples were quickly frozen and sectioned using a cryostat to obtain clean cross-sections suitable for viewing (see Section 3.2.4).

To enhance conductivity and minimize charging effects during imaging, a thin layer of gold (5 nm) was deposited onto the samples using an Emitech K350 sputter-coater (Quorum Technologies Ltd., Ashford, UK). The sputter-coating procedure followed the manufacturer's guidelines, with parameters as specified.

Once coated, the sample stubs containing the mounted samples were carefully introduced into the SEM chamber. They were securely attached and correctly aligned for optimal imaging. SEM parameters were adjusted based on the sample's characteristics and the desired resolution. Given the poor conductivity of the polymer samples and their low melting point, accelerating voltages of approximately 3 - 7 kV were utilized for Secondary Electron detection mode.

Imaging commenced, with adjustments made to focus, magnification, and other settings as necessary to achieve clear and detailed images. Following imaging, the sample stubs were extracted from the SEM chamber, and the samples were stored appropriately for future reference or further analysis.

3.2.4 Cross-sections

Edge samples for microscopic examination were prepared using a Leica CM1950 cryostat (Leica Biosystems Nussloch GmbH, Germany). The cryostat was set to the desired temperature appropriate for the polymer material being analyzed, typically ranging from -20°C to -30°C to ensure optimal sectioning conditions.

The samples, which were previously fixed in an embedding medium (Tissue-Tek® O.C.T. Compound, Sakura Finetek, USA) such as optimal cutting temperature compound, were securely mounted onto the cryostat's sample holder. This ensured stability during the sectioning process and facilitated precise cutting of the samples.

A sharp microtome blade was carefully positioned in the cryostat's cutting

chamber. The blade's angle and orientation were adjusted to ensure optimal sectioning of the sample. The sample was then advanced using the cryostat's motorized feed mechanism, allowing for controlled and consistent slicing of the material.

Sections with a 200 μm thickness were obtained. Each section was carefully collected using a fine brush, cleaned from embedding medium and transferred onto a SEM sample stub coated with carbon adhesive tape (Fig. 3.3).

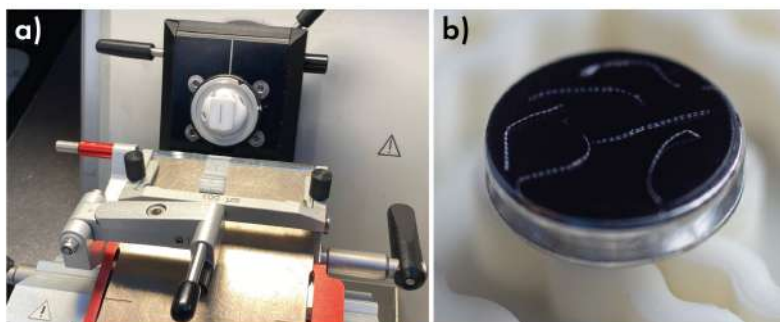


Figure 3.3: Sample in cryoslicing process (a) and sliced samples on SEM stub (b).

The thickness of the polymer films was determined using SEM images analyzed with ImageJ software. Measurements were taken from several points on cryosection images of the films. The method achieved an accuracy of 0.1 microns for images magnified at $2500\times$.

3.2.5 GPC measurements

Gel-permeation Chromatography (GPC) analysis was performed for irradiated and control film to qualitatively determine the loss of molecular weight of polymer after 25 kGy irradiation. For that 2 mg of film were dissolved in 1 ml of THF. 10 μl of solution is then injected into the WATERS GPCV 2000GPC system. The eluted polymer fractions are then detected and quantified using UV photometric detector. However, since there were no standard samples available to calibrate the chromatograph for this specific type of polymer, the data obtained does not provide absolute molecular masses of the polymer before and after irradiation.

3.2.6 Laser microperforation process

A Cobolt TorTM XS 532 nm pulsed laser (50 μ J; 1.9 ns) was employed to microperforate the biopolymer films. The laser light was directed onto the film surface using an 8×0.2 objective lens. Each microperforation was created with three sequential laser pulses, operating at a 1 kHz repetition rate. Film positioning under the laser beam was achieved with a high-precision motorized XY stage (STANDA LTD, Vilnius, Lithuania), offering ± 1 μ m accuracy.

3.2.7 Viscosity measurements

Viscosity measurements were performed with Anton Paar MCR302 rheometer (Anton Paar GmbH, Austria) equipped with a plate geometry setup. Prior to each measurement, the rheometer was calibrated according to the manufacturer's specifications to ensure accurate and reproducible results.

Sample preparation involved carefully transferring the polymer solutions or dispersions onto the rheometer's sample stage, ensuring a uniform and bubble-free layer. The temperature of the sample was controlled and maintained using a Peltier temperature control system integrated within the rheometer, allowing precise temperature regulation from ambient to elevated temperatures.

Once the sample was loaded and equilibrated to the desired test temperature, a cone was lowered to initiate shear flow. The shear rate ($\dot{\gamma}$) was systematically varied across a range of values, typically from low to high shear rates, to obtain a comprehensive viscosity profile of the sample. Each shear rate was maintained until a steady-state viscosity reading was achieved, indicating that the sample had reached equilibrium under the applied shear conditions.

The rheometer's software recorded the torque (τ) and angular velocity data during the measurement, which were then used to calculate the viscosity (η) of the sample using the equation 10:

$$\eta = \frac{\tau}{\dot{\gamma}}; \quad (10)$$

3.2.8 Prolonged drug release investigation

Release measurements

For the prolonged release of drugs from the films, the prepared films were immersed in a 0.1 M PBS buffer (Minimed, Russia) and incubated in a thermoshaker (Biosan TS-100, Biosan, Latvia) at 37°C with constant stirring at 300 rpm for the specified time. Samples were transferred to fresh buffer solution every 1 or 2 days, depending on the experiment's duration.

After the release, the obtained samples were placed in a 96-well plate (Corning 96-well Clear Flat Bottom UV-transparent Microplate), and absorption spectra were recorded using a Tecan Infinite 200Pro Microplate reader (Tecan Trading AG, Switzerland). The absorption spectra of the samples were collected at intervals specified in Table 3.1 with a scan step of 1 nm and a flash count of 12. To determine the concentration, calibration curves were constructed for each investigated substance (Fig. 3.4).

Name	Range, nm	Peak wavelenth, nm
Cefazolin	230-320	271
Methylene Blue dye	450-70	664
Vancomycin	230-320	282
Eosin Y	450-600	515

Table 3.1: Absorption spectra range and characteristic wavelength of used cargo.

Release kinetics evaluation

The drug release kinetics from the polymeric films were evaluated using the DDSolver software. This specialized computational tool is designed for analyzing drug release data and determining the most suitable kinetic models. Initially,

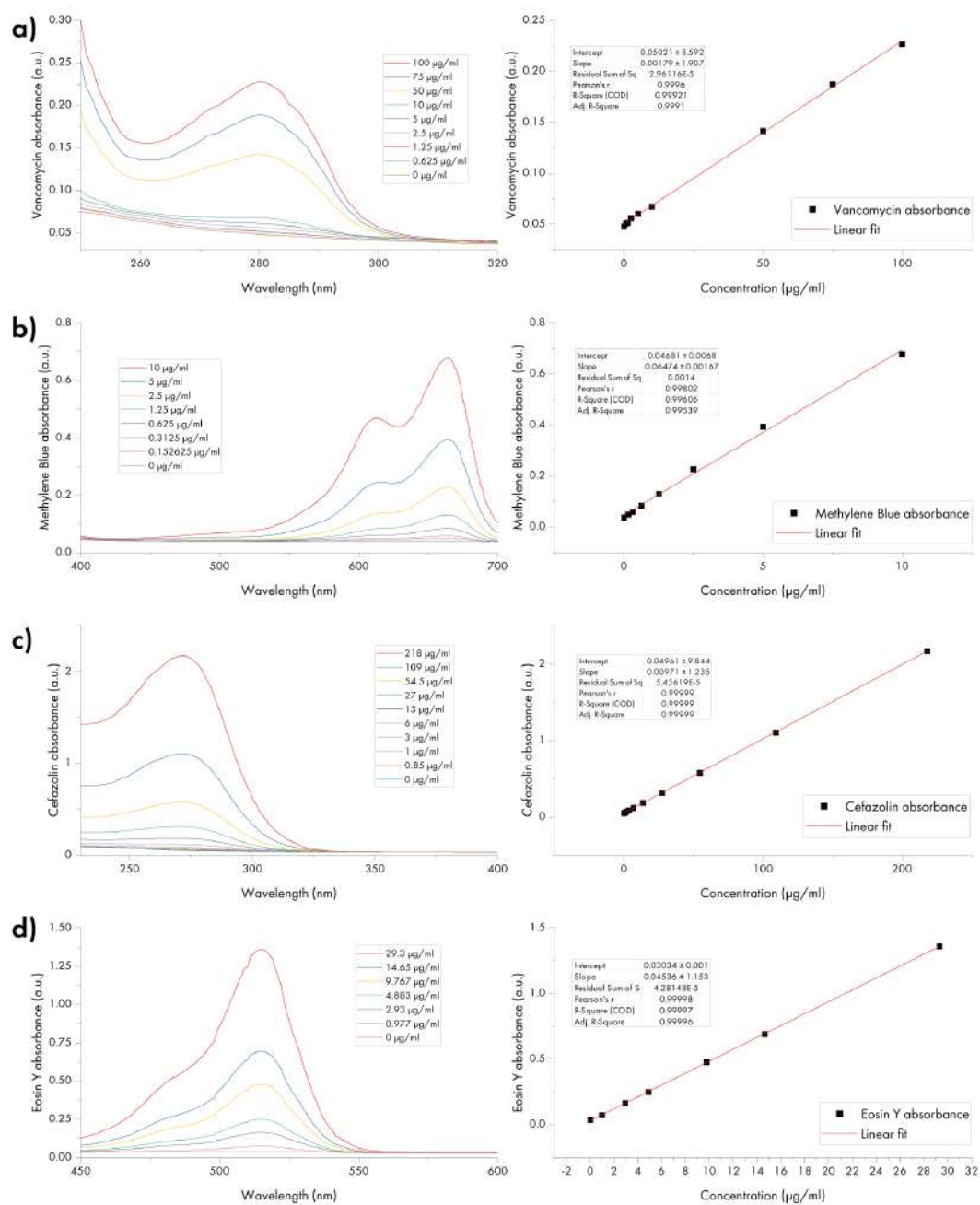


Figure 3.4: Absorption spectra and calibration curves for a) Vancomycin, b) Methylene Blue dye, c) Cefazolin, d) Eosin Y.

films loaded with the drug were prepared as described earlier. At specified intervals, samples of the release medium were collected, and fresh buffer was added to maintain sink conditions.

The acquired release data, which plotted drug concentration against time, were then analyzed using the DDSolver software (Open source). This software provides a range of kinetic models, including zero-order, first-order, Higuchi, and Korsmeyer-Peppas, allowing for a comprehensive examination of the release mechanisms [182].

Each kinetic model was systematically fitted to the release data within the software to find the best fit. The selection was based on parameters like the correlation coefficient (R^2) and other goodness-of-fit metrics. The model with the highest R^2 value and the most physiologically relevant fit was selected to determine the primary release mechanism.

Choosing an appropriate model is vital for accurately assessing drug release properties and comparing dissolution profiles using model-dependent methods. DDSolver offers several statistical criteria to evaluate the goodness of fit of the model, such as the correlation coefficient ($R_{obs-pre}$), coefficient of determination (R^2 or R_{sq}), mean square error (MSE), standard deviation of the residuals (MSE_{root}), Akaike Information Criterion (AIC), and Model Selection Criterion (MSC). Among these, AIC and MSC are commonly used for model identification.

The Akaike Information Criterion (AIC) is a statistical tool used to compare the goodness of fit of different models. Lower AIC values indicate a better fit, and the differences between AIC values across models are crucial for comparison. While AIC values can be positive or negative, interpreting the significance of these differences can be complex due to the unclear distribution of AIC values.

MSC , offered by MicroMath Corporation, is another emerging metric for dissolution data modeling. It represents a normalized version of AIC , independent of data scaling. Typically, the most suitable model exhibits the highest MSC , with values above two to three suggesting a good fit. When assessing mecha-

nistic models, it's essential to consider both the goodness of fit and the model's mechanistic plausibility. While DDSolver calculates these criteria to evaluate the model's goodness of fit, the selection of mechanistic models should also account for their plausibility.

Once the kinetic model was chosen, the DDSolver software determined crucial release parameters, including release rate constants and other relevant variables. These parameters played a pivotal role in understanding the primary mechanisms influencing the release process, whether it was diffusion, erosion, or a combination of both.

Chapter 4. Results

4.1 Introduction to PLACE Technology

High molecular weight biopolymers used in industry usually act as dense membranes, permeable only to low molecular weight gases and water vapors due to sorption-desorption processes. Additionally, these polymers can swell when immersed in water, depending on their chemical composition. Despite their theoretical capacity to retain the entire volume of loaded drugs before degradation, DEC based on such polymer films often initiate substance release earlier due to fabrication defects like micropores and cracks. The release kinetics, primarily governed by diffusion processes, vary based on the magnitude and number of these defects. To achieve ideal zero-order release, it is crucial to minimize film defects and ensure the necessary film "permeability."

A promising approach to address this challenge involves simplifying the drug-eluting film fabrication process and applying the drug layer onto a flat base film using printing methods, eliminating film damage from template interactions. Various manual and automated methods for transferring drugs can be employed, but 3D printing with a CNC-controlled 3D printer emerges as the simplest and most promising option. Proposed technology was named PLACE - Printed Layered Adjustable Cargo Encapsulation. This method offers flexibility, enabling the rapid formation of coatings over large areas and predetermined shapes without physically impacting the film. It surpasses the requirements of stencils for screen printing and stamps for transfer flexographic or gravure printing, as the equipment demands are lower than those for inkjet printing, and the accuracy is significantly higher than simple substrate spraying. On a laboratory scale, a regular 3D printer with minimal upgrades can suffice for implementation.

The next step is to improve the application method and mechanical strength of the coating film. Ensuring both uniform drug coating and adhesion to the base

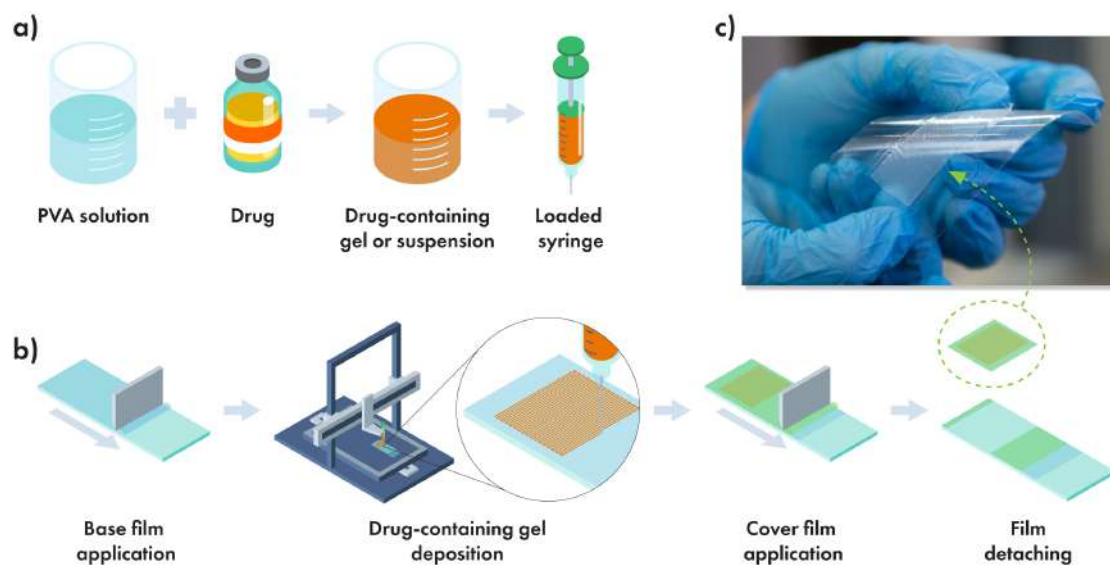


Figure 4.1: The design of the PLACE approach. (a) Mixing of the drug-containing matrix, (b) film fabrication pathway, and freestanding ready-to-use film (c).

film requires considering coating from polymer solutions. Although hot lamination with pre-casted polymer film is possible, it adds an extra step, necessitates precise roll-to-roll lamination equipment, and involves undesired drug heating.

Therefore, the final concept of the new production approach involves three sequential steps: first, forming the base film using the Dr. Blade technique, a robust method for obtaining thick and uniform polymer films; second, printing the required pattern using a 3D printer; and finally, sealing with a cover polymer layer using the Dr. Blade technique again (see Fig. 4.1b). Additionally, the second and third steps can alternate several times to obtain multilayered coatings.

The suggested Dr. Blade technique, also known as doctor blade coating, is utilized in the manufacturing industry to apply a uniform layer of material onto a substrate. It involves using a blade, typically made of metal or plastic, to spread a liquid or viscous material across the substrate's surface. By setting the blade at a precise distance from the substrate, the thickness of the applied layer is controlled. This technique finds widespread use across various industries, including printing, electronics, and coating applications, owing to its simplicity, low solution losses level and ability to yield consistent results [180]. While the Dr. Blade

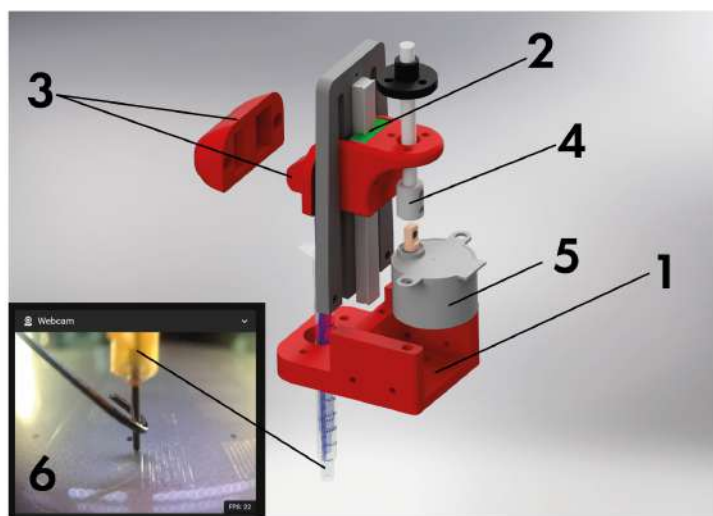


Figure 4.2: Structure of a syringe extruder.

technique can be affected by external conditions, its sensitivity is relatively low, allowing for easy implementation in laboratory settings. Moreover, with appropriate adjustments, this method can be scaled up for industrial-scale production [183].

The core component of the proposed technology is a Computer Numerical Controlled (CNC) machine that dispenses drug-contained solution over the base biopolymer film in a programmable pattern. It can be assembled using a commercial 3D printer with minimal additional parts. In this study, we utilized a 3D printer kit provided by the local manufacturer "VS3D Printers" (Figure 3.1a). It was opted for a direct mechanical syringe pump configuration, where a syringe is attached directly to the printhead, and the pressure on the piston is controlled by a stepper motor. This type of pump is easy to assemble and has a low inertia level. The pumping motor is controlled by a printer host board and operates like a common 3D printer extruder, eliminating the need for extensive firmware modifications.

Since the printing quality and potential print area depend on the weight and dimensions of the printhead, it is necessary to make it as small and lightweight as possible. The final version of the printhead is depicted in Figure 4.2. The printhead

comprises three main parts: a carriage designed for mounting on a linear MGN9 rail (1), a perpendicular railplate with a miniature 7 mm linear guide MGN7 (2), and a detachable piston mounted on it (3). The piston is driven by a screw gear (4) with a screw pitch of 1 mm and a stepper motor (5, mark 28BYJ-48, China). The 28BYJ-48 is a small stepper motor commonly used in various hobbyist projects, robotics, and automation applications. It features a reduction gear mechanism with a gear ratio of about 1:64 to increase torque output up to 450 g*cm and operates on a 12 Volt DC power supply. In full-step mode, the motor has a final resolution of 2056 steps per rotation, which is sufficient for precise dosing of small amounts of liquids. When using a standard 1 ml tuberculin syringe, the theoretical minimum and maximum achievable flow rates are approximately 0.018 and 0.425 ml/min, at rotation speeds of 1 and 24 rotations per minute respectively. Monitoring the printing process is also important. Using a camera next to the needle allows you to monitor the process live (6).

The maximum flow test for the pump was conducted following the methods described in Chapter 3. Given that our coatings were intended to modify the surface of bone implants and dressing material over relatively large areas (several dm²) while ensuring a high drug load up to milligrams per square centimeter, we selected a 23G needle (330 µm ID). This gauge provides a sufficiently narrow extrusion width while allowing for an effective flow. According to the obtained calibration curve, the maximum flow rate of 7 mm³/s for solutions with viscosity similar to water was achieved, which should enable printing speeds of up to 84 mm/s (red graph on Fig. 4.3).

In summary, the proposed approach of combining additive manufacturing methods, specifically 3D printing, with the Dr. Blade technique, offers a scalable and robust manufacturing process for reservoir-based drug-eluting coatings. This method not only simplifies the fabrication process but also ensures uniform drug coating and good adhesion to the base film. With further optimization and validation, this approach holds promise for the development of effective and controllable drug delivery systems.

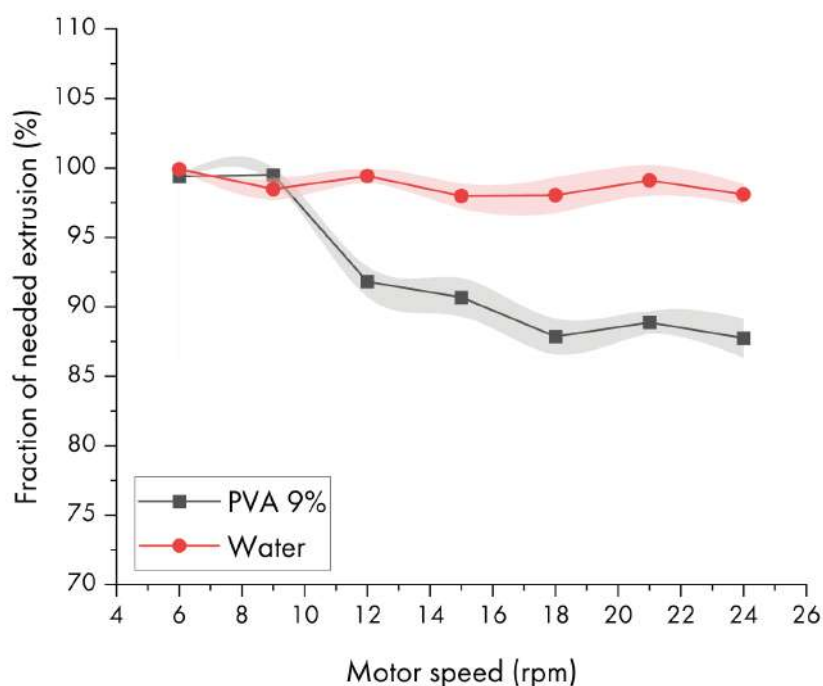


Figure 4.3: Maximum flow test results for water and 9% PVA solution

4.2 Film fabrication and parameter optimization

4.2.1 PVA matrix optimization

The drug loading stage is a critical aspect of the manufacturing process. Printing with aqueous solutions of drugs presents challenges because most biopolymers are hydrophobic and do not wet the substrate well, leading to gaps during printing. Additionally, aqueous solutions are fluid, causing the printed lines to spread out and form spills. Therefore, it is essential to add additives that enhance substrate wetting and provide the necessary viscosity for printing.

Several strict requirements were established as the base: the binding medium for drug particles must be water-based, devoid of harmful and non-biocompatible components, exhibit low reactivity, should not be soluble in organic solvents and possess sufficient viscosity for extrusion through a thin needle while retaining its extruded form. These stringent criteria narrowed down the list of candidates to a single option: polyvinyl alcohol. PVA is FDA-approved for human use, available

in medical-grade formulations, readily dissolves in water to form fluid gels even at low concentrations, and demonstrates inertness when mixed with most of drugs [184, 185, 186, 187]. In this chapter, we explore several critical parameters that influence the fidelity and quality of printed PVA water-based solutions. These parameters include printing speed, molecular weight of PVA, degree of hydrolysis, and solution concentration, all of which play key roles in determining the wetting, spreading, and overall behavior of the solution on the substrate.

The molecular weight (MW) of PVA directly influences the viscosity of the solution, which in turn affects its spreading and printability. Higher (>200 kDa) MW PVA increases solution viscosity, allowing for better control of material spread during printing and enabling the formation of structures with minimal PVA content. However, higher molecular weight also means that the PVA will take longer to degrade and be eliminated from the body, which may be undesirable in biomedical applications [188]. Conversely, lower MW PVA requires higher concentrations to achieve the necessary viscosity for printing, which can complicate the formulation and affect the properties of the final product.

In this study, a moderate MW PVA in the 50-100 kDa range was selected. This choice strikes a balance between achieving the appropriate viscosity for stable deposition and ensuring that the PVA does not persist in the body for extended periods, making it suitable for biomedical applications such as drug-eluting films.

The degree of hydrolysis of polyvinyl alcohol refers to the extent to which acetate groups in the original polyvinyl acetate (PVAc) have been converted to hydroxyl groups. Fully hydrolyzed PVA typically shows enhanced adhesion to hydrophilic substrates and forms stable films, making it suitable for applications requiring strong bonding to polar materials. However, its high hydrophilicity may lead to excessive swelling, particularly in aqueous environments, which can deform the printed structures and affect release kinetics. Conversely, partially hydrolyzed PVA (such as 85% hydrolyzed) offers a more balanced solution. It maintains good solubility while preventing excessive swelling, thereby promoting stability and precision in drug-loaded films.

The concentration of the PVA solution plays a pivotal role in determining the viscosity, which is closely tied to the molecular weight of the polymer. Higher concentrations of PVA in solution result in increased viscosity, improving the control over the printed shape and reducing excessive spreading. However, high concentrations may also cause difficulties in achieving uniform coverage of the substrate and increase the likelihood of clogging during the printing process. In this work, a range of PVA concentrations was tested to find the optimal balance between solution viscosity and printability.

The speed of the printing head directly impacts the wetting and spreading behavior of the PVA solution on the substrate. A slower printing speed allows the solution more time to wet and spread across the surface, leading to uniform coverage and better adhesion. However, excessively slow speeds may cause over-saturation and lead to deformation of the printed structure. On the other hand, faster speeds may reduce the wetting time, causing incomplete spreading and the formation of discontinuities. Optimizing the speed is critical for ensuring a balance between spreading and adhesion, which is essential for achieving consistent and accurate deposition.

In this study, two types of polyvinyl alcohol (PVA) were tested: partially hydrolyzed (PG) with 85% hydrolysis and fully hydrolyzed (FG) variants. A moderate molecular weight range of 70-100 kDa was selected to balance viscosity and spreading behavior. The PG variant had a lower molecular weight of approximately 70 kDa, while the FG variant had a higher molecular weight of about 90-100 kDa. These selections were made to optimize the printing process for stable, high-fidelity drug-eluting films, which were applied to a pre-coated substrate. By adjusting the solution concentration, molecular weight, and degree of hydrolysis, the process was fine-tuned to achieve the desired performance characteristics.

During experiments, it was observed that there was no notable difference in wettability between 85% hydrolyzed and FG PVA on the substrates used. Based on this finding, 85% hydrolyzed PVA was selected to reduce potential swelling within the films. Additionally, solutions of PG PVA exhibited slightly higher

viscosity bearing lower molecular weight, allowing the use of smaller amounts of PVA additive to achieve the desired consistency and viscosity (Figure 4.4d). This approach minimized the polymer content while maintaining control over the printing fidelity and structural stability in the release profiles.

A series of polyvinyl alcohol solutions with concentrations ranging from 3 to 12 wt.% was tested to determine the minimal concentration that allows for uninterrupted extrusion during printing without unnecessary spillage of the PVA solution onto the substrate surface (Figure 4.4a). To obtain a PVA solutions, the required portions of the PVA powder were dissolved in water with stirring and heating in a water bath at 90 C °for 3 hours.

A PVA matrix was applied to a PP substrate, which had been pre-coated with PLGA films, using a modified 3D printer. The sample models for printing were created as solid blocks ($10 \times 10 \times 0.01$ mm) using Fusion360 CAD software and saved as *.stl* files. These models were sliced using PrusaSlicer software with the following settings: a 0.3 mm extrusion width, no solid fill layers at the top or bottom, 50% infill density, a printing speed of 5-20 mm/s, and a travel speed of 100 mm/s. A 50% infill snake-like pattern was chosen for the drug-eluting films (DEFs), as it provided a simple and efficient continuous fill without overlapping lines. The resulting g-code was used directly for the printing process without any further modifications.

This process was conducted under standard conditions using a 23G needle (300 μ m inner diameter) with a Z-offset of 150 μ m (equal to the needle's radius to avoid material buildup). The coated substrates were then dried at 40°C for 10 minutes in a vacuum oven.

The best results were obtained with the 9 wt. % PVA sample, which exhibited a dynamic viscosity of approximately 400 mPa*s (Figure 4.4d). Subsequently, speed and flow calibration were performed to achieve uniform extrusion width with minimal line broadening at the corners (Figure 4.4b and c), resulting in a maximum printing speed of 20 mm/s, solution flow of 1.4 mm³/s, and a line width of about 295 μ m. It should be noted that the use of a viscous gel decreases

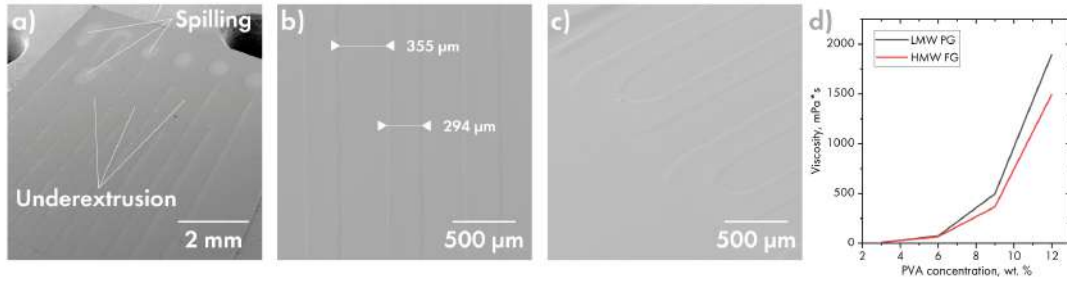


Figure 4.4: Selection of parameters for PVA solution preparation. (a) Print defects when using 6 wt.% PVA solution; line width on a straight section (b) and on turns (c) using 9 wt.% PVA solution; the dependence of the dynamic viscosity of PVA on the concentration (d).

the maximum possible flow rate for the chosen setup to approximately 3 mm³/s (black graph on Fig. 4.3). While this rate is much smaller than that achievable with water, it is still twice the required flow rate.

4.2.2 Drug loading studies

The drug-containing mixtures must meet several requirements. Firstly, the maximum drug loading should not significantly increase the viscosity of the matrix, which could lead to gaps in the print. Secondly, the final printed track should be smooth without any microns-sized roughness that could cause wetting defects.

Cefazolin sodium salt was selected as a model drug due to its high solubility in water (around 250 mg/mL) and widespread use in treating bacterial infections. Three PLGA film samples were prepared, labeled Cef100, Cef200, and Cef400, reflecting Cefazolin concentrations of 100, 200, and 400 mg/mL in a PVA solution matrix. To create these, 100, 200, and 400 mg of Cefazolin sodium salt were dissolved in 1000 μL of 9% PVA solution at room temperature. The mixtures were then centrifuged at 10,000 rpm for 1 minute to remove air bubbles.

Each sample included six PVA solution-printed squares, each measuring 1 cm². For the Cef400 sample, the total drug load per unit area was approximately 843.05 \pm 34.40 $\mu\text{g}/\text{cm}^2$. As the concentration of Cefazolin in the PVA matrix decreased,

the overall drug loading decreased proportionately.

Comparison of samples Cef100 and Cef400 without a cover film revealed increased surface microns-sized roughness due to Cefazolin crystallization (Fig. 4.5). In the Cef100 series, samples were formulated with an approximate 1:1 PVA-to-drug ratio, which effectively minimized Cefazolin crystallization due to the high content of amorphous PVA. As the PVA content decreased, however, crystallized regions became prominent, fully covering the Cef400 sample where the PVA concentration was approximately 20%. Such rough surfaces with microns-sized roughness comparable with film thickness can introduce wetting defects, resulting in numerous micron- and submicron pores and increased susceptibility to mechanical stress, such as bending or pressure, which may damage the film and accelerate drug release.

The crystallization of drugs within delivery systems remains a significant challenge in pharmacology, as it can affect the stability and release profiles of the active ingredient. Incorporating PVA or other water-soluble polymers has become a common approach to counteract this issue, as these polymers can reduce crystallization through steric hindrance and specific intermolecular interactions with the drug molecules [189, 190, 191]. By enhancing the amorphous phase, polymers like PVA provide structural support and help maintain a more uniform, stable film.

In addition to incorporating crystallization inhibitors like surfactants, oligomers, or additional polymers, modifications to the drying process can also be beneficial. For instance, printing on a heated bed or applying warm air can accelerate solvent evaporation, thereby reducing the time available for crystallization to occur.

To investigate this, the same experiment was conducted using a matrix containing 400 mg/ml of Cefazolin, but with printing on a heated bed at 50°C. Accelerating the drying kinetics significantly decreased the crystallization of the drug, as illustrated in Figure 4.6. In summary, the drug-loading stage of the manufacturing process must meet specific criteria to ensure optimal performance. Cefazolin sodium salt, chosen as a model drug, exhibited increased surface roughness due to crystallization in samples with high load. This issue can be addressed by control-

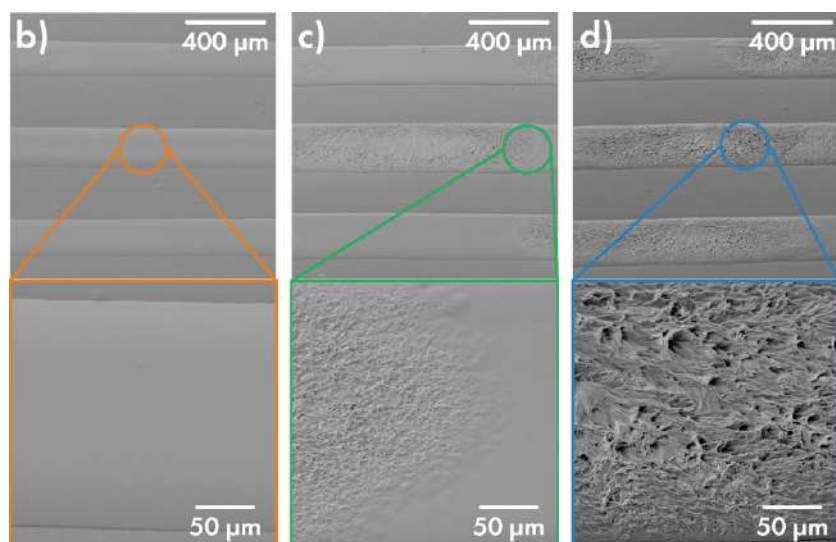


Figure 4.5: SEM image for the surface of uncoated drug tracks for Cef100, Cef200 and Cef400 samples, (a), (b) and (c) respectively.

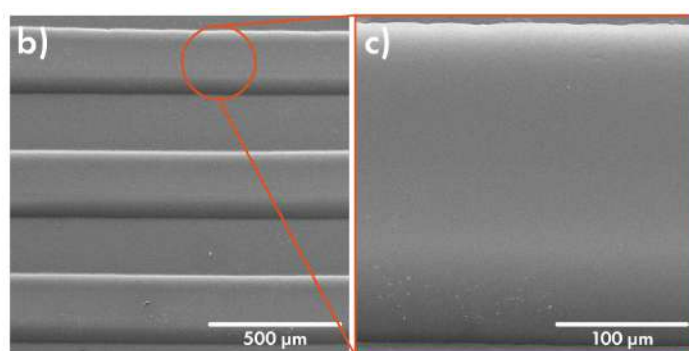


Figure 4.6: SEM image for the surface of uncoated drug tracks for Cef400 sample printed on heated bed.

ling the degree of crystallinity through additives or accelerated drying methods. On the other hand, the required dosage varies greatly for each drug and treatment plan, making it unpredictable. In the experiments described below, a maximum dosage level of 400 $\mu\text{g}/\text{cm}^2$ of DEF was chosen. This dosage should yield approximately 20 $\mu\text{g}/\text{ml}$ per day, ensuring uniform release over the critical first three weeks of patient rehabilitation. This dosage should achieve at least the Minimum Inhibitory Concentration (MIC) for most antibiotics.

4.2.3 Base and cover films forming

The covering film plays a key role in the drug delivery system, particularly in reservoir-based systems where release kinetics are primarily controlled by shell properties. In a basic system, the covering film must be applied without significant wetting defects, be sufficiently thick and durable to withstand the hydrostatic pressure exerted by swelling drugs and PVA, and remain stable throughout the release period. For present work, the polylactic-co-glycolic acid co-polymer was chosen. Its robust characteristics, such as solubility in various solvents, high glass transition point, low hydrophobicity, and moderate hydrolysis resistance, make it a promising material for manufacturing drug-eluting films.

First, a wettability study was carried out to assess the compatibility between polyvinyl alcohol and poly(lactic-co-glycolic acid). Small PLGA film pieces, approximately 200x200x1 μm in size, were fabricated using polydimethylsiloxane contact printing on the PVA film surface and exposed to chloroform vapor. A PDMS stamp with 200x200x200 μm pillars was dip-coated in a 2% PLGA solution in TCM to deposit a thin polymer film on the pillar surfaces. The PDMS stamp with the film was then placed on a slide pre-coated with PVA film and heated to 75°C to imprint the PLGA film squares onto the PVA surface. The slide with the attached films was subsequently placed in a Petri dish containing 300 μl of TCM, sealed, and heated to 50°C for 5 minutes.

This experiment allowed the PLGA to transition to a rubbery flow state with-

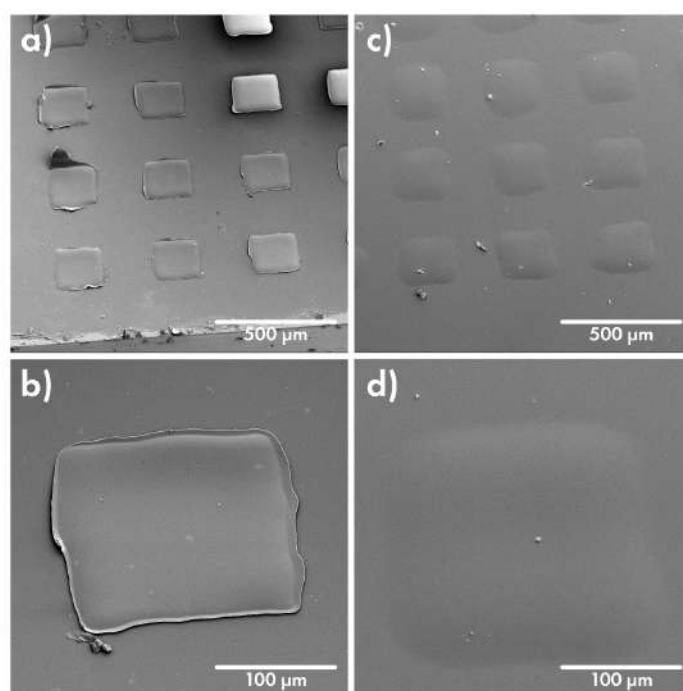


Figure 4.7: (a-b) imprinted PLGA film squares onto the PVA surface before (a-b) and after (b-c) exposure to chloroform vapor.

out heating, thereby simulating conditions similar to the blade coating procedure. Figure 4.7 depicts SEM images of the applied PLGA pieces before (a-b) and after (b-c) exposure to chloroform vapor. It can be observed that after the treatment procedure, the polymer did not form a droplet, but spread, wetting the PVA substrate (c). Nevertheless, wettability defects can occur on curved surfaces of the applied drug. Therefore, an empirical test was conducted on the current system. Five sets of drug-eluting films (DEFs) containing Methylene Blue dye as a model drug were prepared. For this 20 mg of MB were dissolved at ambient temperature in 1000 μL of 9% PVA solution, respectively. The obtained solutions were centrifuged at 10,000 rpm for 1 min to remove the air bubbles. Obtained solution was applied onto PLGA substrates using parameters described in Section 4.2.1. The area of the drug-coated regions was 10 cm^2 . Covering films were applied from PLGA solutions of 1.5, 2.5, 5, 7.5, and 10 wt.% in chloroform to assess coating quality and final covering film thickness. The following parameters were used for both, base and top films - rolling speed 20 mm/s, AG – 50 μm and solution aliquot

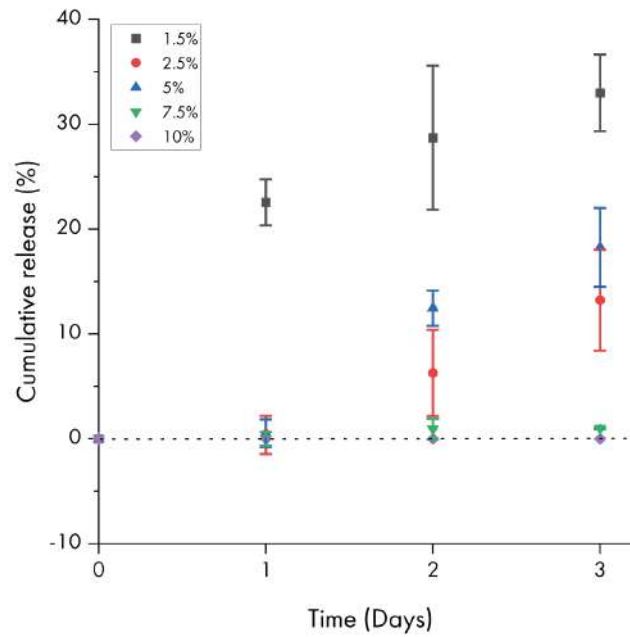


Figure 4.8: Empirical testing of the concentration of the covering solution graph of 500 μl . To assess the leakage of the resulting DEFs, a brief 3-day release experiment was carried out. The corresponding graphs illustrating the results are depicted in Figure 4.8. A moderate rolling speed was selected as optimal for fluid solutions of PLGA in organic solvents. Additionally, an applicator gap of 50 μm was chosen to ensure that the gap adequately covered the printed relief while optimizing the amount of solution utilized. The threshold concentration for successful film formation without defects and with the ability to hold the entire volume of the loaded substance without leakage was found to be 7.5 wt.%. In the other samples, stochastic defects leading to drug leaks were observed.

This variation can be attributed not only to the increasing proportion of polymer in the solution but also to the non-linear increase in viscosity. Generally, as the viscosity of the solution increases, the thickness of the resulting film also increases. This is because higher viscosity solutions tend to spread less readily under the blade due to shear thickening, leading to a thicker layer being deposited onto the substrate. Thus, the 1.5% PLGA solution was highly fluid and formed a micron-sized film, while the 10% solution was very viscous and resisted spreading,

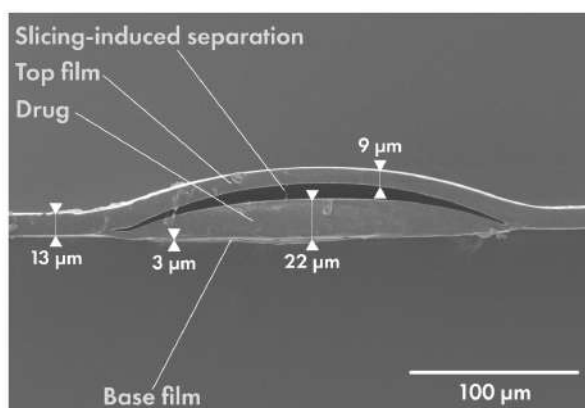


Figure 4.9: SEM image of PLGA film's edge

resulting in thick and uneven films.

In summary, an optimal film thickness of top film approximately 10 μm was achieved using a 7.5% PLGA solution. The viscosity measurements yielded the result of 66 mPa*s for such solution. The resulting film was cut into strips using cryo-tome cutting and observed via SEM. The microphotograph is presented in Figure 4.9. The overall film thickness in the drug-filled regions is about 35 μm, with the thickness of the PLGA film between tracks measuring approximately 9 μm. The experiment demonstrated that at this thickness, film defectiveness was notably reduced, while the solution remained convenient to handle. These parameters were employed for subsequent experiments. The free-standing 10 μm film was tested in a diffusion cell to obtain information about the permeability of pure PLGA films for small molecules. The test was conducted as follows: a circle of 16 mm diameter was cut from the PLGA film using a punch paper cutter and mounted between two flanges of a horizontal cell (Fig. 4.10a). A Methylene Blue saturated solution was introduced into the donor compartment, while distilled water was introduced into the receptor compartment and mixing was initiated as presented in Figure 4.10b. At predetermined time intervals, samples were taken from both compartments. The concentration of the model dye substance in each compartment was determined spectrophotometrically by UV-Vis spectroscopy at a constant wavelength of 664 nm. The experimental conditions for all experiments

were as follows: 5 ml of Methylene Blue drug solution was added to the donor compartment of the diffusion cell, 5 ml of distilled water was added to the receptor compartment, the working temperature was 37 °C, and the mixing speed was set to $n = 100$ rpm.

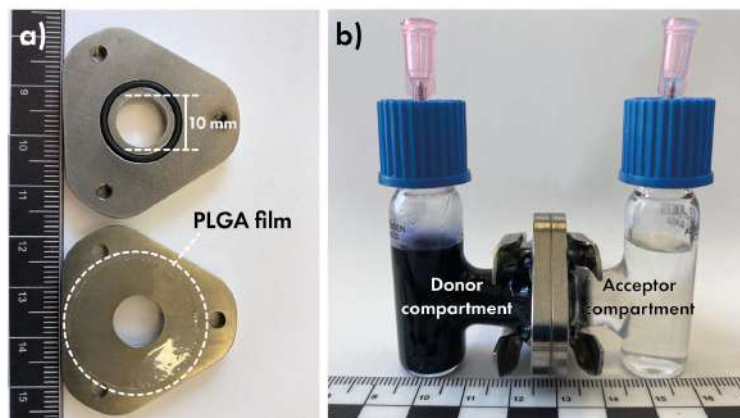


Figure 4.10: (a) Film holder made of acid-resistant stainless steel. (b) Diffusion cell

Incubation for 7 days demonstrates the absence of Methylene Blue diffusion through the polymer film, which is coherent with non-defective PLGA films. It should be noted that despite the absence of drug molecule diffusion, osmotic-driven diffusion was observed via changes in the volumes of solutions in compartments and the concentration of the donor solution (see Fig. 4.11).

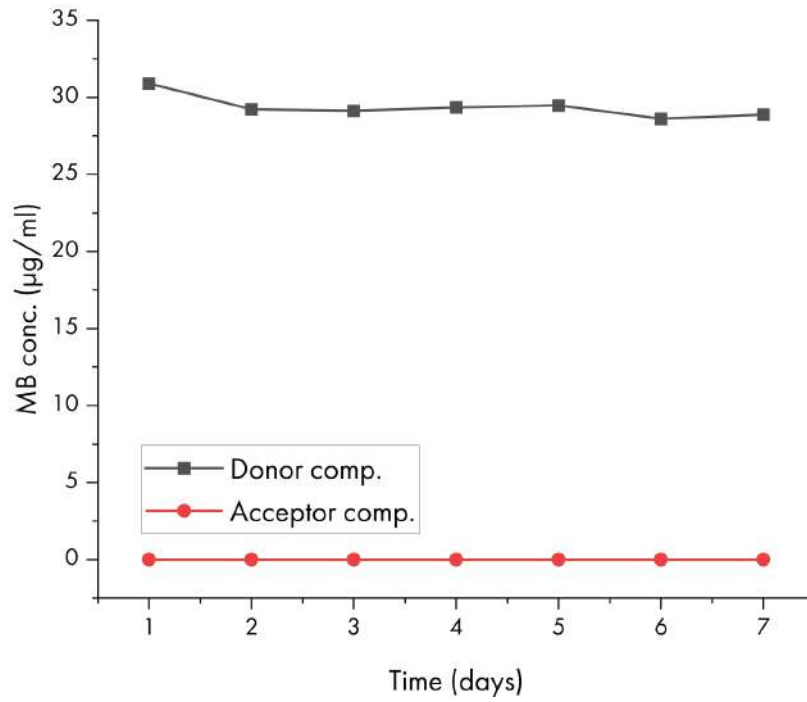


Figure 4.11: Test of permeability of PLGA film

The primary technique utilized for producing PLGA films in this study involves several sequential steps:

1. **Base Film Application:** A 7.5% PLGA solution in chloroform was used to apply the initial base film. The coating process was carried out at a rolling speed of 20 mm/s with an applicator gap (AG) of 50 µm. The coated substrates were then dried at 40°C for 10 minutes in a vacuum oven.
2. **Medicinal Solution Coating:** The base film was subsequently coated with medicinal PVA solution using a 23G needle (ID 300 µm) with a Z-offset of 150 µm. The gel flow rate was set to approximately 850 µL/h, with a printhead linear speed (LS) of 20 mm/s and an acceleration of 5000 mm/s². After applying the gel, the substrates were dried again at 40°C for 10 minutes in the vacuum oven.
3. **Top Film Application:** The final step involved applying a top film using the same 7.5% PLGA solution in chloroform. The process was performed

at a rolling speed of 20 mm/s and an applicator gap (AG) of 50 μm . The substrates were then dried at 40°C for 10 minutes in the vacuum oven to complete the film fabrication process.

4.3 Drug release characterization

4.3.1 Quantification of the vancomycin elution from PLACE films

Vancomycin, an antibiotic drug, was chosen for *in vitro* testing (Fig. 4.12). It is a glycopeptide antibiotic medication utilized in the treatment of bacterial infections, particularly effective against Gram-positive bacteria such as methicillin-resistant *Staphylococcus aureus* (MRSA) and *Clostridium difficile*. Vancomycin functions by inhibiting the synthesis of bacterial cell walls, thereby halting bacterial growth and replication. Typically administered as vancomycin hydrochloride, it boasts a high solubility of approximately 300 mg/ml and notable stability, making it a recommended choice for antimicrobial DDSs [192]. Due to its good stability and high solubility, it will serve as a highly soluble drug model throughout the work.

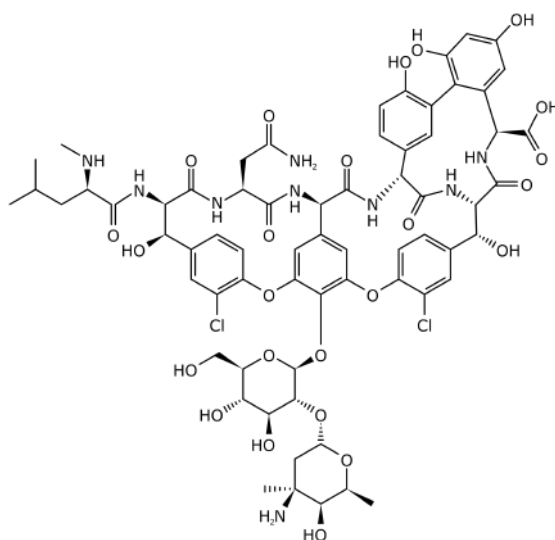


Figure 4.12: Chemical structure of vancomycin

Two sets of PLGA film samples, labeled as Vanc100 and Vanc200, were pre-

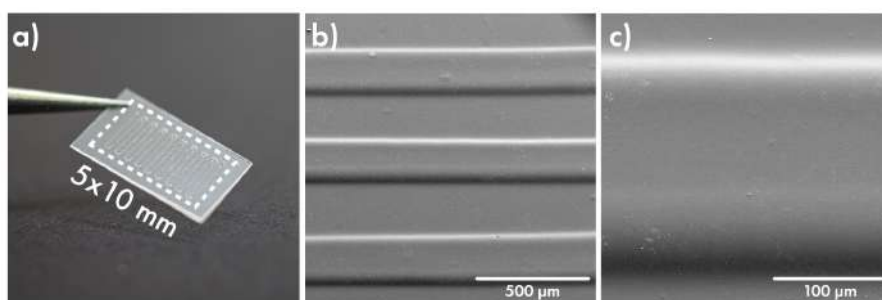


Figure 4.13: PLACE film on PP substrate (a) and microimages of drug-filled stripes (b-c).

pared for each concentration of Vancomycin in a PVA solution matrix at 100 mg/ml and 200 mg/ml, respectively. Obtained gel was applied onto PLGA substrates using parameters described in Section 4.2.3. Each set comprised six gel-printed squares, with each square having an area of $0,5 \text{ cm}^2$ (Fig. 4.13a.). The total drug loading was determined based on the sample area, resulting in a loading of $437 \pm 12 \text{ } \mu\text{g}/\text{cm}^2$ and $212 \pm 9 \text{ } \mu\text{g}/\text{cm}^2$ for the Vanc200 and Vanc100 sets respectively.

SEM images of the film's surface are depicted in Figure 4.13b,c. The cover film evenly covers the relief of the drug layer. For easy handling and to eliminate the contribution of release through the base film, all films were left on the PP substrate.

Figure 4.14 shows the in-vitro drug release study of vancomycin, with the concentration of the drug measured at different time intervals, and the cumulative release curves.

From the data, it is evident that the percentage of drug release of vancomycin increases slowly over time. For the Vanc100 group, the percentage of drug release is about 3% at 1 day, gradually increasing to 14% by the 27th day. In terms of the Vanc200 set, minimal drug release of 0.8% is observed at 1 day, gradually increasing to 18% by the end of screening.

Table 4.1 summarizes the findings from a kinetic drug release investigation of vancomycin using a DD (differential dissolution) solver [182]. Various mathemati-

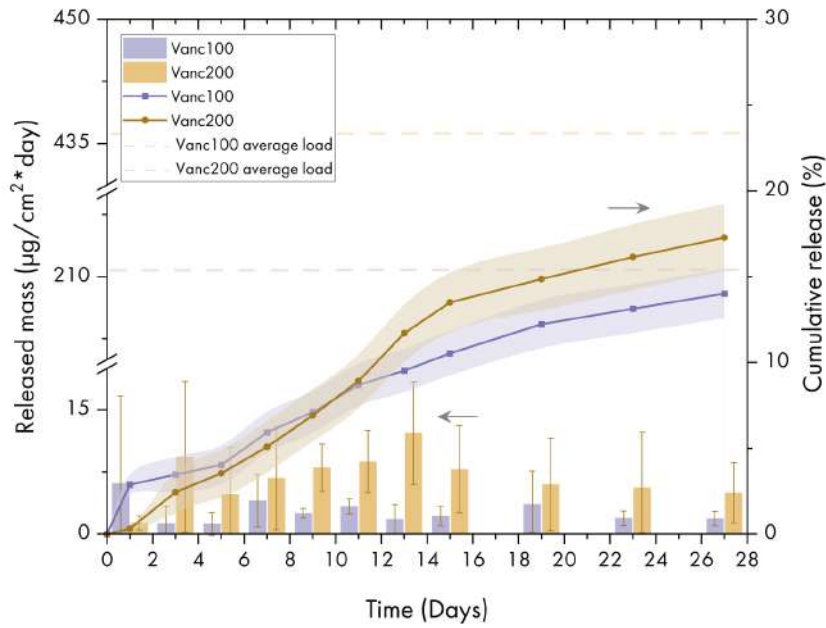


Figure 4.14: Daily and cumulative release profiles for the Vancomycin-loaded samples with 100 and 200 mg/ml of PVA matrix Vancomycin added.

	$R_{obs-pre}$	R^2	MSE	MSE_{root}	AIC	MSC
Peppas-Sahlin	0.9893	0.9787	0.4676	0.6838	20.5113	3.3028
Korsmeyer-Peppas	0.9892	0.9784	0.4208	0.6487	18.6488	3.4721
Higuchi	0.9856	0.9524	0.8360	0.9143	25.3576	2.8622
First Order	0.9855	0.8511	2.6122	1.6162	37.8907	1.7229
Hopfenberg	0.9855	0.8511	2.9038	1.7040	39.8956	1.5406
Zero Order	0.9815	0.8119	3.3004	1.8167	40.4629	1.4890

Table 4.1: Kinetic drug release study of Vanc100 group from DDSolver. Goodness of fit parameters.

cal models, including zero-order, first-order, Higuchi, Korsmeyer-Peppas, Hopfenberg and Peppas-Sahlin were examined to assess their suitability for describing vancomycin release. The assessment included evaluating goodness of fit (GOF) parameters such as $R_{obs-pre}$, R^2 , MSE , MSE_{root} , AIC , and MSC .

The analysis highlights that the Peppas-Sahlin and Korsmeyer-Peppas models showed an exceptional fit, with respective values of $R_{obs-pre} = 0.9893$, $R^2 = 0.9787$ for Peppas-Sahlin and $R_{obs-pre} = 0.9892$, $R^2 = 0.9784$ for Korsmeyer-Peppas. While other models varied in their fit quality, the Higuchi model also showed a relatively good fit. However, it is important to note that the zero-order release

	Parameter	Value
Korsmeyer-Peppas	k_{KP}	1.974
	n	0.624
Peppas-Sahlin	k_1	0.754
	k_2	1.341
	m	0.346

Table 4.2: Kinetic drug release study of Vanc100 group from DDSolver. Best fit values.

model had notably poor goodness-of-fit values, suggesting it may not adequately represent the release dynamics of PLACE films.

The underperformance of the zero-order model implies that the drug release from PLACE films is not controlled solely by a constant-rate process. Instead, factors such as diffusion, polymer relaxation, swelling, and matrix erosion appear to play a substantial role, leading to deviations from ideal zero-order kinetics. The Higuchi model, while effective, assumes diffusion as the main release mechanism, which may limit its applicability in cases where other mechanisms are active.

In contrast, the Korsmeyer-Peppas model's adaptability enables it to account for multiple release mechanisms, including diffusion, swelling, and erosion, making it well-suited for capturing the complex release profiles of PLACE films. The diffusion exponent n derived from this model provides further insights into whether the release follows Fickian (diffusion-controlled) or non-Fickian (anomalous) kinetics, aiding in the identification of the predominant release mechanisms. Similarly, the Peppas-Sahlin model offers flexibility, allowing for a more nuanced analysis of release dynamics influenced by both diffusion and polymer relaxation mechanisms.

Moving on to the Korsmeyer-Peppas model, the parameter n has a value of 0.624, indicating that the drug release follows a non-Fickian diffusion mechanism and is influenced by additional mechanisms such as polymer relaxation, swelling, erosion, or other complex processes within the polymeric matrix.

The Peppas-Sahlin model has best-fit values of k_1 and k_2 of 0.754 and 1.341, respectively, and a diffusion exponent m of 0.346. This model is applicable when the transport mechanism indicates a combined effect of chain disentanglement, ero-

	$R_{obs-pre}$	R^2	MSE	MSE_{root}	AIC	MSC
Peppas-Sahlin	0.9874	0.9750	1.3011	1.1407	31.7693	3.1446
Korsmeyer-Peppas	0.9825	0.9631	1.7098	1.3076	34.0699	2.9355
First Order	0.9802	0.9597	1.6803	1.2963	33.0373	3.0294
Hopfenberg	0.9801	0.9596	1.8703	1.3676	35.0568	2.8458
Zero Order	0.9743	0.9436	2.3521	1.5336	36.7367	2.6931
Higuchi	0.9851	0.8517	6.1819	2.4863	47.3664	1.7267

Table 4.3: Kinetic drug release study of Vanc200 group from DDSolver. Goodness of fit parameters.

	Parameter	Value
Peppas-Sahlin	k_1	-7.345
	k_2	7.010
	m	0.252
Korsmeyer-Peppas	k_{KP}	1.311
	n	0.834
First Order	k_1	0.009
Zero Order	k_0	0.806

Table 4.4: Kinetic drug release study of Vanc200 group from DDSolver. Best fit values.

sion, or swelling of hydrophilic polymer for drug release. The ratio of relaxational over Fickian contribution was calculated by Equation 6 and ranged from 1.78 to 5.77. $R/F > 1$ indicates that the relaxational contribution was predominant over the diffusional contribution.

Similar findings were noted for the Vanc200 series. Both the Peppas-Sahlin and the Korsmeyer-Peppas models demonstrated the best GOF parameters, with $R_{obs-pre}$ values of 0.9874 and 0.9825, and R^2 values of 0.9750 and 0.9631, respectively. The Zero order model and other models exhibited high levels of goodness of fit parameters, whereas the Higuchi model showed relatively lower values of GOF (see Tab. 4.3). In the Korsmeyer-Peppas model, the parameter n has a value of 0.834, suggesting that the drug release exhibits non-Fickian anomalous transport, influenced by both diffusion and relaxation mechanisms(see Tab. 4.4).

The Peppas-Sahlin model yields best-fit values of k_1 and k_2 as -7.345 and 7.01, respectively, alongside a diffusion exponent m of 0.252. The notably negative value of k_1 suggests a minimal influence of the Fickian diffusion mechanism on

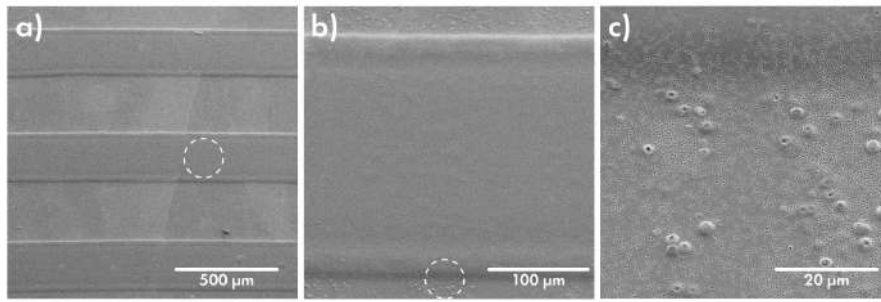


Figure 4.15: SEM images of films after release in PBS.

the drug release process. Additionally, the constants for zero-order release and first-order release correspond to 0.806 and 0.009, respectively. Notably, the value of k_1 for the First order model approaches zero, indicating that factors other than the concentration gradient predominantly control the rate of drug release. These factors may include matrix erosion, swelling, or other complex processes within the polymeric matrix.

Overall, the two best-fit models suggest that the linear release of vancomycin from Vanc100 and Vanc200 is supported by non-Fickian kinetics and involves several mechanisms. This aligns well with the system, as it encompasses both the possible erosion of the PLGA coating film and the influence of the swelling drug layer with its gradual leaching. Moreover, the tracks of swollen PVA can be regarded as a kind of diffusion barrier, slowing down the diffusion of the drug load to large membrane defects and potentially smoothing out possible burst release.

Considering the release curves outside of mathematical models, it can be concluded that the system exhibits a linear burst-less release of a small amount of load, likely associated with leakage through defects. The analysis of samples post-release did not reveal any visible microdefects or porosity. The analysis of samples post-release did not reveal any visible defects or porosity. However, examination through SEM microphotographs showed noticeable microporosity on the cover film of drug-containing containers (see Fig.4.15)

Overall, the load retention of the resulting film was significant, with more than 80% remaining inside the film after a month. Given the therapy's importance in

the first 2-3 weeks and the fact that the lifespan of PLGA in the body is 2-3 months, it would be sensible to slightly accelerate the release of the drug to maximize its amount during therapy while avoiding an avalanche-like yield of substance residues during bulk hydrolysis of the coating film. Nevertheless, already at this stage, it has been shown that PLACE films are capable of long-term retention of large doses of drugs and release them without an initial burst effect. The possibility of varying the amount of drug inside the film has been demonstrated. Such films may be suitable for covering temporarily placed MIDs, such as urethral catheters, providing additional antimicrobial function throughout the duration of insertion.

4.3.2 Impact of laser microperforation

Laser microperforation of a MB loaded biodegradable film

In this section, we aim to showcase a method for accelerating drug release from films without altering their composition, focusing on two model substances: Vancomycin, representing a highly soluble drug, and Methylene Blue (MB), a dye with limited solubility of about 30-40 mg/ml (Fig. 4.16). Small doses of MB were employed to simulate the behavior of poorly soluble toxic drugs, such as cytostatics commonly used in tumor treatment. The approach involves enhancing the permeability of the polymer film by creating a series of holes with a specified diameter using laser ablation.

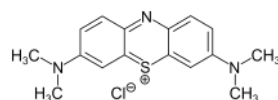


Figure 4.16: Chemical structure of Methylene Blue dye.

Effect of hole diameter on elution rate. A series of films loaded with MB were produced using PLGA polymer, as outlined in Section 4.2.3. A sample of 20 mg of dye per 1 ml of matrix was used. Optical and SEM images of a typical sample is presented in Figure 4.17a. The total MB load was measured at $35 \pm$

9 $\mu\text{g}/\text{cm}^2$. Experimental data revealed a linear correlation between laser energy and hole diameter within the 15 to 50 μJ range (Fig. 4.17). Specifically, the diameters of holes for laser energies of 15 μJ , 35 μJ , and 50 μJ were 18 ± 2.3 μm , 22 ± 2 μm , and 24 ± 2.5 μm , respectively. These measurements were taken from optical images analyzed using ImageJ software. Although the laser wavelength of 532 nm is not absorbed by PLGA, it is absorbed by the MB dye. This absorption creates a plasma ball that damages the coating and forms a hole. Despite the small variations in hole diameters (up to 25% difference), the area affected by the laser scales significantly, increasing up to 1.7 times due to the area expanding with the square of the diameter.

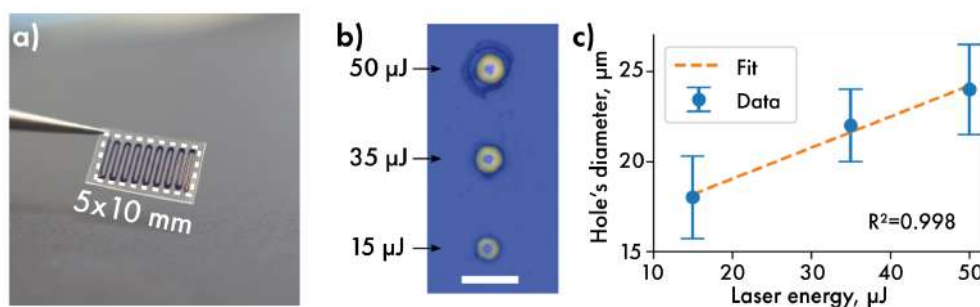


Figure 4.17: (a) Optical image showing microperforations created at various laser energies. Scale bar is 50 μm . (b) Relationship between laser energy and hole diameter for MB-loaded PLGA films. The average diameter of ten holes produced at each energy level is shown.

To examine how the diameter of the holes affects the rate of elution, a flow cell experiment was conducted. The results, shown in Figure 4.18, reveal noticeable differences in the elution zone widths for holes of varying sizes. Figure 4.18c illustrates these differences, with over 90% of the cargo being released. On average, about 50% of the total drug payload was released, but the width of the elution zones varied depending on the hole size. Specifically, the widths of the zones were 860 ± 50 μm for 24 μm holes, 625 ± 45 μm for 22 μm holes, and 300 ± 40 μm for 18 μm holes (Figure 4.18e).

To quantify the amount of eluted MB, a reference for 0% elution as the initial

average intensity of the MB stripe (I_{E0}) and 100% elution as the average intensity of the MB-free surrounding (I_{E100}) were established. The intensity of each pixel ($I_{x,y}$) in the image of the MB-loaded film, captured after 24 hours in the flow cell, was then used to calculate the relative amount of eluted MB (EC) using Equation 11:

$$EC[\%] = \frac{I_{x,y} - I_{E0}}{I_{E100} - I_{E0}} \times 100; \quad (11)$$

To determine the relative elution rate (ER) of MB, the intensity of each pixel ($I_{x,y,t}$) over time was analyzed. First, each time-series intensity value was converted to relative elution using Equation 11. Then, to find the rate of elution change, the difference in relative elution between successive time points was computed using Equation 12:

$$ER[\%/min](t) = \frac{I_{x,y,t_i} - I_{x,y,t_{i+1}}}{\Delta t}; \quad (12)$$

The highest relative elution rates were mapped for each pixel to create the 2D map shown in Figure 4.18d. The results revealed that the elution rate was about 0.6%/min near the laser-created holes and decreased to 0.1%/min as the distance from the holes increased. The width of the area where the elution rate drops to the average level matches the width of the region where MB was fully released after 24 hours in the flow cell.

Quantification of the MB elution depending on the number of holes. To quantify MB elution, a spectrophotometric calibration was performed, showing a linear relationship between the absorption at 664 nm and MB concentration for levels under 10 $\mu\text{g/ml}$ (Figure 3.4). To assess how the number of holes affects elution rate, four sets of PLGA film samples were prepared. A diameter of about 10 μm was chosen for the holes, as sizes below 18 μm are suitable for medium- to long-term drug release. The samples were categorized as follows: (0H) no holes, (1H) 1 hole, (2H) 2 holes, and (4H) 4 holes. A six with an MB concentration of 20

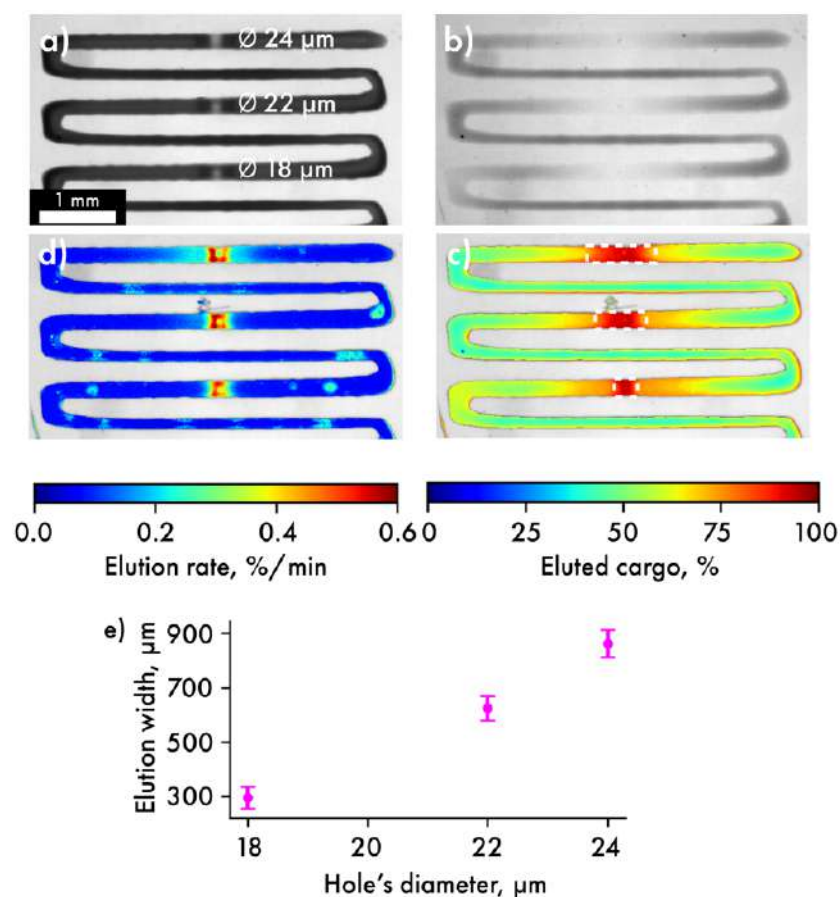


Figure 4.18: (a) Initial view of an MB-loaded film placed in a flow cell. (b) Appearance of the MB-loaded film after 24 hours in a high-flow environment. (c) Pseudo-colored map showing the amount of MB released from films with microperforations of various diameters after 24 hours in a high-flow setting. (d) Pseudo-colored map displaying the maximum elution rate observed for different hole diameters and their surrounding areas. (e) Graph showing how the diameter of the holes affects the width of the elution zone where over 90% of the substance is released.

mg/ml was used for drug printing, applied to the PLGA substrates according to the parameters described in Section 4.2.3. Each group contained six PVA-printed squares, each with an area of 1 cm^2 , and the total drug loading was calculated to be $35.05 \pm 9.30 \mu\text{g}/\text{cm}^2$.

Quantitative data regarding MB elution corresponding to the number of holes are presented in Figure 4.19a, while Figure 4.19b illustrates the locations of laser-made holes for the different sample groups. Notably, all perforated groups exhibited linear, or zero-order, elution kinetics. GOF parameters for the Zero order model fitting are presented in Table 4.5. The release values from non-perforated samples were on the verge of detection and can be considered as negligible.

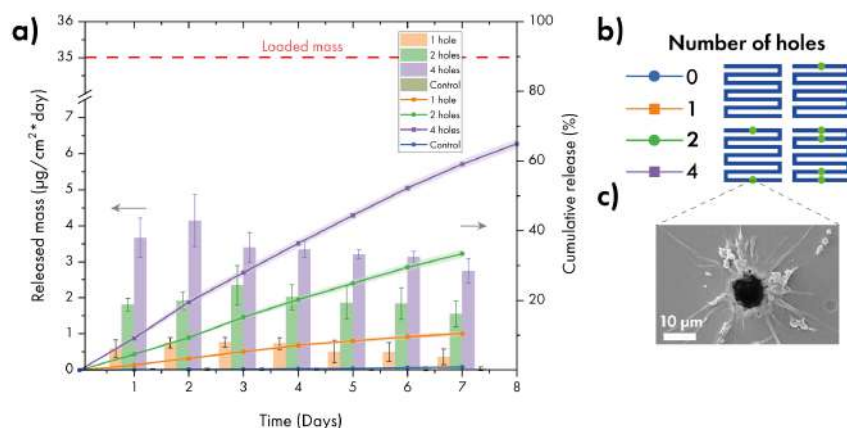


Figure 4.19: (a) MB elution data over one week, based on the number of laser-created holes.(b) Positions of the holes in different sample groups (0, 1, 2, and 4 holes) are indicated by green circles. (c) SEM image of a laser-induced hole, with an average diameter of $10 \mu\text{m}$.

The elution rates calculated by k_0 (see Tab. 4.6) were $0.23 \pm 0.06 \mu\text{g}/\text{day}$ for one microperforation, $0.68 \pm 0.13 \mu\text{g}/\text{day}$ for two microperforations, and $1.23 \pm 0.1 \mu\text{g}/\text{day}$ for four microperforations. The consistent linear elution rate can be explained as follows: A small volume around each laser-made hole allows the drug to diffuse into the surrounding environment. Simultaneously, the remaining sample continuously replenishes this volume with drug, facilitated by the swelling

	$R_{obs-pre}$	R^2	MSE	MSE_{root}	AIC	MSC
1 hole	0.9934	0.9761	0.0458	0.1937	-9.8308	3.9374
2 hole	0.9977	0.9905	0.1592	0.3978	1.5918	4.4032
4 hole	0.9978	0.9903	0.5247	0.6829	8.2865	4.5425

Table 4.5: GOF parameters for the Zero order model fitting

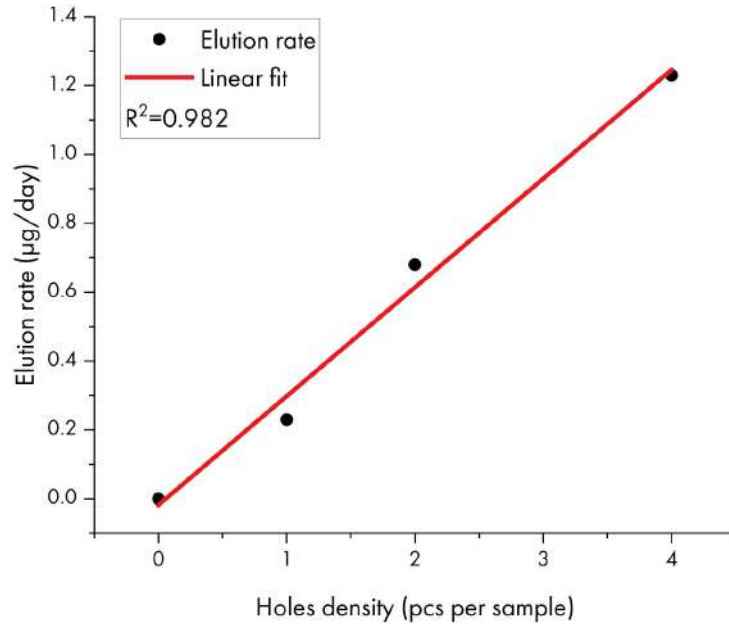


Figure 4.20: The linear dependence between the elution rate and the number of holes.

of the dye-containing PVA hydrogel, which absorbs water through the cover film. This results in a steady, zero-order release of the drug. The data shows a linear relationship (Fig. 4.20) between the number of holes and the elution rate, with each additional hole contributing approximately 0.3 µg/day to the overall release.

It's important to note that the linear dosing regime is disrupted after 7-8 days of the experiment. Taking set with four microperforations as an example, a

	Parametr	Value	Rate (µg/day)
1 hole	k_0	0.644 ± 0.176	0.23 ± 0.06
2 hole	k_0	1.957 ± 0.369	0.68 ± 0.13
4 hole	k_0	3.506 ± 0.281	1.23 ± 0.1

Table 4.6: Best fit values for the Zero order model fitting

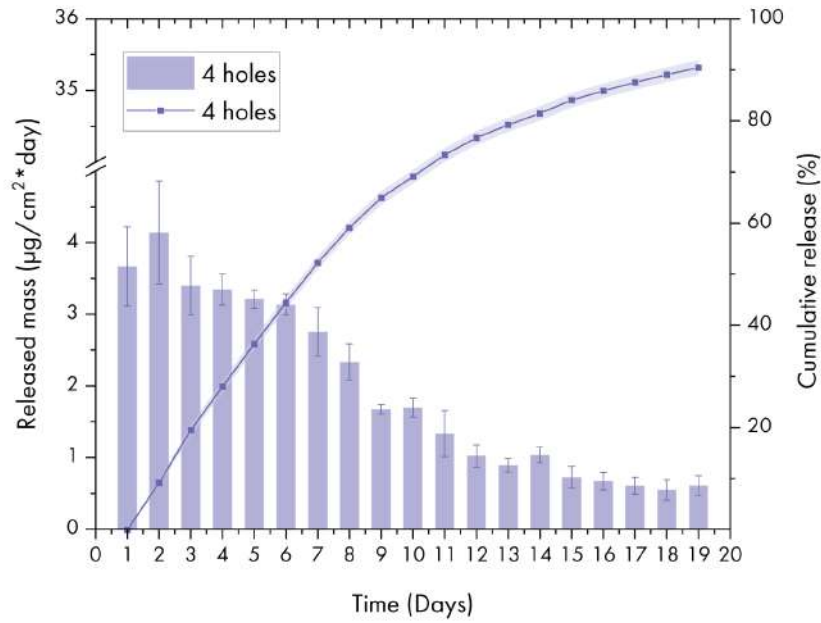


Figure 4.21: Two-week MB elution data for 4H sample.

significant slowdown in drug release becomes evident (Fig. 4.21). This slowdown could be attributed to the geometric design of the reservoir, which consists of a long strip with a hole in its center. Initially, as long as the rate of drug diffusion to the hole matches the rate of its diffusion to the surrounding medium, the release proceeds monotonically. However, once the area of empty PVA grows large enough to noticeably impede drug diffusion to the hole, the release rate from the film also decreases. As shown in Table 4.7, the data fits well with models considering impact of non-Fickian diffusion.

The findings reveal that the Peppas-Sahlin and the Korsmeyer-Peppas models demonstrated strong goodness of fit, yielding $R_{obs-pre}$ of 0.9893, $R^2=0.9787$ and $R_{obs-pre}$ of 0.9892, R^2 of 0.9784 respectively. While other models displayed varying levels of goodness of fit parameters, the Higuchi model also demonstrated relatively robust fit.

The Peppas-Sahlin model provides best-fit values of k_1 and k_2 as 7.332 and -0.362, respectively, with a diffusion exponent m of 0.736. A larger k_1 value suggests that the Fickian diffusion mechanism is predominant. The small and negative value of k_2 indicates that the non-Fickian diffusion mechanism influences the drug

	$R_{obs-pre}$	R^2	MSE	MSE_{root}	AIC	MSC
Korsmeyer-Peppas	0.9916	0.9832	0.2165	0.4587	12.6032	3.8313
Peppas-Sahlin	0.9992	0.9984	0.0259	0.1523	-14.1183	6.0581
Higuchi	0.9897	0.8772	1.3549	1.1180	32.3371	2.1868

Table 4.7: GOF parameters for the 8-14 day range for samples with four microporations.

	Parametr	Value
Korsmeyer-Peppas	k_{KP}	12.129 ± 1.577
	n	0.384 ± 0.043
Peppas-Sahlin	k_1	7.332 ± 1.167
	k_2	-0.362 ± 0.115
	m	0.736 ± 0.054

Table 4.8: Best fit values for the 8-14 day range for samples with four microporations.

release process, but its effect is minimal. In the Korsmeyer-Peppas model, the parameter n has a value of 0.384, suggesting that the drug release follows a hindered Fickian diffusion regime, that is consistent with physical process suggested above.

Laser microperforation of a Cefazolin loaded biodegradable film

To investigate the effect of microperforations on films with a high drug load, films loaded with Cefazolin antibiotics were selected. The preparation process was similar to the Vancomycin-loaded films described in Section 4.2.3, with some modifications. Cefazolin was incorporated into the matrix at a concentration of 200 mg per 1 ml of matrix. Additionally, 3 wt. % of Oil Red O dye was added to the PLGA solution to create a top film capable of absorbing 532 nm laser light, as Cefazolin itself does not absorb in this wavelength range.

To fine-tune the laser parameters, a series of perforations were created with varying repetition rates (Fig. 4.22a). Achieving the desired hole size of approximately 15-18 μm was possible with a minimal repetition rate of 3 pulses (Fig. 4.22b).

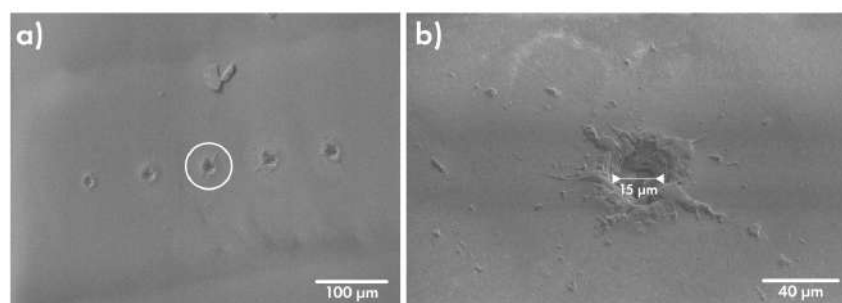


Figure 4.22: (a) Series of perforations were created with varying repetition rates, hole made with repetition rate of 3 pulses

Quantification of the Cefazolin elution depending on the number of holes. To assess the elution of Cefazolin, a spectrophotometric calibration was conducted, revealing a linear correlation between the absorption value at 271 nm and Cefazolin concentration for levels below 10 $\mu\text{g/ml}$ (Figure 3.4). Samples were prepared according to the previously described method to investigate the impact of the number of holes on the elution rate. The samples were categorized into four groups: (1) no holes; (2) 1 hole; (3) 2 holes; and (4) 4 holes.

All samples were then incubated in PBS solution for a duration of two weeks, with the PBS solution being changed daily and stored refrigerated. Upon completion of the experiment, all samples were defrosted to room temperature to assess the elution of Cefazolin using a plate reader. However, no Cefazolin-related peaks were observed in the UV-Vis absorption spectra (Figure 4.23, green line - characteristic for Cefazolin). Instead, a drifting peak around 280-300 nm was noted for all non-frozen and defrosted samples, as shown in part of the normalized profiles on Figure 4.23 (light blue lines). According to the literature, this observed peak is characteristic of Cefazolin degradation products [193], indicating complete degradation of Cefazolin in PBS starting within the first few days.

To ascertain if the drug degraded within the films, one of the control samples was cut into small pieces and incubated for 10 minutes in DI water. The obtained spectra, depicted as the red line in Figure 4.23, displayed a main peak located at 280 nm, accompanied by a broad shoulder in the 270 nm region, which may

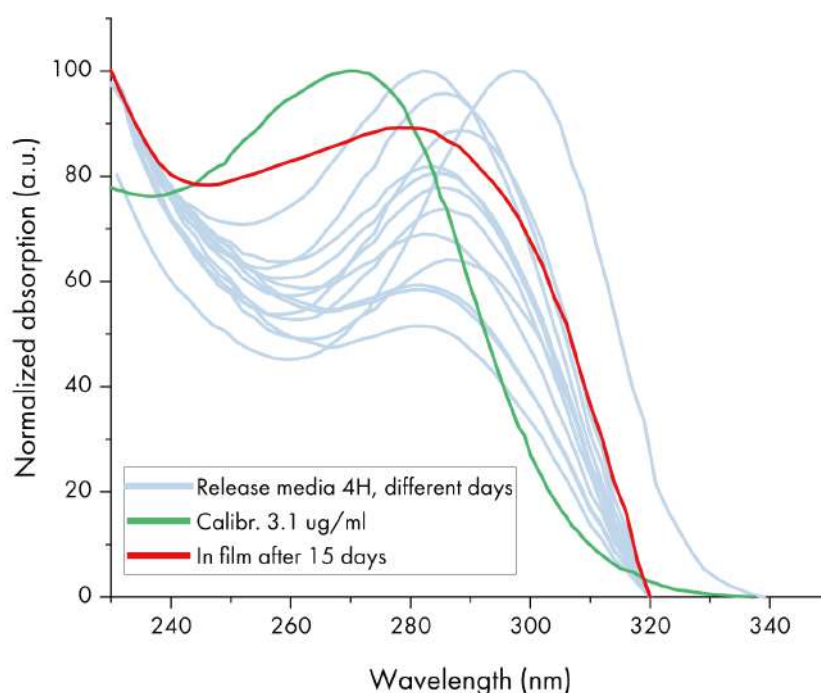


Figure 4.23: Spectra of Cefazolin (in green), its residue (in red) and variations of its degradation products in different days (in blue).

suggest the presence of non-degraded Cefazolin. However, due to the poor stability of Cefazolin, it was decided to utilize Vancomycin, which had previously demonstrated optimal properties.

Laser microperforation of a Vancomycin loaded biodegradable film

To explore the impact of microperforations on films with a high drug load, we selected films loaded with Vancomycin antibiotics. The preparation process closely resembled that outlined in Section 4.2.3, with a few adjustments. Vancomycin was incorporated into the matrix at a concentration of 200 mg per 1 ml of matrix. Additionally, we added 3 wt. % of Oil Red O dye to the PLGA solution to create a top film capable of absorbing 532 nm laser light, as Vancomycin itself does not absorb in this wavelength range. By employing a repetition rate of 3 pulses, we achieved the desired hole size of approximately 15-18 μm (Fig. 4.24b). The total drug loading was determined based on the sample area, resulting in a loading of

$499 \pm 2 \mu\text{g}/\text{cm}^2$ for Vanc200LP samples.

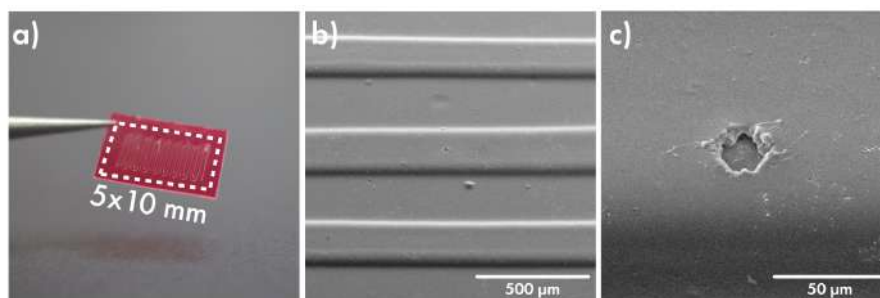


Figure 4.24: Samples photo (a) and SEM images of laser-perforated film (b-c).

Quantification of the Vancomycin elution depending on the number of holes. Quantitative data regarding Vancomycin elution corresponding to the number of holes are presented in Figure 4.25. The release of a large load of highly water-soluble drug differs significantly from the release of a small load of MB. While there was notable variation among samples within each group, the differences between groups were not particularly pronounced. This discrepancy may stem from the composition of the films; unlike the methylene blue samples, where 80% of the load consists of poorly soluble PVA, in this experiment, the films contain only about 30% of it. The rest of the chamber volume is filled with highly water-soluble Vancomycin, which also acts as an osmogen. Consequently, diffusion inside the chambers is not significantly hindered, but there is significant pressure buildup within them, also as a fast drug erosion rate. As a result, during the initial days, a substantial amount of the loaded substance is released, typically ranging from 40-80 $\mu\text{g}/\text{ml}$, gradually decreasing to 15-30 $\mu\text{g}/\text{ml}$ over time. Any potential differences in hole diameter may lead to noticeable variations in release rates. Interestingly, the sample with the highest number of holes exhibits the least variation, likely due to the rapid decrease in hydrostatic pressure within the chambers.

The rough fitting of averaged release profile reveal that the Peppas-Sahlin and the Korsmeyer-Peppas models demonstrated strong goodness of fit, yielding $R_{obs-pre}$ of 0.9998, $R^2=0.9996$ and $R_{obs-pre}$ of 0.9990, R^2 of 0.9979 respectively.

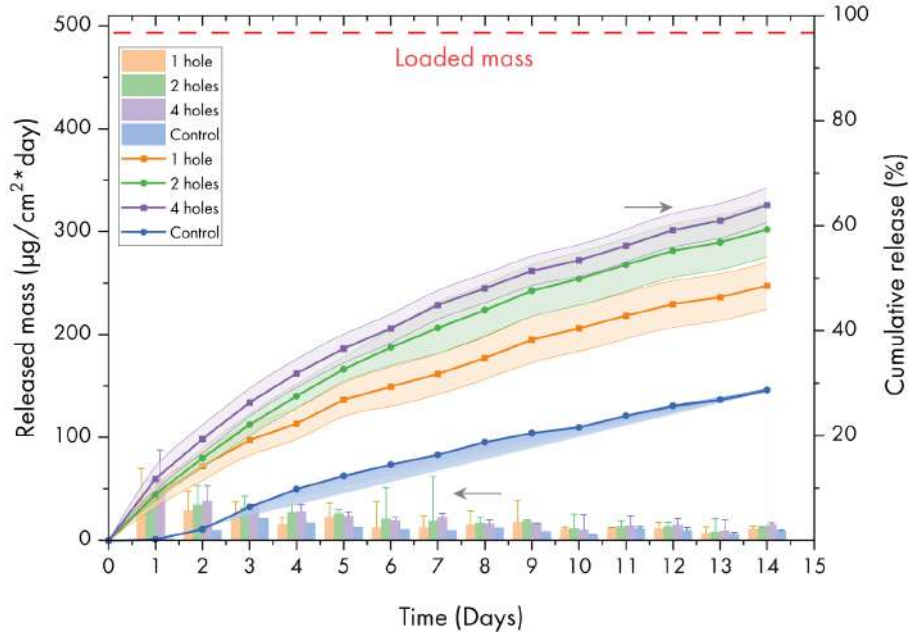


Figure 4.25: One-week MB elution data depending on the number of laser-made holes for Vanc200LP samples

	$R_{obs-pre}$	R^2	MSE	MSE_{root}	AIC	MSC
Peppas-Sahlin	0.9998	0.9996	0.1801	0.4243	17.5576	6.9905
Korsmeyer-Peppas	0.9984	0.9967	1.2841	1.1332	46.2248	5.0793
Higuchi	0.9970	0.9883	4.2959	2.0726	63.4507	3.9309
First-order	0.9947	0.9715	10.4318	3.2298	76.7587	3.0437
Zero-order	0.9707	0.8406	58.3702	7.6400	102.5879	1.3218

Table 4.9: GOF parameters for the 1-14 day range for samples with four microporations.

While other models displayed varying levels of goodness of fit parameters, the Higuchi model and First-order model also demonstrated relatively robust fit (Table 4.9). Given the best-fit values obtained from the Peppas-Sahlin model, where $k_1 = 12.682$, $k_2 = -0.545$, and the diffusion exponent $m = 0.750$, we can draw several conclusions about the drug release mechanism from the polymeric system under study.

Firstly, the parameter k_1 represents the rate constant of drug release, with a higher value indicating faster release kinetics. In this case, $k_1 = 12.682$, suggesting that the drug release from the polymer matrix occurs at a relatively fast rate.

	Parametr	Value
Peppas-Sahlin	k_1	12.682
	k_2	-0.545
	m	0.750
Korsmeyer-Peppas	k_{KP}	14.047
	n	0.580

Table 4.10: Best fit values for the 1-7 day range for samples with four microperforations.

Secondly, k_2 is a parameter associated with the mechanism of drug release. The value of $k_2 = -0.545$ implies that the release mechanism is not purely Fickian diffusion. Instead, a negative k_2 value indicates a combination of diffusion and another process, likely polymer relaxation or erosion. Lastly, the diffusion exponent m provides insight into the nature of the release mechanism. With $m = 0.750$, this exponent falls between 0.5 and 1.0, which characterizes a non-Fickian or anomalous diffusion process. This means that the drug release is governed by a combination of both diffusion through the polymer matrix and the relaxation of the polymer chains. In summary, the given values indicate that the drug release from the polymeric system is characterized by a relatively fast release rate and follows a non-Fickian mechanism, where both diffusion and polymer relaxation play significant roles in the overall release process.

In the Korsmeyer-Peppas model, the parameter n has a value of 0.580, suggesting that the drug release follows non-Fickian anomalous transport, influenced by both diffusion and relaxation mechanisms. This finding is consistent with a real system featuring both swellable and erodible drug and PVA.

SEM images for 4-hole after release samples demonstrates, that release occurs predominantly in perforated zones (dashed lines in Figure 4.26). The flat stripes of the empty reservoirs are clearly visible. At the same time, the zone to the right, without perforations, still shows remains of the substance in stripes.

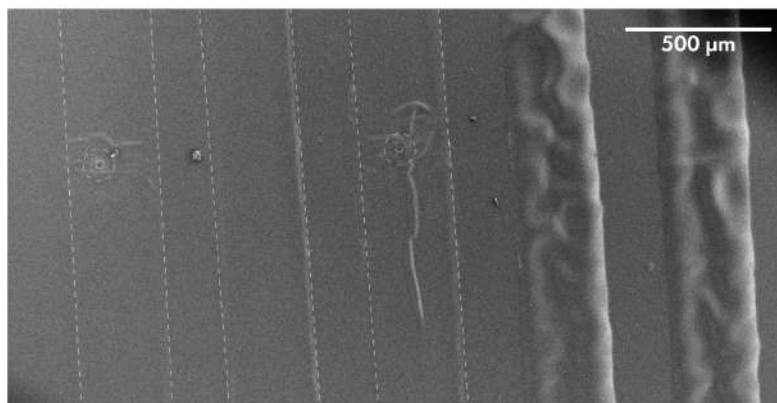


Figure 4.26: SEM images for 4-hole after release samples.

This section demonstrated that laser perforation has emerged as a promising method for tailoring the release profiles of drugs from PLACE films, along with highlighting the role of the diffusion and erodible layer of PVA and its mixtures with the drug. While accelerated release is crucial for certain drugs to ensure therapeutic efficacy, the slow diffusion of drugs through the PVA matrix can sometimes hinder the desired release rates. Simultaneously, the erosion of the hydrophilic drug/PVA hydrogel structure has shown to significantly influence drug release. This indicates a shift in the drug release mechanism from diffusional to relaxation or erosion-controlled release. These limitations underscore the need for a more refined approach to modulate drug release.

Moving forward, transitioning from creating a small number of larger holes to generating numerous smaller holes can offer a solution. This controlled porosity approach can lead to a more uniform drug release system, mitigating the drawbacks associated with slow diffusion through the PVA matrix. Such advancements promise to enhance the versatility and efficiency of laser perforation techniques in tuning drug release from PLACE films.

4.3.3 Influence of porogen agents

To create a film with regulated porosity, diverse porogens can be utilized. Typically, these are polymers soluble in both water and organic solvents. PEG and

PVP emerge as prime choices for porogenic additives, both being FDA-approved for medicinal use, emphasizing their biomedical applicability and safety. PEG and PVP were selected as inert additives in this work due to their biocompatibility and solubility in both water and the initial polymer solution, making them convenient for achieving controlled porosity in the final films. These additives can dissolve and leach out in vivo without adverse effects, facilitating gradual drug release through the pores left behind. Traditional solid porogenic agents, such as salts, sugars, and gelatin nanoparticles, present greater challenges for submicron porosity creation, as they require precise dispersion and stabilization to prevent agglomeration [194, 195, 196, 197]. Furthermore, the use of solid porogens in biological applications can introduce risks of inflammatory responses, osmotic imbalance, or unexpected immune reactions due to residual particles. PEG and PVP offer a simpler, safer alternative for generating consistent porosity without these complications. Consequently, the use of PEG and PVP as porogens enables direct application of the porogen-containing layer onto the drug-loaded layer, eliminating the need for post-processing steps such as leaching or etching. This streamlined process minimizes the risk of drug loss or degradation, ensuring a more efficient production and reliable performance of the final film.

Nevertheless, incorporating hydrophilic porogens such as PEG and PVP into a hydrophobic PLGA matrix can pose challenges due to potential phase separation, impacting film uniformity and performance. The molecular weight (MW) of these additives significantly influences their compatibility with PLGA. Lower MW additives generally exhibit better miscibility with PLGA than their higher MW counterparts. This propensity is attributed to the ease with which smaller molecules permeate and disperse within the polymer matrix.

It can be stated from the literature, that additives with low molecular weights addition range from 10 to 30 wt.% , the miscibility is typically optimal. At this range, the additive molecules can effectively interact with the PLGA chains, promoting homogeneity and reducing phase separation. This results in films with more uniform porosity and controlled drug release profiles.

Porogen	MW, Da
PEG 400	400
PEG 2000	2000
PEG 8000	8000
PVP K17	12000
PVP 55k	55000
PVP K90	1300000

Table 4.11: Porogens tested in presented work.

In the present work, various types of PEG and PVP listed in Table 4.11 were evaluated for their miscibility with Corbion PLGA 5010. The ideal outcome for this study was to achieve interconnected clusters or groups of pores with sizes comparable to the thickness of the film, uniformly distributed across the film area.

For the experiment, specific quantities of these additives were added to a 7.5% PLGA solution to create mixtures at 10 and 20 wt.% based on the dry film weight. The resulting solutions were stirred intensively for 2 hours and processed similarly to conventional PLGA films.

Use of PEG as pore-generating agent

For high molecular weight PEG, uncontrollable phase separation during films casting was evident. Optical images (Fig. 4.27) revealed that PEG 2000 (b) and 8000 (a) formed large clusters, some measuring hundreds of microns, which floated on the surface of the PLGA. The size and distribution of these clusters were inconsistent and did not correlate with the amount of additive, suggesting complete immiscibility. While applying the mixtures at elevated temperatures (40-45°C) reduced the cluster size slightly, the results still were far from producing a uniform film.

The mixtures with PEG 400 exhibited similar results when films were applied under ambient conditions. However, when applied at elevated temperatures using

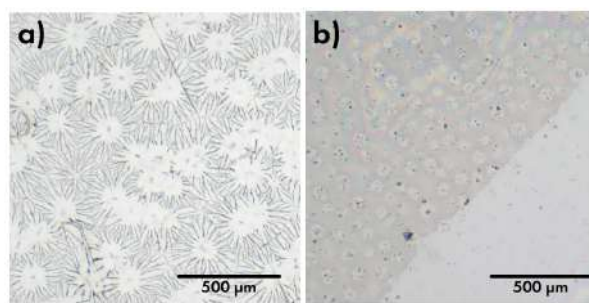


Figure 4.27: Optical images of PLGA films with 10% of PEG 8000 (a) and partly immersed in water PEG 4000 (b).

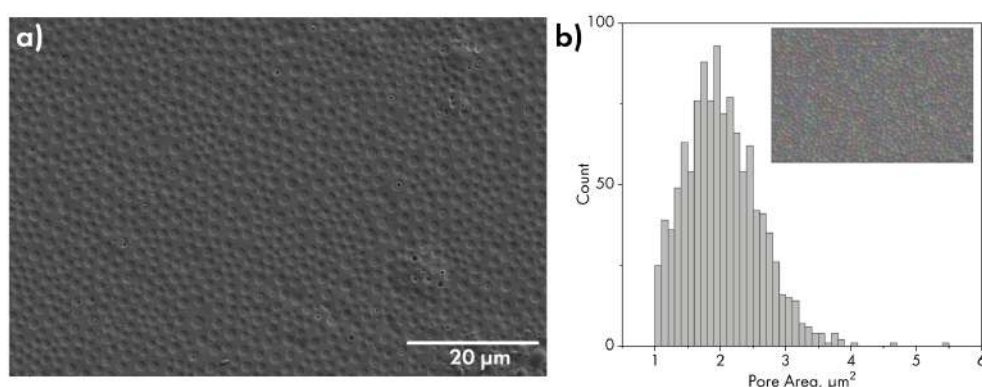


Figure 4.28: SEM micrographs of sample with 10% PEG 400.

a heated table, homogeneous films were obtained for the 10% mixture. The film with higher concentration of PEG 400 demonstrated randomly distributed large PEG droplets on the surface of film.

To assess the distribution of PEG in the films, they were immersed in water for 1 hour to remove the porogenic additive. SEM micrographs are shown in Figure 4.28. Small PEG-rich droplets can be observed on the film's surface, which could easily melt during SEM acquisition. After the washing procedure, semicircular recesses are visible. This suggests that although a well-ordered structure was achieved, such porosity cannot be utilized as a transport channel for drugs, as most of the liquid PEG is concentrated on the top surface of the PLGA film as a big $2 \mu\text{m}^2$ droplets.

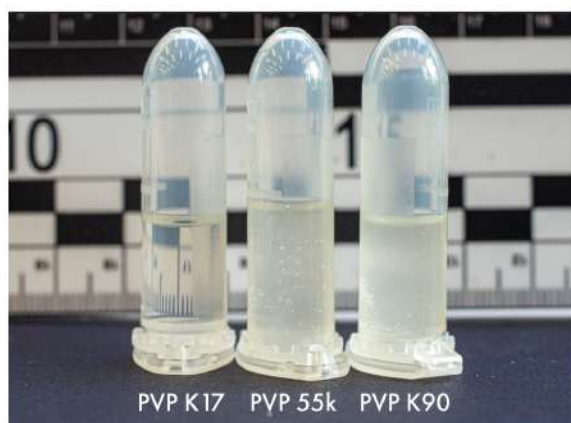


Figure 4.29: Emulsification of PLGA solutions with the addition of 10% PVP 55k (a) and K90 (b), clear mixture with PVP K17 (c).

Use of PVP as pore-generating agent

For PVP, immiscibility with PLGA was evident even in the solutions. Stratification of PLGA solutions was observed with the addition of 10% PVP 55k and K90 (Fig. 4.29a and b respectively). Additionally, a notable increase in viscosity was observed in solutions containing PVP K90, attributed to its longer polymeric chains. Solutions containing the shorter PVP K17 remained clear, stable, and maintained their initial viscosity levels (Fig. 4.29c). Films were prepared both at ambient conditions and on a heated substrate. For films prepared without heating, significant phase separation was evident, with observable hexagonal cells indicating PVP-rich regions (Fig. 4.30a) for 10% of additive and complete phase separation for 20% PVP (Fig. 4.30b). The most homogeneous films were achieved using a heated table (Fig. 4.30c). Clusters of PVP, measuring only 0.5 to 2 microns in size, appeared during the long-term accumulation of an image due to the heating of the film by an electron beam. The average area of these clusters was calculated to be approximately $0.25 \mu\text{m}^2$ (Fig. 4.30d and e).

Despite the efforts to achieve a homogenous distribution of PVP clusters, complete uniformity could not be attained. The cryo-section analysis of the film reveals a gradient in the cluster size and distribution, with both parameters in-

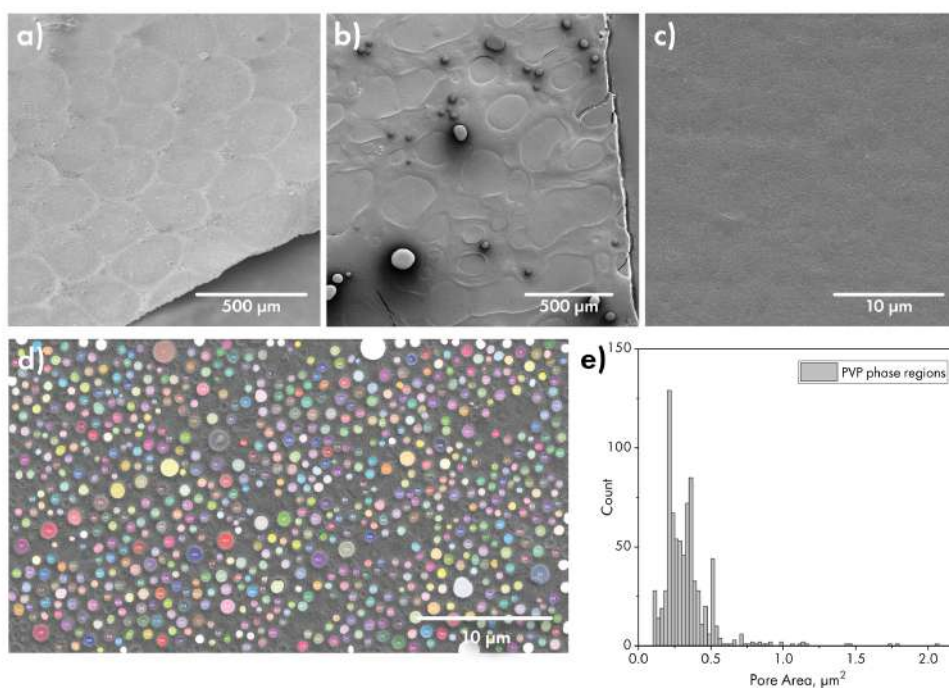


Figure 4.30: PVP-rich regions were observed for samples with 10% additive (a), while complete phase separation occurred at 20% PVP (b) in non-heated samples. The most homogeneous films were achieved using a heated table with 10% PVP K17 (c and d). The cluster size distribution histogram for these samples is shown in image (e).

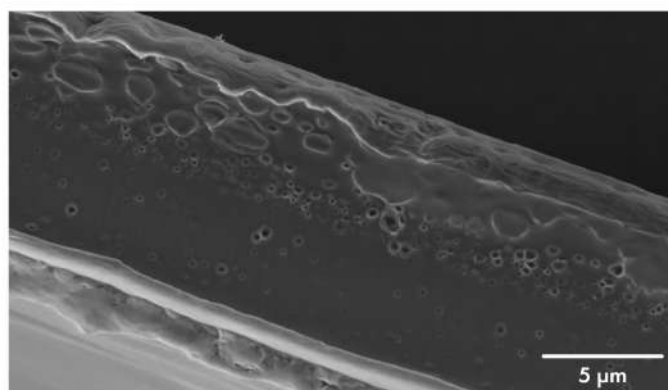


Figure 4.31: The SEM image of the edge of the PLGA film containing 10 wt.% of PVP K17

creasing from the bottom surface toward the top (Fig. 4.31). This results in a heterojunction-like structure between the two polymers. In such a configuration, the formation of a substantial number of through-pores is unlikely. However, this arrangement is expected to enhance the film's hydrophilicity, leading to increased swelling and the development of water-filled nanopores. Consequently, these factors would improve the film's permeability and accelerate its degradation rate.

Quantification of the Methylene Blue elution from PLGA films containing 10% and 20% PVP K17

To assess the impact of PVP addition, this approach was initially applied to films containing MB. Spectrophotometric calibration was conducted to evaluate the elution of MB, revealing a linear correlation between the absorption value at 664 nm and MB concentration for concentrations below 100 $\mu\text{g/ml}$ (Figure 3.4). Six samples were prepared for each PVP concentration following the main method described in section 4.2.3. However, there was a variation in the composition of the top films, with 10% and 20% PVP K17 added respectively, while maintaining the rolling temperature at approximately 45°C. The total drug loading was determined based on the sample area, resulting in a loading of $122 \pm 13 \mu\text{g/cm}^2$ for all samples.

The SEM images of the resulting films are depicted in Figure 4.32. The films

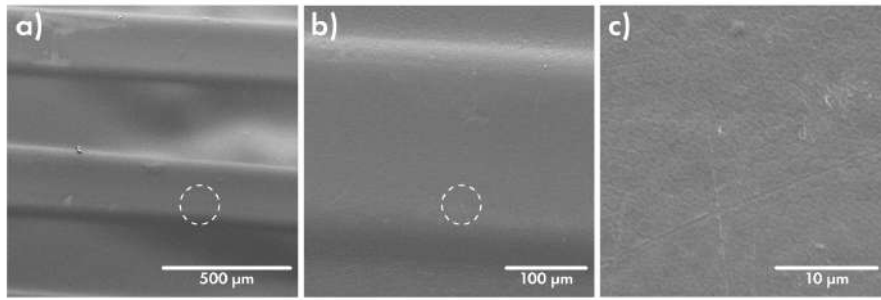


Figure 4.32: Microphotographs of samples surface.

appear smooth and homogeneous until clusters of PVP, only a few microns in size, appear during prolonged exposure to an electron beam, likely due to heating of the film. Figure 4.33 illustrates the daily and cumulative release profiles for the samples described above. The addition of 10% PVP resulted in a consistent release of approximately 30% of the loaded cargo over the course of three weeks. The observed variability in the daily release values could be attributed to the non-uniform distribution of PVP clusters, both in terms of number and size, across different samples. The area of the sample might not be sufficient to mitigate the impact of this factor through averaging. Adding 20% PVP led to an accelerated burst release, with 80% of the dye released within the first 24 hours. These unfavorable results can be attributed to phase separation and the formation of large PVP clusters on the film's surface, resulting in the formation of large pores.

When compared to laser-perforated films, it is notable that the release profile closely resembles the profile obtained using films with two laser-perforated holes. Additionally, gradual deceleration in release is evident, which may serve as evidence of suboptimal pore size and distribution.

Although the findings indicate a strong goodness of fit for the Peppas-Sahlin model, with $R_{obs-pre}$ of 0.9926 and $R^2=0.9848$, the large deviation in the BFV for this model may be attributed to variations in sample quality. Consequently, drawing a definitive conclusion for this model is challenging. The negative value of k_1 indicates an initial burst release, which means that there is a rapid release of the drug from the formulation at the beginning of the process. The value of m being

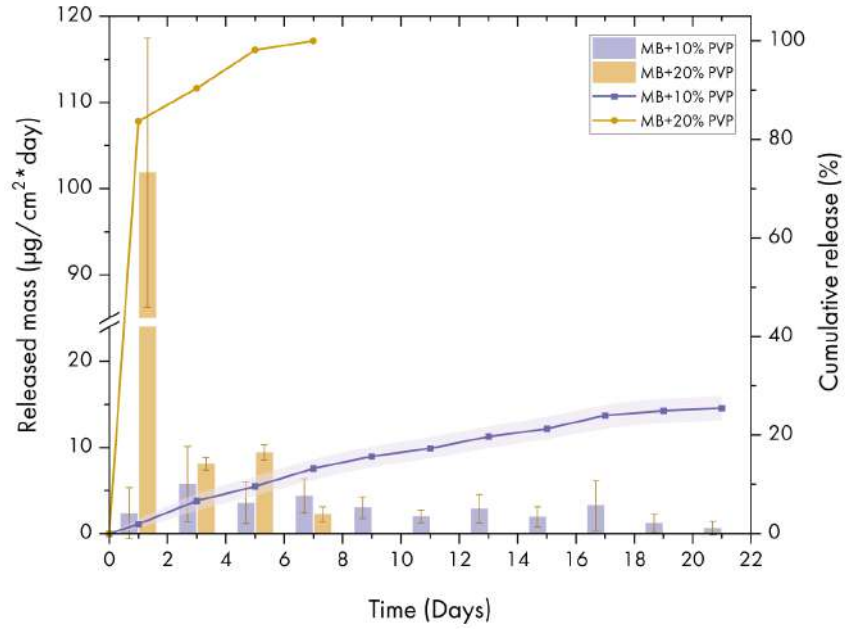


Figure 4.33: Daily and cumulative release profiles for the MB-loaded samples with 10% and 20% PVP added.

	$R_{obs-pre}$	R^2	MSE	MSE_{root}	AIC	MSC
Peppas-Sahlin	0.9926	0.9848	7.2171	2.6844	61.5883	3.7368
Korsmeyer-Peppas	0.9790	0.9552	20.5784	4.4689	73.6965	2.8054
First-order	0.9835	0.9540	20.2144	4.3350	71.4151	2.9809
Hopfenberg	0.9834	0.9540	22.0861	4.5309	73.4310	2.8258
Higuchi	0.9828	0.9288	27.2319	5.2150	77.2269	2.5338
Hixson-Crowell	0.9743	0.9121	39.7665	5.9536	78.9979	2.3976
Zero-order	0.9420	0.7382	121.6429	10.1431	91.9231	1.4034

Table 4.12: GOF parameters for the samples with 10% PVP K17

	Parametr	Value
Korsmeyer-Peppas	k_{KP}	10.197 ± 6.934
	n	0.614 ± 0.117
Peppas-Sahlin	k_1	-13.847 ± 32.505
	k_2	19.468 ± 24.574
	m	0.434 ± 0.330

Table 4.13: Best fit values for the 8-14 day range for samples with four microperforations.

less than 0.5 indicates that the release is primarily controlled by swelling and relaxation mechanisms rather than purely diffusion-controlled. However, the broad confidence intervals for constants and m indicate some uncertainty in the model fitting due to deviation between samples. On the other hand, the Korsmeyer-Peppas model yields lower GOF values with $R_{obs-pre} = 0.9790$ and $R^2=0.9552$, but it presents more adequate values for BFV. The parameter n has a value of approximately 0.6, suggesting that the drug release follows non-Fickian anomalous transport, influenced by both diffusion and relaxation mechanisms, which is consistent with a real system featuring both swellable and soluble PVP.

Figure 4.34 presents SEM microphotographs of samples containing 10% PVP (a-c) and 20% PVP (d-f). Notably, samples with 20% of additive were only incubated in PBS for one week until full drug release, while samples with 10% PVP were incubated for 3 weeks before the experiment was halted.

Observing the sample with 20% PVP, it's apparent that the drug-containing stripes have completely fall off, forming a fold in the middle. Upon closer inspection, the surface of the sample reveals numerous micron-sized craters where the PVP was originally located. These craters vary in size from 1 to 8 microns, with the surface appearing smooth overall, but larger craters exhibiting submicron-sized pores. This suggests that due to the high amount of additive, the phases did not separate optimally, resulting in large heterogeneities that accelerated drug release from the films even in the absence of significant hydrolysis of PLGA.

In contrast, the sample with a lower percentage of PVP exhibits a different appearance. The film and stripes appear highly swollen, likely due to the penetration of water deep into the films facilitated by the presence of hydrophilic PVP. The polymer surface appears rough, with no traces of craters. Closer inspection reveals significant porosity due to erosion and hydrolysis. Despite this, the reservoirs remain relatively voluminous and hold more than 70% of the load.

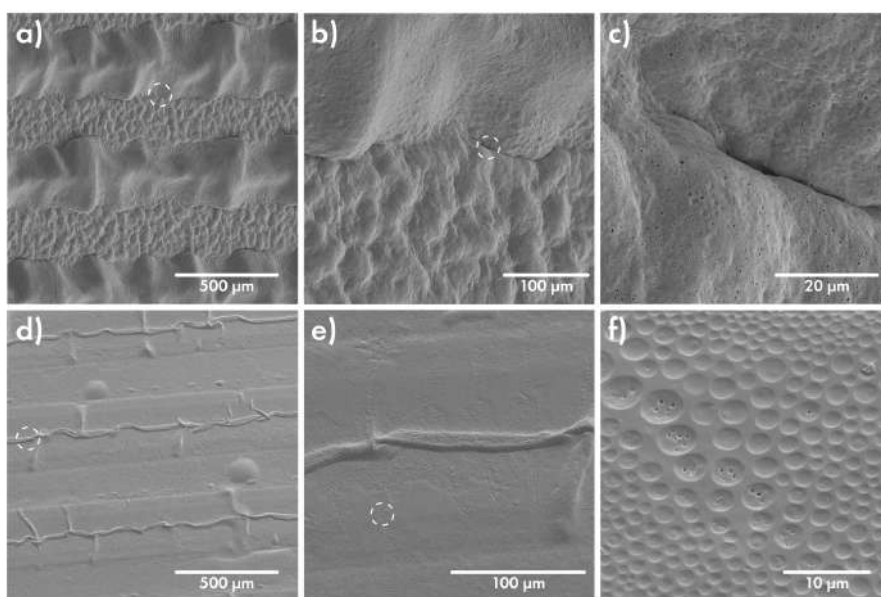


Figure 4.34: SEM microphotographs of samples with loaded MB and containing 20% PVP (a-c) and 10% PVP (d-f).

Quantification of the Vancomycin elution from PLACE films containing 10% PVP K17

For the films containing Vancomycin, a porogen incorporation approach was also taken with only a lower concentration of PVP (10%) due to previous issues with MB release. Six samples were prepared following the main method described in section 4.2.3. However, there was a change in the composition of the top films, with 10% PVP K17 added, while maintaining the rolling temperature at approximately 45°C. The total drug loading was determined based on the sample area, resulting in a loading of $499 \pm 2 \mu\text{g}/\text{cm}^2$ for all samples.

The SEM images of the resulting films are presented in Figure 4.35. Initially, the films exhibit a smooth and homogeneous appearance (Fig. 4.35a). However, upon prolonged exposure to an electron beam, clusters of PVP, measuring only a few microns in size, become evident (Fig. 4.35b), likely as a result of film heating. Figure 4.36 displays the daily and cumulative release profiles for the aforementioned samples. The cumulative release exhibits a complex profile, with an average zero-order release of about 40% of the loaded substance by day 4, accompanied by

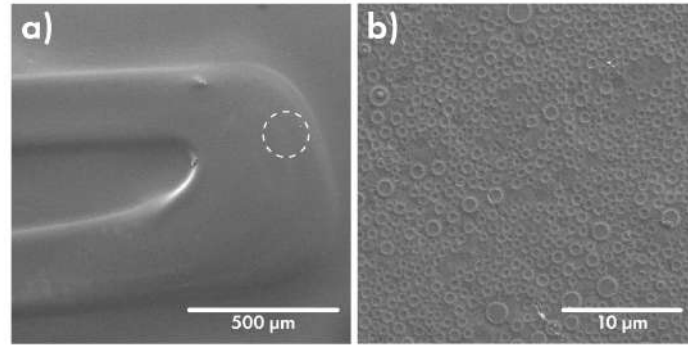


Figure 4.35: SEM microphotographs of sample with loaded Vancomycin and containing 10% PVP

	$R_{obs-pre}$	R^2	MSE	MSE_{root}	AIC	MSC
Day 1-5						
Zero-order	0.9969	0.9899	3.2529	1.8036	18.7340	3.8985
Day 5-14						
Peppas-Sahlin	0.9986	0.9972	0.2722	0.5218	12.4481	5.2792
Korsmeyer-Peppas	0.9971	0.9941	0.5023	0.7088	17.9095	4.7330
First-order	0.9984	0.8369	12.3486	3.5141	49.1077	1.6132

Table 4.14: GOF parameters for the samples with 10% PVP K17

daily doses ranging significantly from 40 to 100 μg . Subsequently, there is a gradual slowdown in release, with daily average doses ranging from 50 to 15 μg . The variability observed in the daily release values may be attributed to the uneven distribution of PVP clusters, both in terms of quantity and size, among different samples. The sample area may not be adequate to offset this factor through averaging. Furthermore, the difference in release speed compared to the previous release of MB can be explained by the lower amount of insoluble PVA in the drug layer, as well as the higher solubility of Vancomycin itself. In comparison to laser-perforated films, it is noteworthy that the substance's release rate is higher due to the more even distribution of pores.

Since the averaged release profile is biphasic, fitting of each phase was rough estimated separately. In the first phase we used data from days 1-5, in the second phase from 5 to 14. GOF parameters are presented in Table 4.36.

As mentioned earlier, the behavior observed during the first 4 days follows

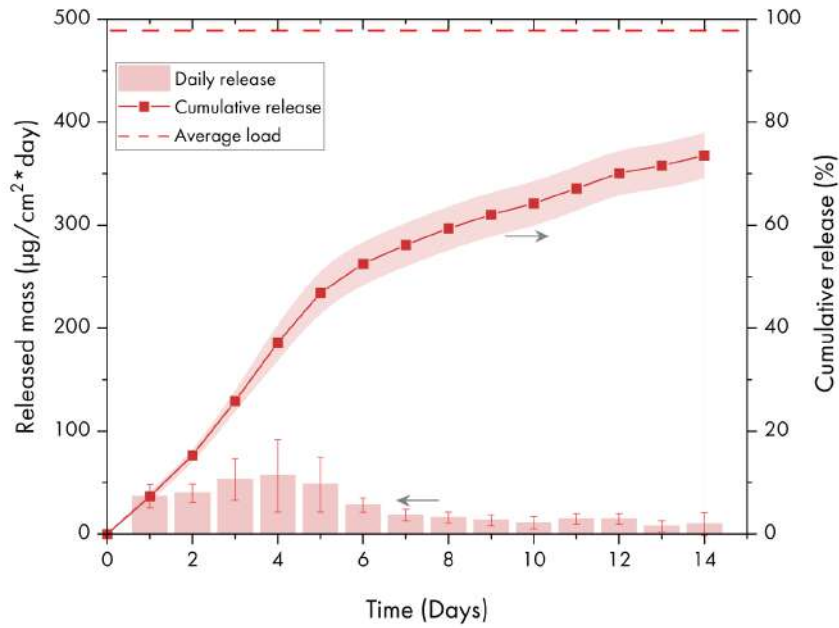


Figure 4.36: Daily and cumulative release profiles for the Vancomycin-loaded samples with 10% PVP added.

	Parametr	Value
Zero-order	k_0	9.059
Peppas-Sahlin	k_1	21.199
	k_2	-1.331
	m	0.617
Korsmeyer-Peppas	k_{KP}	24.689
	n	0.417

Table 4.15: Best fit values for the 5-14 day range for samples with four microperforations.

a Zero-order equation. It can be hypothesized that the gradual dissolution of PVP and the swelling of PVA contributed to this phenomenon. Subsequently, the release profile from days 5 to 14 aligns reasonably well with the Peppas-Sahlin and Korsmeyer-Peppas models.

The findings for the second release phase indicate a strong goodness of fit for the Peppas-Sahlin model, with $R_{obs-pre}$ of 0.9986 and R^2 of 0.9972, and for the Korsmeyer-Peppas model, with $R_{obs-pre}$ of 0.9971 and R^2 of 0.9941. A larger value of k_1 suggests that the Fickian diffusion mechanism is predominant. The small and negative value of k_2 indicates that the non-Fickian diffusion mechanism influences

the drug release process, but its effect is minimal. This is quite physical for a highly porous system with a small amount of diffusion-retarding PVA inside. In the Korsmeyer-Peppas model, the parameter n has a value of 0.417, suggesting that the drug release follows almost First-order kinetics ($n=0.45$). However, the value of R^2 for this model is not ideal. Since the coefficient n for the Korsmeyer-Peppas model is slightly lower than 0.45, which is typical for hindered diffusion, it can be assumed that this is due to the presence of PVA inside and overall variability between samples.

Figure 4.37 presents SEM microphotographs of samples containing 10% PVP (a-c) after 5 days of incubation in PBS, and after all 2 week period (d-f).

By day 5, more than 40% of the cargo had been released, causing the strips to lose volume in the middle, although some substance remained at the edges. The entire sample surface exhibits uniform coverage with PVP craters and micron and submicron pores. After spending two weeks in a buffer solution, the samples appear more or less the same with slightly swollen regions between the drug stripes, possibly due to water penetration deep into the films facilitated by the presence of hydrophilic PVP. The polymer surface appears rough, devoid of any crater-like features, but closer examination reveals significant porosity resulting from erosion and hydrolysis. The stripes have completely lost their volume.

Therefore, the incorporation of pore formers like PVP can significantly hasten the release of small doses of poorly soluble drugs. By adjusting the PLGA/PVP ratio, the release profile can be finely tuned over several weeks. However, it's crucial to note that induced porosity may also accelerate polymer hydrolysis significantly. Hence, careful optimization is necessary to ensure gradual release of most cargo before complete decomposition, thereby preventing a delayed burst effect.

In the scenario of a large load of highly water-soluble drugs, the release occurs more rapidly. Each day, the film liberates approximately 7-10% of the loaded substance, making it ideally suited for post-operative therapeutic applications.

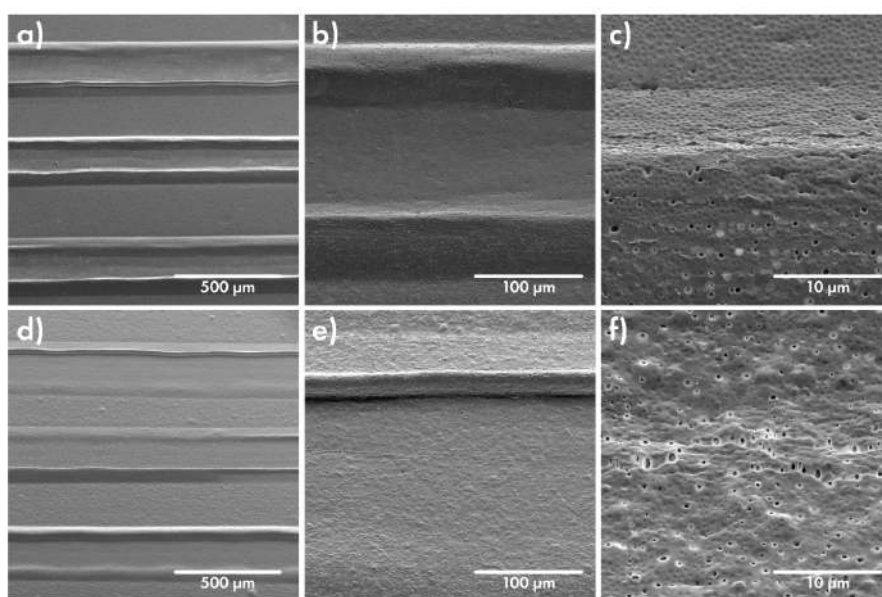


Figure 4.37: SEM microphotographs of samples with loaded Vancomycin and containing 10% PVP (a-c) after 5 days of incubation in PBS, and after all 2 week period (d-f).

4.4 E-beam sterilization and film stability

4.4.1 Impact on PLGA films

Since electron beam sterilization is the only available and suitable method for polymeric films sterilization, it was aimed to investigate its impact on drug release from PLGA films. To begin, neat PLGA films were prepared using a 7.5% solution of PLGA in chloroform, resulting in a film approximately 8 μm thick. Half of this film was then sent to the Tecleor sterilization plant and subjected to a total dose of 25 kGy, a standard dose for medical implantable devices.

Subsequently, both the irradiated and control samples were immersed in a 0.01 M PBS solution and incubated for 1 month at 37°C. Each week, one of the irradiated samples was removed from the PBS, washed with deionized water, and collected to acquire SEM images.

Figure 4.38 illustrates the four irradiated samples, which were incubated for 1, 2, 3, and 4 weeks respectively, alongside the control sample incubated in PBS



Figure 4.38: Irradiated PLGA films and control (non-irradiated) sample after 1-4 week incubation in PBS.

for 4 weeks. It is evident that the optical density of irradiated films increases significantly after 3 weeks of incubation due to pore formation. In contrast, the control samples maintained their initial optical density even after 1 month in the PBS solution.

When examined using SEM, the samples showed distinct changes over the incubation period in PBS. After the first week, the sample surface appeared smooth without any evidence of pore formation (Fig. 4.39a). By the second week, noticeable porosity emerged, with micron-sized pores covering the entire film surface unevenly, often concentrating in dense islands. These irregularities may be attributed to defects and abrasions present on the film, acting as hydrolysis concentrators (Fig. 4.39b).

In Fig. 4.39c, a coral-like structure of partly hydrolyzed PLGA film is evident after 3 weeks of incubation in PBS. It's important to note that after this period, the irradiated film became fragile, as shown in the upscaled photo (Fig. 4.40b). By the fourth week in PBS, the polymer film exhibited a fragile and loose foam-like structure (Fig. 4.39d). It appears that surface hydrolysis predominates before 4 weeks, with approximately half of the film depth undergoing hydrolysis on the side facing the buffer solution, while the other side, protected by the PP substrate, remains smooth and dense (Fig. 4.40b).

However, SEM images do not reveal nano-sized pores, making it impossible to

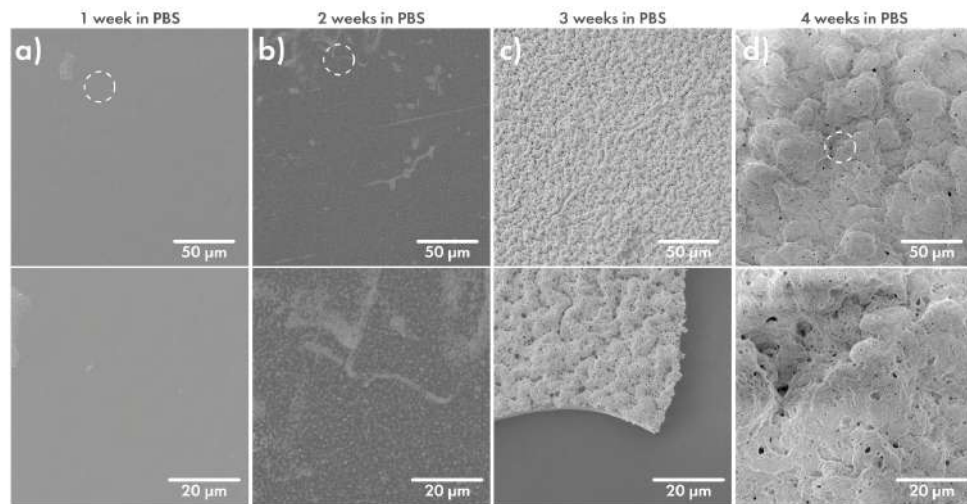


Figure 4.39: SEM microphotographs of Irradiated PLGA films after 1-4 week incubation in PBS.

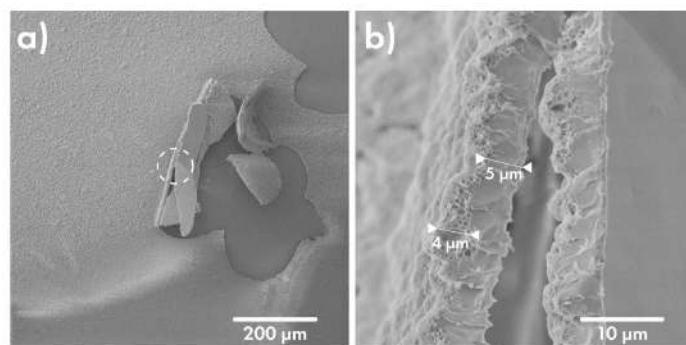


Figure 4.40: Up-scaled photo of 3-week incubated sample

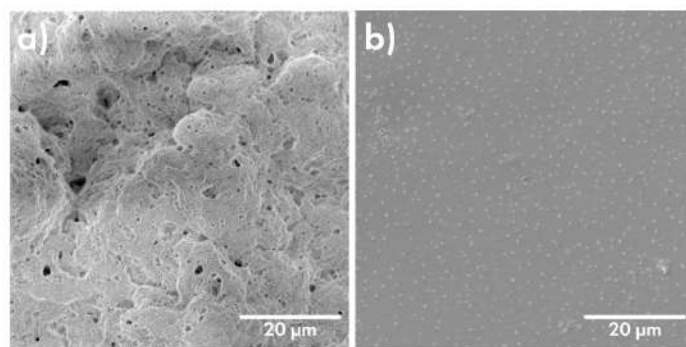


Figure 4.41: Surface of Irradiated PLGA film (a) and control (non-irradiated) sample (b) after 4 week incubation in PBS.

assess bulk hydrolysis for this timeframe. Nevertheless, after four weeks, the film was fully hydrolyzed, demonstrating an avalanche-like hydrolysis process.

Upon examination of the control sample incubated for one month, a similar stage of hydrolysis was observed compared to the second week of the irradiated sample. Only small sub-micron pores began to appear on the surface of the control sample (Fig. 4.41). Such acceleration of hydrolysis process can be attributed to significant chain cutting during irradiation. Gel-permetation Chromatography (GPC) analysis was performed for irradiated and control film to qualitatively determine the loss of molecular weight of polymer after 25 kGy irradiation. However, since there were no standard samples available to calibrate the chromatograph for this specific type of polymer, the data obtained does not provide absolute molecular masses of the polymer before and after irradiation (Tab. 4.16). Instead, it allows for the assessment of relative changes in masses, offering insight into the extent of the sterilization's impact.

The data in the Table 4.16 represents the results of GPC analysis for PLGA polymer before and after irradiation. Before irradiation (0 kGy), the number average molecular weight (M_n) of the PLGA polymer is 63748 g/mol, while the weight average molecular weight (M_w) is 135858 g/mol. The Polydispersity Index (PDI), calculated as the ratio of M_w to M_n , is 2.13.

After irradiation with a dose of 25 kGy, significant changes in the molecular

	M_n	M_w	PDI
0 kGy	63748	135858	2,13
25 kGy	16577	80182	4,8

Table 4.16: Data from GPC analysis for PLGA polymer before and after irradiation.

weight distribution of the PLGA polymer are observed. The M_n decreases to 16577 g/mol, indicating a reduction in the average molecular weight of the polymer chains. Similarly, the M_w decreases to 80182 g/mol. Consequently, the PDI increases to 4.8, reflecting a broader molecular weight distribution compared to the non-irradiated sample.

These results suggest that irradiation has led to chain scission and degradation of the PLGA polymer, resulting in a decrease in molecular weight and an increase in polydispersity. Such changes in molecular weight distribution can impact the mechanical properties, stability, and performance of the polymer in various applications, including drug delivery systems and biomedical implants.

4.4.2 Impact on release properties

To assess the impact of PVP addition, this approach was initially applied to films containing MB. Spectrophotometric calibration was conducted to evaluate the elution of MB, revealing a linear correlation between the absorption value at 664 nm and MB concentration for concentrations below 100 µg/ml (Fig. 3.4). Twelve samples were prepared following the main method described in section 4.2.3. Half of this samples was then sent to the Tecleor sterilization plant and subjected to a total dose of 25 kGy, a standard dose for medical implantable devices. Resulted films were incubated in 0.01 M PBS for 19 days to assess release profiles, depicted on Figure 4.42 . There is a significant difference in the drug release profiles between the control samples and the samples irradiated at 25 kGy.

For the control samples, approximately 9% of the drug was released over a period of 19 days. This indicates a slow and sustained release of the drug from the

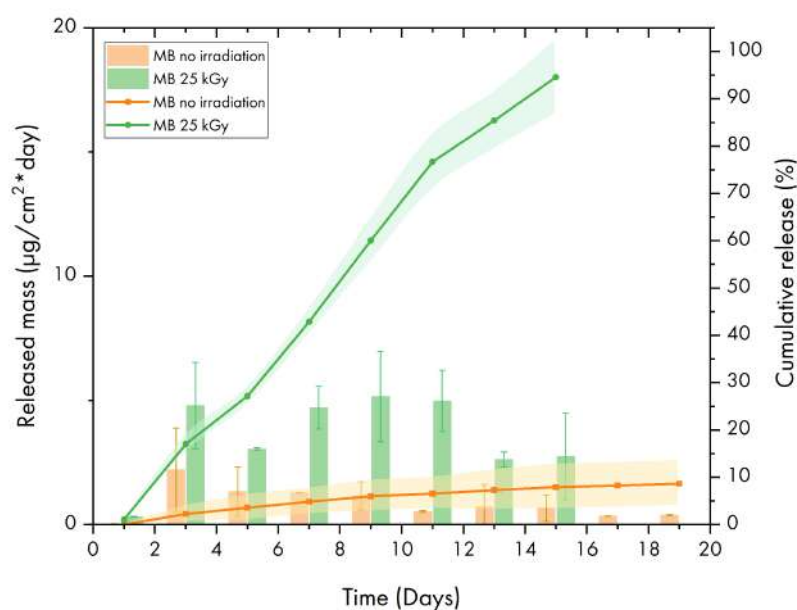


Figure 4.42: Daily and cumulative release profiles for the MB-loaded samples. Irradiated (in green) and non-irradiated (in orange).

polymer matrix over time. In contrast, the samples irradiated at 25 kGy exhibited a much higher cumulative drug release, with approximately 94% of the drug being released by day 15. This suggests a rapid and extensive release of the drug from the polymer matrix, possibly due to changes induced by the irradiation process.

The SEM images provide valuable insights into the microstructure of the samples, particularly highlighting differences between the control and irradiated samples. For the control samples, the SEM image reveals a lack of porosity, indicating a relatively dense and uniform structure (Fig. 4.43). Only wrinkles due to film stretching due to PVA swelling are visible on Figure 4.43b. This suggests that the polymer matrix maintains its integrity without significant degradation or damage. In contrast, the SEM image of the irradiated samples shows extensive destruction by hydrolysis, resulting in large holes and a porous structure, particularly in the drug-containing tracks (Fig. 4.43b-c). This confirms that the irradiation process has caused significant degradation and disruption of the polymer matrix, leading to increased porosity.

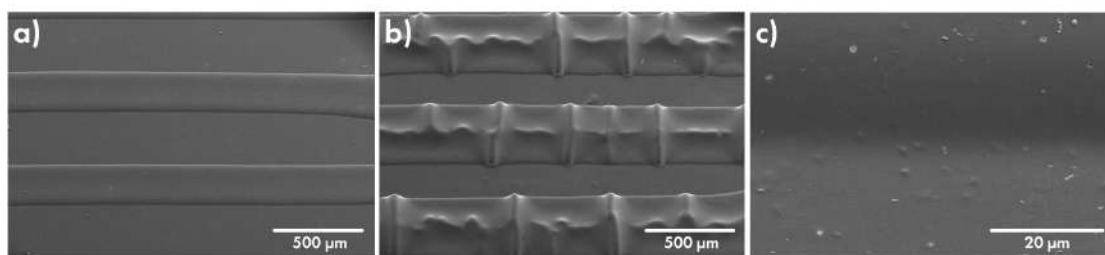


Figure 4.43: (a) Control sample surface before release; (b-c) Sample surface after incubation for 19 days in PBS.

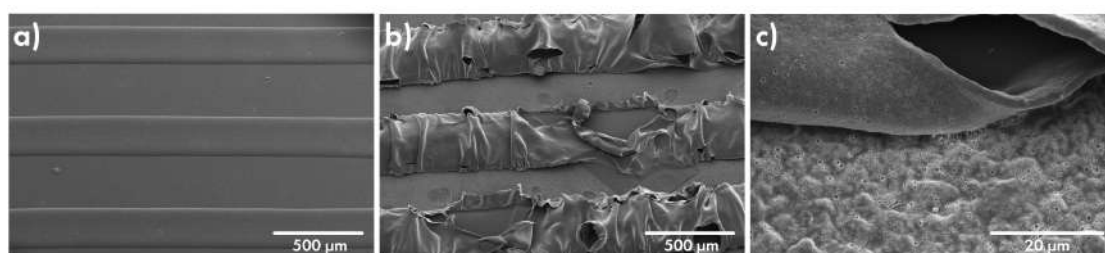


Figure 4.44: (a) Irradiated sample surface before release; (b-c) Sample surface after incubation for 15 days in PBS.

The data clearly demonstrate that irradiation at 25 kGy significantly accelerates drug release from the polymer matrix compared to the control samples, underscoring the impact of radiation on the material's drug release behavior. With the observed decrease in M_w and increase in polydispersity index post-sterilization, several implications for PLGA DDS emerge.

Firstly, adjustments to drug loading may be necessary to achieve the desired release profile post-sterilization, as alterations in molecular weight can affect drug release kinetics. The decrease in M_w also accelerates polymer matrix degradation, potentially leading to a heightened burst release of the drug. Strategies to mitigate this effect, such as modifying polymer composition may be warranted to maintain controlled release.

Furthermore, the impact of altered molecular weight and polydispersity on the long-term stability of the DDS necessitates stability studies to assess post-sterilization shelf-life and storage conditions. Exploring alternative sterilization methods or op-

timizing electron beam sterilization parameters may help minimize adverse effects on polymer properties. Considering the potential implications on in vivo performance, including pharmacokinetics and biodistribution, further investigations, including animal experiments, are essential to ensure the safety and efficacy of the sterilized DDS.

While irradiation accelerates polymer degradation to approximately three weeks, aligning well with the two-week release period, it may not be suitable for extended drug release without optimization, such as dose reduction. Thus, meticulous evaluation of polymer property changes post-sterilization is imperative for the consistent and predictable performance of PLGA DDS.

4.5 Multilayered film development

Since films are produced by the sequential deposition of individual layers, this process can be carried out either in several iterations, resulting in multilayer films with various additives, or by loading drugs separately into one layer. This feature allows the use of PLGA films for combination drug therapy, enabling the simultaneous administration of multiple chemotherapeutic agents. The goal is to achieve improved efficacy, enhanced pharmacokinetic properties, a synergistic effect, and reduced toxicity.

To evaluate the multilayer approach, a large-area film was created with alternating layers of PVA matrix, featuring pink and yellow fluorescent colorants, applied on a PLGA-coated PP substrate. Each PVA layer was separated by a PLGA film. The film, which covers an area of 36 cm², is depicted in Figure 4.45a, with an optical image shown in Figure 4.45b. The SEM image of the cryosection in Figure 4.45c shows the thickness of various layers: the drug layer is approximately 13 μm thick, the separating PLGA films are around 2 μm each, and the top covering film ranges from 10 to 15 μm.

Such a structure, depending on the thickness and quality of the separating layers, can enable sequential drug release. A simpler and more commonly used

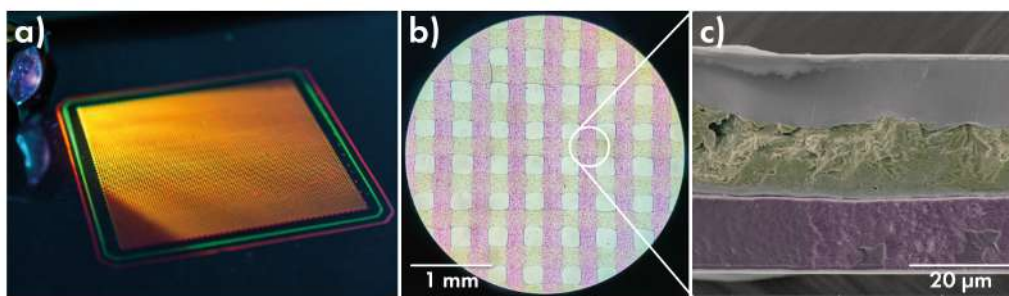


Figure 4.45: Large-area multilayered film under UV light (a), its optical image (b) and SEM image of cross-section (c).

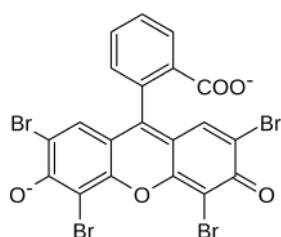


Figure 4.46: Formula of Eosine Y dye.

option is to release two drugs simultaneously. To simulate this approach, two dyes were chosen—Methylene Blue and Eosin Y—since both have fairly narrow absorption bands and can be detected in solution simultaneously (molecular formula of Eosin Y is presented on Fig. 4.46). The Figure 4.47b shows the obtained films, where the drugs were applied in the form of interpenetrating combs. Eosin, with good solubility close to that of drugs (about 500 μg/ml), was used as a drug model with a loading of 100 mg/ml in the PVA matrix. Methylene blue was used in a 20 mg/ml matrix load. To ensure rapid drug release, holes were made in the "teeth" of the comb. For MB, every strip was perforated, and for EY, every second strip was perforated to try to equalize the release rates of the substances (Fig. 4.47a , green dots). The figure shows normalized spectra of release solutions by day (a), as well as daily and cumulative release curves for multi-drug films (b). It can be observed that the release of MB is uneven, with a slight burst release on the first day followed by an increasing rate by day 6. In total, about 22% of the loaded 32 mg of substance was released by the end of the week. The release of

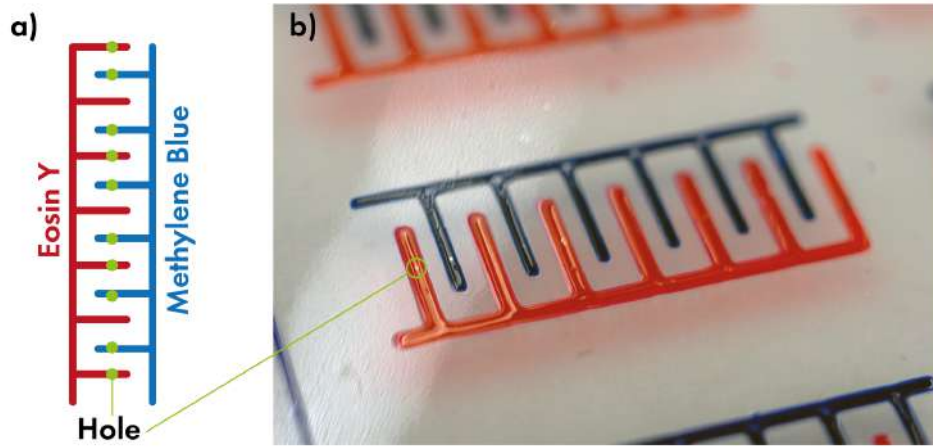


Figure 4.47: Perforation scheme (a) and resulting multi-drug films (b).

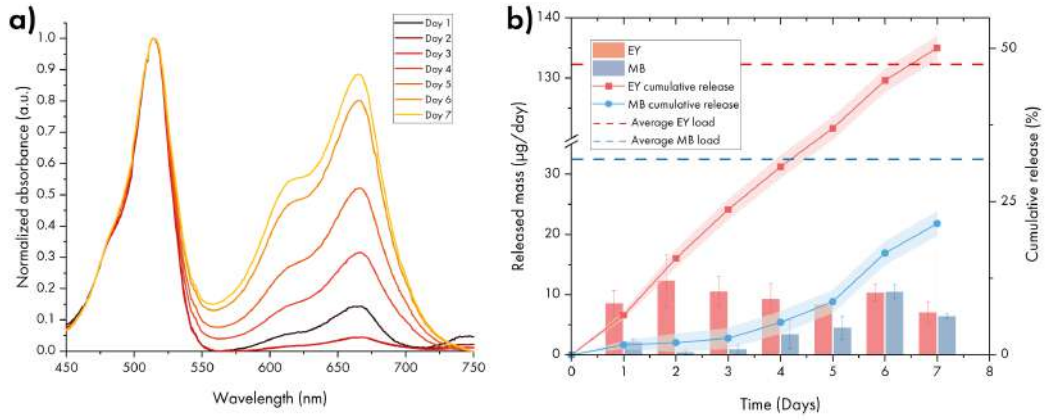


Figure 4.48: Absorption spectra of release solutions, day 1-7 (a). Daily and cumulative release curves for multi-drug films (b).

EY, on the other hand, is close to linear and fits the Zero-order equation perfectly (Table 4.17). Over the course of seven days, half of the loaded dye was released.

	$R_{obs-pre}$	R^2	MSE	MSE_{root}	AIC	MSC	
EY							
Zero-order	0.9983	0.9963	1.1762	1.0845	18.8656	4.9972	[H]
MB							
Peppas-Sahlin	0.9931	0.9856	1.2317	1.1098	20.5426	3.3559	

Table 4.17: The best GOF parameters for the multi-drug samples

Given the values for the Peppas-Sahlin model for MB dye release with $k_1 = 0.328$, $k_2 = 0.064$, and $m = 1.431$ (Table 4.18), we can conclude that the drug

	Parametr	Value
Zero-order	k_0	9.059
Peppas-Sahlin	k_1	0.328
	k_2	0.064
	m	1.431

Table 4.18: Best fit values for the 5-14 day range for samples with multiple drugs.

release from the polymeric system primarily follows a Super Case II transport mechanism. This indicates that the release mechanism is dominated by polymer relaxation, swelling, or erosion processes, with the diffusion mechanism playing a significant but less dominant role. The moderate value of k_1 suggests that Fickian diffusion is still an important component of the release process, while the smaller value of k_2 indicates that the relaxation-controlled release mechanism is less influential. The diffusion exponent m being greater than 1 signifies that the release rate increases over time due to substantial polymer relaxation or swelling.

At the same time, EY releases linearly with a fairly high rate constant $k_0 = 9.059$, which suggests that the substance diffuses through the holes at a constant speed. By comparing these two dosing regimens, several conclusions can be drawn. First, there is insufficient acceleration of the MB release. The release of MB is hampered by diffusion through a large amount of PVA, whereas molecules of highly soluble EY quickly diffuse to the exit point. This observation leads to the conclusion that combining poorly and highly soluble drugs in one coating requires much more precise tuning of their release, especially if the drugs must be released in close dosages.

Overall, the proof of concept for multidrug films is demonstrated, showcasing the potential and versatility of this technology. Possible difficulties, such as the uneven release rates between different drugs, have been identified. Nevertheless, the flexibility of the technology allows for varying the volume of medicine by layering less soluble drugs in multiple layers and better controlling the release through fine-tuning laser perforation. This adaptability can be crucial for optimizing combination drug therapies and achieving desired release profiles.

Chapter 5. PLACE Technology: application and adhesion Studies

5.1 Description of methods and research objects

Medical adhesive or adhesion system typically consists of a set of natural or synthetic monomers and oligomers or a polymer solution in an organic solvent. For adhesives used for functionalizing implantable devices, a comprehensive list of requirements is presented. First and foremost, adhesives must be biocompatible - not exert toxic effects on the patient, not cause irritation or allergic reactions, and have approval for use within the body. The adhesives used should also be bioresorbable, with the resorption time determined by the functional coating's working time (FT), and should not be less than that to prevent premature coating delamination; it should also not greatly exceed the FT for proper integration of the implantable device into the body. Adhesive systems should not contain components that dissolve the surface of the implant and/or polymer films. The compositions used should provide sufficient adhesion to the surface of the implant and be insoluble upon contact with body fluids. Convenience and ease of use are also important. Parameters such as the conditions and duration of possible adhesive storage, the number of components in the adhesive system, the viscosity of the active composition, and the speed of initial polymerization (life of the activated adhesive in liquid state) are considered. Several options for adhesive systems were considered during the analysis of the Russian market for medical adhesives:

1. Adhesives based on cyanoacrylate compositions, available under the trade names Sulfacrylate (Russia), Dermabond (USA), and others. Such medical adhesives are a mixture of the monomer 2-octyl cyanoacrylate with functional additives. Cyanoacrylate compositions have excellent adhesion to polymers and metals, are bioresorbable, have a long shelf life, and are inexpensive to manufacture. Among the disadvantages of such adhesives, undesirable chemical activity of the monomers

present in them can be distinguished, capable of partially dissolving the surface of biopolymers, and rapid adhesive polymerization. For testing, Sulfacrylate glue was selected - a surgical adhesive consisting of three main components: ethyl ester of α -cyanoacrylic acid, butyl acrylate, and methacrylate-3-oxysulphan, responsible, respectively, for the composition's polymerization, its elasticity, and antibacterial activity. Complete bioresorption of the adhesive occurs within 30–45 days from the moment it is applied to living tissue. The adhesive composition has high fluidity, allowing for uniform distribution of the composition over the surface of the implant in the form of a thin film; the polymerization rate of the adhesive system is about 30 seconds.

2. Adhesives based on silicone compositions (synthetic rubbers), actively used in prosthetics and implantology - Provox® (Sweden), Technovent (UK), Factor II (USA). Such adhesives are used in the construction of prostheses, as well as for fixing prostheses and other medical devices on human skin. In the polymerized state, silicone adhesives are completely inert and safe for the body; the compositions provide good adhesion to metals and have a long lifespan. However, this type of adhesive is not bioresorbable, so it was not used in the tests.

3. Fibrin adhesives are a two-component system consisting of fibrin and thrombin, isolated from doses of donor plasma or autologous plasma, i.e., the patient's own plasma. When the adhesive components are mixed, they form a dense fibrin film with excellent adhesion to living tissue. At the same time, in the scientific literature, the adhesion of fibrin glue to metals and polymers has not been adequately considered, which, in combination with other disadvantages of fibrin adhesives, namely: high cost ($>15,000$ rubles/ml), short shelf life (<4 hours at room temperature), and the risk of allergic reactions to foreign proteins; does not allow considering fibrin compositions as a reliable adhesive for testing.

4. Due to the insufficient supply of adhesives on the market, the thermal bonding method was also used for testing. The essence of the method lies in pre-coating the implantable device with a thin (several microns) layer of biopolymer from which drug-containing films are made. After placing the films on the implant,

the product undergoes a film baking process in a drying cabinet at the glass transition temperature of the biopolymer. The advantages of this method include the absence of the need to use other components, except those already used for the production of drug films; convenience of coating the implant, the possibility of adjusting the position of the drug film. However, the use of this method imposes additional conditions, namely: the need to take into account the increased final thickness of the coating when predicting the degradation time of the polymer, the need to select thermally stable drug substances, since the temperature range of 55-65°C is used for the baking of the main biopolymers (polylactic acid (PLA), polycaprolactone (PCL), polyglycolic acid (PGA), and its copolymers).

5.1.1 Materials used

As a model implant, samples obtained from LLC "Thios" were used, representing titanium plates measuring 20x20x4 mm with different surface roughness. Drug-containing films made from a copolymer of PLA and PGA in a ratio of 50:50

-

PURASORB® PDLG 5010 50:50 ratio (Corbion, Netherlands) were used for coating. The model drug used was the antibiotic Cefazolin (Lekko, Russia). The linear dimensions of the film samples were 8x12 mm.

5.1.2 Surface investigation of titanium Samples

Scanning electron microscopy was used to examine the surface of the obtained titanium samples. The overall appearance of the samples and microphotographs of the sample surfaces are shown in Figure 5.1.

The surface of the polished titanium sample is a flat plane with small scratches about 2-4 microns wide, left by the polishing abrasive. The surface roughness of the unpolished sample is significantly higher, with grain sizes of 10-15 microns. The surface of the sample with a trabecular structure is similar in roughness to the unpolished sample at the micro level, but on a macro scale, it resembles a

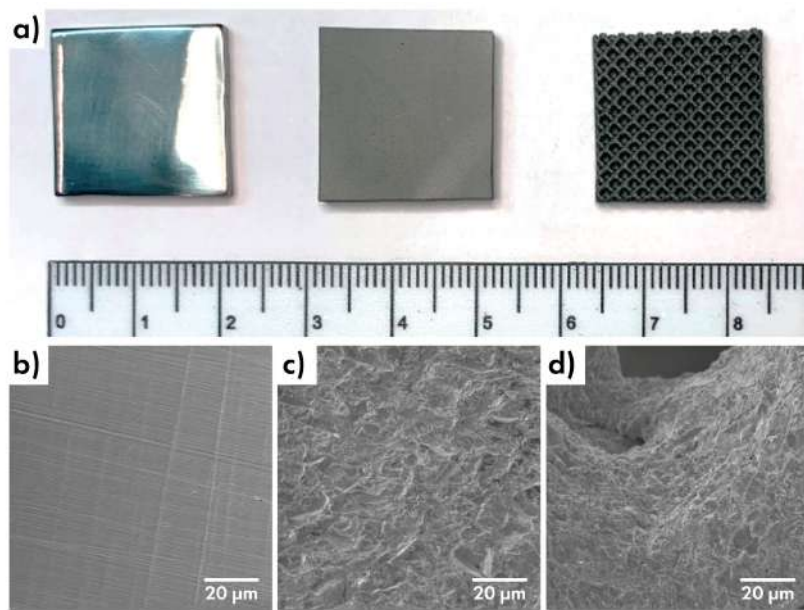


Figure 5.1: A - General view of the samples, from left to right: sample with a polished surface, sample with a rough surface, sample with a trabecular structure. B - Microphotograph of the polished sample surface, C - Microphotograph of the rough surface sample, D - Microphotograph of the sample surface with trabecular structure.

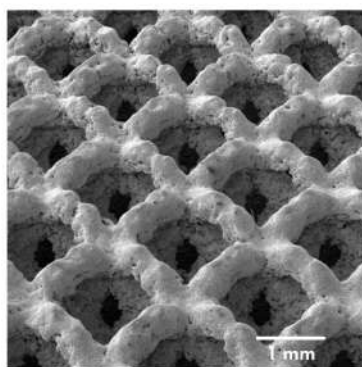


Figure 5.2: Microphotograph of the sample surface with trabecular structure.

volumetric mesh with a step between the peaks of about 2 mm (Fig. 5.2).

5.1.3 Fixation procedure

For the reproducibility of test conditions, it was decided to test fixation with Sulfacrylate and thermal bonding simultaneously. For thermal fixation, 3 μ l of a 10% PLGA solution in acetone was spread over half of the titanium sample surface, which was then dried in a drying cabinet for 30 minutes at 45°C. The sample was then wetted with ethyl alcohol to facilitate positioning and initial adhesion of the drug-containing films. After fixing the films, the titanium samples underwent thermal treatment in a drying cabinet for 30 minutes at 55°C.

For adhesive fixation of the polymer film with the drug on the surface of titanium samples, 1 μ l of Sulfacrylate adhesive was evenly spread in a thin layer over the remaining half of the sample surface. Subsequently, the drug film was fixed.

5.1.4 Evaluation of the reliability of polymer film fixation on the surface of a prosthesis with variable surface roughness and relief

To study adhesion under conditions close to those inside the body, prepared samples were placed in a physiological solution and incubated at 37°C for 7 days. After this period, the condition of the films was recorded, and a qualitative assessment of polymer film adhesion was conducted using the shear method. For

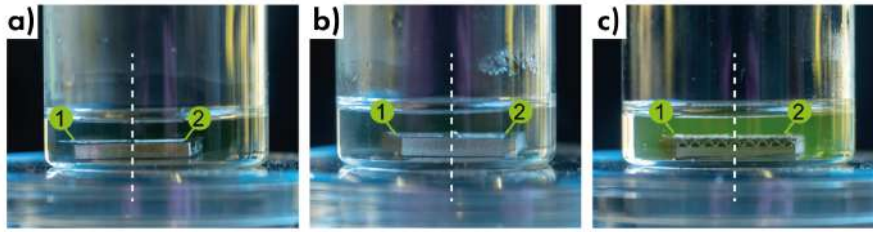


Figure 5.3: Samples with fixed films under a layer of physiological solution after 7 days of incubation. 1 - films fixed on Sulfacrylate, 2 - thermally fixed films. A - sample with a polished surface, B - sample with a rough surface, C - sample with a trabecular structure.

this purpose, samples incubated in the physiological solution were placed in a test setup consisting of a press with a soft pressing plate and loaded to a value of 25 g/cm². The surface of the pressing plate was covered with nitrile to provide the required coefficient of friction. Then, the loaded sample was slowly moved parallel to the surface of the pressing plate, thus pulling it out of the setup.

The criteria for assessing fixation reliability are the absence of film delamination, or the delamination of the film edge not exceeding 10%, or partial delamination not exceeding 20% over the entire area of the film after testing.

After 7 days of incubation in the physiological solution at 37°C, no delamination of drug-containing films was observed for both Sulfacrylate and thermally fixed films.

When testing film adhesion to metal using the shear method, the best results were obtained for the polished sample. After the test, the films remained uniformly fixed over the entire area (Fig. 5.4, A1 and A2). For rough samples, the results were worse; in particular, on sample B2 shown in 5.4, areas of film delamination are noticeable. Similar results were obtained for the sample with a trabecular surface structure (Fig. 5.4B, C1 and C2), where after testing, the edges of the films began to delaminate.

Analyzing the obtained data, it can be concluded that the surface roughness of the sample plays an important role in ensuring maximum adhesion. For the pol-

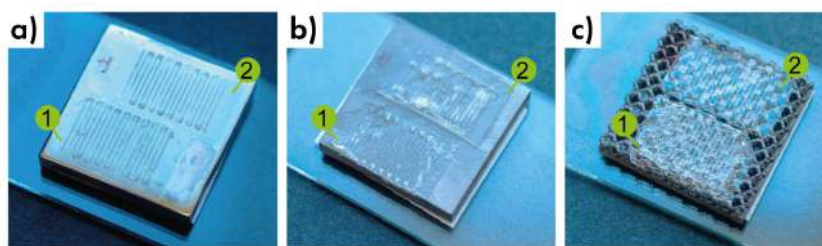


Figure 5.4: Samples with fixed films after qualitative assessment of polymer film adhesion using the shear method. 1 - films fixed on Sulfacrylate, 2 - thermally fixed films. A - sample with a polished surface, B - sample with a rough surface, C - sample with a trabecular structure.

ished sample, the contact area between the sample and the drug film is maximum, and the applied adhesive layer allows smoothing out all surface irregularities. The multimodal surface of the unpolished sample does not allow for even distribution of the adhesive over the surface and has a smaller contact area with the drug film compared to the polished sample. This results in weak adhesion of the film in areas of minimal contact and partial delamination from the sample upon physical impact. The surface of the sample with a trabecular structure allows fixing the film only on the peaks of the trabecular mesh, with the contact area being minimal, effectively, about 25% of the film area is fixed to the sample. With such fixation, unsecured edges and corners inevitably remain, which may result in delamination of the film upon physical impact.

According to the adhesion assessment criteria, both fixation methods - adhesive fixation with Sulfacrylate and thermal fixation - proved to be sufficiently reliable for solid samples. After testing on the polished sample, there were no delaminations or any defects. For the rough sample, the area of the delaminated film was calculated by analyzing the digital image. For the film fixed on Sulfacrylate, the total area of manifested defects was 2%. The defect area for the thermally fixed film was 6%, manifested as distributed defects, and about 5% as a delaminated film edge. The worst results were obtained for the titanium sample with a trabecular surface structure. The area of delaminated edges on trabecular samples was

about 23%, exceeding the specified criteria.

5.2 Evaluation of the effectiveness of methods for coating complex-shaped products with polymer films containing drugs

5.2.1 *Description of methods and research objects*

As part of the evaluation of the effectiveness of methods for applying polymer coatings containing drugs, two individual hip joint endoprotheses made of titanium served as the medical products with complex shapes. On one prosthesis, polymer coatings were applied using the patch method, which involves manufacturing and fixation of multiple small fragments of drug-containing polymer coating ($2\text{--}3\text{ cm}^2$) on the surface of the product, while the other prosthesis was coated using the template method, which involves placing and fixing relatively large fragments of drug-containing polymer coating ($10\text{--}15\text{ cm}^2$) on the product surface, which are cutouts of the prosthesis made according to its three-dimensional model. For both application methods, drug-containing coatings were made of a biocompatible and biodegradable polymer (a copolymer of PLGA and PGA in a 50:50 ratio - PURASORB® PDLG 5010 (Corbion, Netherlands)) with a thickness not exceeding $15\text{ }\mu\text{m}$, containing the antibacterial substance cefazolin at a concentration of $400\text{ }\mu\text{g}/\text{cm}^2$.

The effectiveness of coating methods is understood based on the following criteria: 1. Efficient and rational use of polymer raw materials and the possibility of its reuse; 2. Time spent on placing and fixing drug-containing polymer coatings; 3. Convenience and feasibility of applying polymer coatings.

5.2.2 *Patch method of application*

To evaluate the effectiveness of the patch method, the necessary number of polymer coating fragments with an area of 3 cm^2 was manufactured, representing

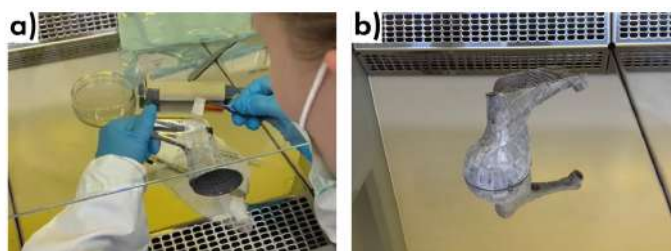


Figure 5.5: A - Procedure for applying a drug-containing polymer coating to the surface of an individual endoprosthesis using the patch method. B - Final view of the endoprosthesis with the drug coating.

a rectangle with sides of 1.5 and 2 cm, respectively. Figure 5.5A-B illustrates the procedure for applying the polymer coating in the form of patches to the surface of an individual titanium endoprosthesis, as well as the final result. Medical cyanoacrylate adhesive was used to fix the drug-containing polymer film to the prosthesis surface. 1 μ l of adhesive was evenly spread in a thin layer over an area of 1 cm² on the polished surface of the implant. Subsequently, the polymer film with the drug was fixed on the prosthesis by lightly pressing the polymer film with the drug onto the surface of the implant with the applied adhesive layer. On areas of the prosthesis with relief (areas for osseointegration), the adhesive consumption per unit area is 2-4 times higher compared to polished areas. This is due to the penetration of the adhesive into the complex relief and pores of this part of the prosthesis.

To fully coat the endoprosthesis with drug-containing polymer films using the patch method, 6 person-hours were spent. This inefficiency of the method is primarily due to the lack of a "plan" for the coating procedure. Essentially, the task boils down to covering the complex shape of the endoprosthesis, including spherical and cylindrical parts, bends, recesses, etc., with patches of fixed area and shape. The operator had to devise the placement of coating elements during their application and also adjust the shape of the patches by cutting them "on-site." Such a correction procedure leads to waste - parts of the drug-containing polymer coating (up to 10% of the initial total area of the patches). These waste materials,

including polymer, cannot be reused because the procedure for separating the polymer from the drug and other coating components is complex and impractical. In addition to the above-mentioned shortcomings of the method, it is worth noting a decrease in the quality of the finished product's appearance, caused by the presence of randomly oriented patches of coating with drugs of different shapes and areas on its surface. Despite the mentioned shortcomings of the method, this technology, due to its simplicity of implementation, may be suitable for coating individual custom-made endoprostheses of almost any shape for scientific research purposes. However, its application for commercial purposes for mass coating of various endoprostheses does not seem feasible.

5.2.3 Template method of application

The template method of application is based on the concept of creating fragments of a polymer coating containing drugs according to the shape and size intended for application to specific, pre-determined areas of the endoprosthesis surface. In total, several such polymer films cover the entire area of the prosthesis, repeating its surface relief as much as possible. The first stage of the template application method involves preparing a 3D model of the individual endoprosthesis. Typically, the 3D model of the prosthesis is represented as an *.stl file. The peculiarity of this format is the representation of model surfaces as triangles of varying area. Cutting such surfaces is associated with a number of difficulties, particularly due to the variable density of the triangular mesh, which may result in an excessive number of faces in certain areas of the template or the inability to create seams in the required surface area due to insufficient mesh density in that area. The surface retopology process (simplification and isotropization of mesh topology) is often applied to models obtained from sculpting or 3D scanning. There are several software packages available freely that allow for semi-automatic retopology of 3D models and can be used for commercial purposes. One such package is the Instant Meshes software (Open source). The program accepts 3D models in the

*.obj format as input data. Figure 5.6A-B shows the interface of the program, the initial model of the individual prosthesis loaded into the program, and the result of the program's work - a uniform square mesh formed on the surface of the 3D model of the implant, respectively. The main parameters for mesh configuration are the number of polygons (Figure 5.6A3) and the "comb" tool (Figure 5.6A4) used for local mesh orientation, particularly in areas of holes and complex curvature (transition from a sphere to a plane, etc.). For a typical model presented in Figure 5.6B, the number of polygons sufficient for forming a uniform mesh ranges from 20,000 to 25,000. For other types of prostheses, this number may increase or decrease according to the complexity of the model. Figure 5.7A-B shows a comparison of the same surface area of the 3D model in its initial *.stl format and after retopology in the Instant Meshes program, respectively. A uniform square mesh with minimal polygons different from the square is clearly observed. Meshes of this type significantly facilitate the task of placing seams on the model's surface for its cutting.

The second stage of the template method involves marking seams (lines along which the 3D model will be cut) on the surface of the implant model. This operation can be performed in several programs distributed freely with the ability to use for commercial purposes. In the context of this scientific research, Blender software was used - free and open-source software for working with 3D models in various formats.

When cutting the model, it is necessary to avoid forming sections of the template that have clearly pronounced curvature along two directions (spherical and other areas), especially when it comes to the cups of hip joint prostheses. Failure to comply with these limitations will result in the formation of folds and the inability of the coating to "fit" properly. Although polymer coatings are stretchable and deformable, excessive mechanical stress resulting from the placement and fixation of knowingly incorrectly cut coatings on the prosthesis surface can lead to the integrity of the coating being compromised and changes in the kinetics of drug release.

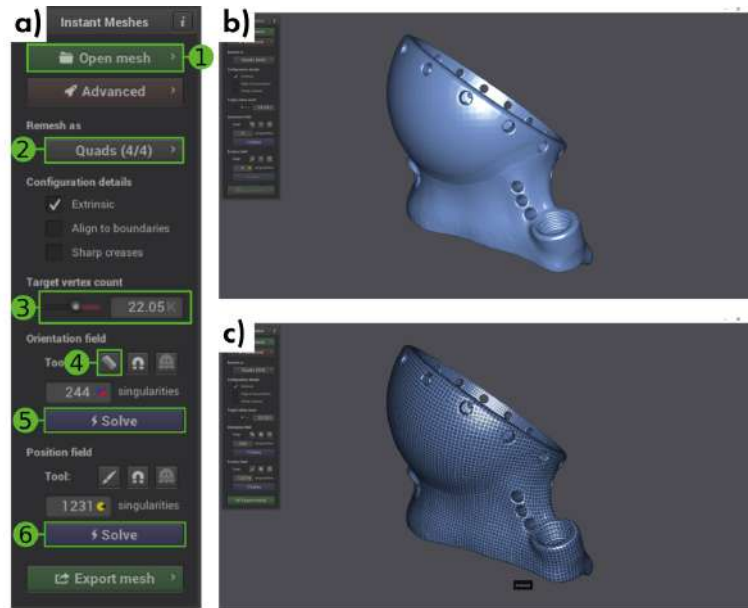


Figure 5.6: A - main control elements of the Instant Meshes program; 1 - model loading button, 2 - type of polygons used for mesh construction, 3 - number of polygons used for mesh construction, 4 - "comb" tool for manual local mesh orientation in areas of complex model geometry, 5,6 - buttons for building the orientation field of the mesh and the mesh itself, respectively. B - initial model loaded into the program, C - result of the program's work - a uniform square mesh formed on the surface of the 3D model.

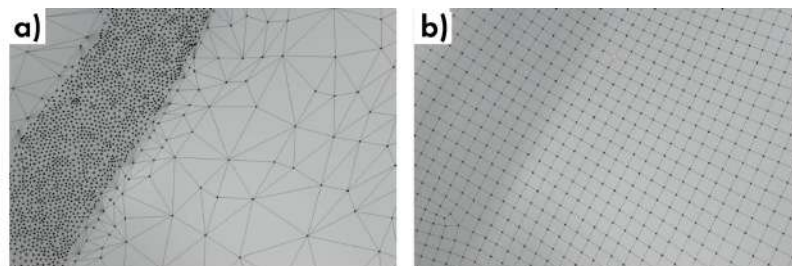


Figure 5.7: A - initial representation of the surface area of an individual prosthesis in *.stl format in the form of a triangular mesh of varying density. B - the same surface area, presented in the form of a uniform square mesh after semi-automatic retopology of the surface in the Instant Meshes program.

To indicate seams on the model surface, the necessary polygons are selected using the "Face select" tool. After selection, pressing the "Ctrl-E" key combination brings up a context menu from which the "Mark seam" option is chosen. Thus, on the model surface, a zone of polygons highlighted in red appears, indicating the seam along which the model will be cut. This operation is repeated as many times as necessary to apply the desired number of seams. Figure 5.8A-B presents the model of an individual hip joint prosthesis loaded into the Blender program with seams applied to its surface, as well as the result of cutting - a set of polymer coating shapes intended for placement on specific areas of the product, respectively. In Figure 5.8A, a calibration cube with a known side length was added to the model to maintain scale. The greatest number of seams was placed on the spherical part of the implant (Figure 5.8A1) for correct cutting, as well as on the area with a large diameter threaded hole (Figure 5.8A2), since this area of the model has a complex transition between geometries. The cutting of the 3D model of the prosthesis, presented in Figure 5.8B, is used for the production of polymer coatings of the required shape using the patented PLACE (printable adjustable cargo encapsulation) technology. Due to the manufacturing peculiarities, coating elements (patches) are formed on a single polymer substrate, from which they need to be cut out. The cutting process can be performed automatically using plotters with a rotary blade or laser cutting machines. Polymers used to create drug-containing coatings can be cut using commercially available laser radiation sources, such as a CO₂ laser.

For fixing the polymer film with medication on the prosthesis surface, medical cyanoacrylate adhesive was used. 1 μ L of adhesive was evenly spread in a thin layer over an area of 1 cm² on the implant surface. Afterward, individual cut pieces were fixed onto the prosthesis surface. The 3D model of the implant was used to orient the polymer coating fragments, with alignment based on the fastening holes on the cup for precise placement of the medication coating fragments in the required position. Figure 5.9A-B illustrates the process of applying drug-containing polymer coatings to the surface of an individual hip joint prosthesis using the die-

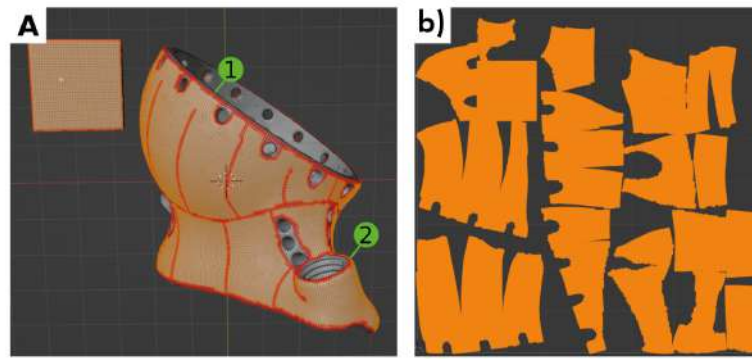


Figure 5.8: A - model of an individual implant after retopology with seams applied to it, along which the model will be cut. 1,2 - areas of the model with curvilinear geometry requiring a greater number of seams for cutting them into flat shapes. B - cutting of the prosthesis model along seams used to create individual drug-containing coatings.

cut method and the final result, respectively. The fixation of one polymer coating fragment took from 2 to 5 minutes depending on its size and shape. Taking into account the number of fragments, applying the polymer coating to the entire implant can take up to 90 minutes. Thus, the die-cut method is significantly more productive (at least 4 times) compared to the patch method. With the proper experience in placing polymer coating fragments on standard products, the application speed can be increased. Additionally, the polymer remaining on the substrate after cutting out the coating fragments can be reused since these areas do not contain medication or other components. This fact significantly increases the efficiency of raw material usage.

It's also worth noting the improvement in the external appearance of the product with polymer coatings compared to the patch method. When using the die-cut method, the polymer coating fragments and junction seams are uniformly oriented, and the fragments themselves cover a relatively larger area of the prosthesis surface, making the coating visually more cohesive.

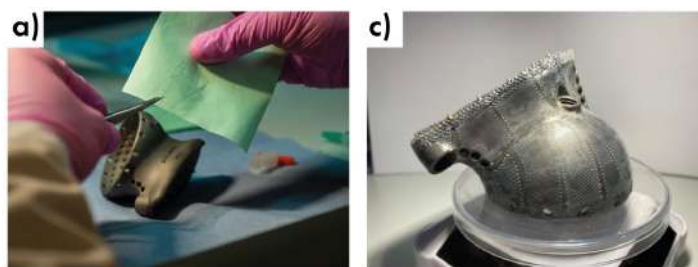


Figure 5.9: A - the process of applying drug-containing polymer coatings to the surface of a complex-shaped individual prosthesis using the die-cut method. B - the final appearance of the prosthesis with modified polymer film surfaces.

5.2.4 Conclusive remarks on applicability.

The research has shown that the template method of applying drug-containing coatings surpasses the patch method in all criteria. Specifically, the application procedure takes significantly less time (90 minutes), and the polymer raw material remaining after cutting patches of the required shape can be reused. Moreover, the produced polymer coatings are designed for specific parts of the prosthesis, making their application convenient and understandable. With training, the application time can be significantly reduced when applying coatings to standard products.

A search for adhesives and adhesive systems available for use was conducted, and their characteristics were evaluated, leading to the identification of the best options: medical cyanoacrylate adhesive and thermal bonding using a biopolymer.

The reliability of fixing polymer films on the surface of a prosthesis with variable roughness and different relief was evaluated using the proposed methods. According to the adhesion evaluation criteria, both fixation methods, cyanoacrylate adhesive bonding and thermal fixation, proved to be sufficiently reliable for solid samples. The largest area of defects was 11% detachment of the film for thermally fixed film on a rough surface sample. No visible defects were observed on films fixed on polished samples. The area of detached edges on trabecular samples exceeded 20%, attributed to the surface structure features and small contact area of drug films with the titanium surface.

In conclusion, both proposed systems, cyanoacrylate adhesive bonding and thermal fixation, are sufficiently reliable for fixing polymer films on the surface of a titanium prosthesis. The best adhesion results are achieved with minimal surface roughness of the samples. Increasing roughness, accompanied by a decrease in the contact area of the films with the prosthesis surface, reduces the quality of adhesion and requires the application of thicker layers of adhesive. In the case of prostheses with three-dimensional macrostructure, such as trabecular surface structure, the contact area between the implant surface and the drug film is insufficient for its reliable fixation. Films adhered to such surfaces may detach during implant installation and use. Additionally, applying films to the trabecular part of the prosthesis reduces access to trabecular voids and may likely lead to complications during osseointegration. Based on these facts, the research team concludes that applying films to the trabecular part is not advisable.

The results obtained in this research can be actively used to implement the procedure for creating and applying drug-containing polymer coatings in the production process of individual endoprostheses of complex shapes with various surface typologies. Below are the main advantages of working with films produced using the PLACE technology compared to other methods of forming thin polymer films on the surface of various medical devices (spraying, immersion, etc.):

1. The ability to finely adjust the kinetics of drug release by changing the permeability of its top layer during coating production.
2. Rational and efficient use of the drug component, as well as precise control of its absolute content in the coating due to automatic and localized placement of the drug layer on the surface of the polymer film.
3. The ability to achieve significant absolute values of drug substances per unit area of the coating ($>400 \text{ } \mu\text{g}/\text{cm}^2$), which significantly exceeds existing analogs.

Chapter 6. Economic feasibility, future outlook, and final conclusions

6.1 Cost-effectiveness and production feasibility of biodegradable PLACE films for medical applications

The economic viability and scalability of biocompatible, biodegradable films for drug delivery are promising, driven by the affordability of materials, feasible manufacturing methods, clinical benefits, regulatory compatibility, and long-term market potential.

Material Costs: The choice of medical-grade, biobased polymers provides an affordable base for these films, particularly as domestic suppliers in Russia can meet the demand, reducing import-related expenses. The films themselves are extremely thin, meaning that the material consumption remains low, even for mass production, further enhancing cost-effectiveness. Solvent-based processes also provide an efficient use of polymer solutions, allowing for precise deposition and minimal waste. Complementary materials, such as polyvinyl alcohol (PVA) and polyvinylpyrrolidone (PVP), are readily available at very low costs, making them ideal for structural support or porogen functions within the films. While the primary solvents used in production are economical, any shift toward more environmentally friendly solvents, like ethyl acetate or ethyl lactate, would increase costs slightly, though it might be justified by regulatory and market demands for sustainable practices.

Manufacturing Feasibility: The selected synthesis techniques, including 3D printing and direct coating, offer high scalability and versatility. These methods can readily be adapted to both small and large-scale production requirements. For applications that require individual, patient-specific implants, the current manufacturing setup can support a limited production volume, approximately hundreds of devices per year. However, this technology can be scaled up through a roll-to-

roll (R2R) production line, which would allow the high-throughput manufacture of standardized films for larger-scale clinical needs, potentially reaching tens of thousands of units per year. This flexibility ensures that the technology can be adapted from small-batch to mass production settings without major overhauls in infrastructure.

Clinical Benefits and Demand: The controlled-release and biodegradable characteristics of these films offer distinct clinical advantages. Localized drug delivery, enabled by the films' controlled-release mechanisms, can lower systemic side effects and improve patient compliance by providing sustained therapeutic effects at the target site. This is particularly beneficial in applications requiring infection prevention and combination drug therapies, such as wound care, implant coatings, and other localized treatments. By reducing infection rates, these materials could potentially shorten hospital stays, improve recovery times, and minimize the need for repeat interventions, thereby addressing a significant clinical demand in the market.

Regulatory and Safety Considerations: The use of biocompatible polymers was specifically chosen to facilitate regulatory approval, as these materials reduce the risk of adverse reactions and enhance patient safety. This simplifies the regulatory pathway, given that patient safety and predictable biodegradation are fundamental requirements in medical material approval processes. However, incorporating drugs into the films demands stringent regulatory oversight, as special conditions are needed to ensure drug stability and efficacy. Producing these films in sterile conditions, rather than relying on post-sterilization by radiation, preserves both the physical properties of the film and the therapeutic integrity of the drug. Leveraging the infrastructure of an existing clean room within a prosthetics production facility could streamline compliance with sterilization and regulatory standards while minimizing costs associated with additional facility requirements.

Long-term Potential and Return on Investment (ROI): These films' potential to improve clinical outcomes has a direct positive impact on ROI. By reducing the incidence of infections and the need for follow-up interventions, these mate-

rials could lower the overall healthcare costs associated with implant procedures and wound care. Furthermore, their adaptability for various therapeutic applications, combined with high scalability, suggests a strong long-term potential for both clinical adoption and financial sustainability. The market demand for safe, biodegradable, and effective drug-delivery systems positions this technology favorably for investment and clinical expansion, potentially achieving sustainable revenue through its broad applicability and patient-centered benefits.

6.2 Future directions and perspectives

The developed technology for controlled drug delivery using biodegradable polymer films offers a promising foundation for further innovation and clinical applications. Future work will aim to refine and expand upon the initial findings to optimize performance, enhance sustainability, and explore new biomedical applications. One key focus is the exploration of more stable porogens that offer both reliability and compatibility with biological systems. Investigating alternative polymers, such as poly(2-ethyl-2-oxazoline) or even biodegradable PVA nanoparticles, could allow for improved porosity control, greater material stability, and enhanced biocompatibility, leading to more finely tuned drug release profiles. Expanding the potential applications of these multilayered (ML) films is another exciting avenue. The technology shows promise for developing advanced wound healing patches that combine prolonged antimicrobial release with tissue regeneration properties. Additionally, the films could be adapted as self-expanding meshes suitable for endoscopic delivery, providing non-invasive, targeted treatment options for hard-to-reach areas in the body. To align with environmentally conscious practices, there is a strong motivation to develop greener production methods. This would involve replacing commonly used solvents with more bio-friendly options, such as ethyl acetate or ethyl lactate. Such a shift could reduce environmental impact and improve safety in manufacturing, making the process more sustainable and suitable for larger-scale production. Pilot testing in col-

laboration with SamSMU will serve as a critical step for process improvements and validation of clinical efficacy. Early-stage trials will help fine-tune technology parameters, optimize drug release kinetics, and address scalability challenges, providing data essential for regulatory approval and wider clinical adoption. Lastly, expanding the technology to encapsulate non-soluble drugs, peptides, and biologics represents a compelling future direction. By modifying the film structure and porogen composition, this platform could be adapted to deliver a broader range of therapeutics, including those that present solubility challenges, thereby broadening the clinical applications and treatment options available through this innovative material technology. In summary, these future steps will build on the success of the current work to advance the applicability, scalability, and sustainability of these films, ensuring their continued relevance in diverse medical fields and facilitating their transition from the lab to clinical settings.

6.3 Conclusion

Reservoir systems offer precise control over drug release kinetics but face challenges in manufacturing of such DEC. To address this, a coupling of additive manufacturing methods with reservoir-based systems was proposed. This approach named PLACE (Printed Layered Adjustable Cargo Encapsulation) aims to offer universality, scalability, and precise control over drug release profiles, benefiting both surface modification of medical devices and the creation of free-standing films for drug elution.

By simplifying the drug-eluting film fabrication process and applying the drug layer onto a flat base film using 3D printing, film damage from template interactions is eliminated. The Dr. Blade technique for forming the base film ensures thickness and uniformity, while 3D printing allows for rapid coating formation over large areas and predetermined shapes without physically impacting the film. The proposed technology utilizes a Computer Numerical Controlled (CNC) machine that dispenses drug-contained PVA solution over the base biopolymer film

in a programmable pattern. This CNC machine, assembled using a commercial 3D printer with minimal additional parts, offers flexibility and scalability for both laboratory and industrial settings.

Overall, The PLACE approach enhances the scalability and robustness of manufacturing processes for drug-eluting coatings. Through sequential steps of base film formation using the Dr. Blade technique, 3D printing of drug-contained PVA solution, and sealing with a cover polymer layer, precise control over drug release profiles is achieved. Preliminary tests have shown promising results, achieving control over the dosage of the drug, the shape of needed DEC's, and enabling printing speeds of up to 84 mm/s, allowing standard DEC's to be printed in minutes. This integrated approach addresses the challenges in manufacturing reservoir-based delivery systems, offering a promising solution for enhancing scalability and robustness in the production of drug-eluting coatings.

The evaluation and optimization of loading capacity per unit area of drug-eluting coatings (DEC's) are crucial for ensuring controlled and effective drug delivery. To address challenges related to printing aqueous solutions of drugs, enhance substrate wetting and provide necessary viscosity, Polyvinyl alcohol (PVA) was suggested as a promising option due to its FDA approval for human use, availability in medical-grade formulations, and compatibility with water-based solutions. Optimal dynamic viscosity for printing, enabling uniform extrusion without spillage onto the substrate surface, was selected and amounted to 370 mPa*s.

In the subsequent drug loading stage, Cefazolin sodium salt was chosen as a model drug due to its high water solubility and common use in treating bacterial infections. PLGA film samples with varying concentrations of Cefazolin were prepared and characterized. The ability to control the range of loaded medication was shown. Possible difficulties and limitations of the method, such as crystallization of the substance and an increase in the viscosity of concentrated solutions, were identified, and possible solutions were also shown.

The covering film's role in the drug delivery system was assessed, focusing on factors such as wettability, thickness, and durability. Poly(lactic-co-glycolic acid)

50:50 polymer was chosen as the covering film material due to its robust characteristics. The fabrication process for PLACE films involved sequential steps, including the initial application of a base film, followed by the deposition of medicinal hydrogel and the final application of a top film. These steps ensured controlled drug loading and effective film formation, contributing to the optimization of loading capacity per unit area for DEC's. For each step, optimal printing and application parameters were determined, allowing the production of low-defect films for long-term drug therapy. The parameters are listed in the Table 6.1.

As part of the work, the possibility of using films for prolonged release of a drug for more than 3 weeks without burst release was demonstrated. Methods have been proposed for a controlled increase in the rate of drug release through laser microperforation of films and the addition of pore-generating agents such as PEG or PVP. By selectively perforating the coating surface with laser energy, micro-sized pores can be created, enabling controlled drug release. This technique offers high spatial resolution and can be tailored to achieve specific release rates. Ability to control the release from films with both small ($40\text{-}100\text{ }\mu\text{g}/\text{cm}^2$) and large (up to $500\text{ }\mu\text{g}/\text{cm}^2$) loading's of drugs was shown.

Similar results were obtained for films containing the addition of polyvinylpyrrolidone as a porogen. It was demonstrated that PVP can be selectively removed after coating deposition, leaving behind porous structures that modulate drug diffusion rates. Using the example of small loads of Methylene Blue, the ability to significantly change the release of the substance from a one-week burst to a sustained duration of more than 2 weeks is shown. Sustained release for a large load of Vancomycin was demonstrated; the medicine was released completely and systematically within two weeks, falling within the required time of therapy.

The testing of the technology included studying the impact of radiation sterilization by accelerated electrons on drug-eluting coatings (DEC's). It was observed that neat polymer films underwent accelerated degradation under radiation. Additionally, irradiated PLACE films exhibited significantly accelerated drug release. Recommendations for optimizing sterilization procedures are suggested based on

Manufacture Stage	Optimized parameters and features needed to film forming	Resulted Features
Base film	Dynamic viscosity for solutions in TCM 70 mPa*s. Equal 7.5 wt.% solution of Corbion 5010 PLGA CS = 20 mm/s; AG = 50 μ m	Film thickness = 3-5 μ m
Cover film	Dynamic viscosity for solutions in TCM 70 mPa*s. Equal 7.5 wt.% solution of Corbion 5010 PLGA CS = 20 mm/s; AG = 50 μ m	Film thickness = 8-10 μ m
Drug layer	Needle size 23G Flow = 0.85 ml/h Printing speed = 15 mm/s Heating 40-50 °C Optimal drug conc. 20-200 mg/ml of matrix Infill 50% ZO = 150 μ m	Line width = 295 μ m Drug dose up to 500 μ m

Table 6.1: Base parameters for PLACE film for manufacturing

these findings.

In the testing phase, the template method for applying drug-containing coatings was compared to the patch method, and the former was found to be superior in terms of time efficiency and material reuse. Adhesive options for fixing polymer films on prosthetic surfaces were evaluated, with medical cyanoacrylate adhesive and thermal bonding identified as the best options. Adhesion reliability was tested on 3D-printed titanium blanks with varying surface roughness. It was concluded that both bonding methods are reliable on smoother surfaces but less effective on trabecular surfaces. Detachment was observed on rougher surfaces, suggesting caution when applying films to such areas. This research provides valuable insights for implementing drug-containing polymer coatings on complex-shaped endoprostheses, highlighting the advantages of using PLACE technology over other methods.

Finally, the following principles outcomes were achieved:

1. **Versatility:** This technology is versatile, accommodating a wide range of drug doses. For instance, it can handle small doses (40-100 $\mu\text{g}/\text{cm}^2$) for applications requiring precise drug administration, such as hormone therapy. Simultaneously, it can manage larger doses (up to 500 $\mu\text{g}/\text{cm}^2$) for acute treatments, like antibiotic delivery.
2. **Tailored Release Profiles:** With methods such as laser microperforation and the addition of porogens, PLACE allows for tailored release profiles. For instance, burst release can be mitigated to prevent sudden spikes in drug concentration, ensuring a smoother therapeutic response over time.
3. **Flexibility in Application:** PLACE technology can be adapted to various medical scenarios. For example, it can be used to create coatings for individual medical implants, providing localized drug delivery to prevent infections or promote tissue integration.

Overall, presented PLACE technology offers a customizable and adaptable

approach to drug delivery, promising improved patient outcomes and enhanced treatment efficacy across a wide range of medical applications.

Bibliography

- [1] “Sterilization for Medical Devices | FDA.”
- [2] S. J. Hong and M. K. Hong, “Drug-eluting stents for the treatment of coronary artery disease: A review of recent advances,” *Expert Opinion on Drug Delivery*, vol. 19, no. 3, pp. 269–280, 2022.
- [3] P. Shah and S. Chandra, “Review on emergence of nanomaterial coatings in bio-engineered cardiovascular stents,” *Journal of Drug Delivery Science and Technology*, vol. 70, apr 2022.
- [4] A. Kastrati, A. Dibra, J. Mehilli, S. Mayer, S. Pinieck, J. Pache, J. Dirschinger, and A. Schömig, “Predictive factors of restenosis after coronary implantation of sirolimus- or paclitaxel-eluting stents,” *Circulation*, vol. 113, pp. 2293–2300, may 2006.
- [5] J. C. Messenger, K. K. Ho, C. H. Young, L. E. Slattery, J. C. Draoui, J. P. Curtis, G. J. Dehmer, F. L. Grover, M. J. Mirro, M. R. Reynolds, I. C. Rokos, J. A. Spertus, T. Y. Wang, S. A. Winston, J. S. Rumsfeld, and F. A. Masoudi, “The National Cardiovascular Data Registry (NCDR) data quality brief: The NCDR Data Quality Program in 2012,” *Journal of the American College of Cardiology*, vol. 60, pp. 1484–1488, oct 2012.
- [6] R. A. Byrne, M. Joner, and A. Kastrati, “Stent thrombosis and restenosis: What have we learned and where are we going? the Andreas Grüntzig Lecture ESC 2014,” *European Heart Journal*, vol. 36, pp. 3320–3331, dec 2015.
- [7] S. H. Im, S. J. Park, J. J. Chung, Y. Jung, and S. H. Kim, “Creation of polylactide vascular scaffolds with high compressive strength using a novel melt-tube drawing method,” *Polymer*, vol. 166, pp. 130–137, mar 2019.

- [8] J. Fu, Y. Su, Y. X. Qin, Y. Zheng, Y. Wang, and D. Zhu, “Evolution of metallic cardiovascular stent materials: A comparative study among stainless steel, magnesium and zinc,” *Biomaterials*, vol. 230, p. 119641, feb 2020.
- [9] Z. Tu, Y. Zhong, H. Hu, D. Shao, R. Haag, M. Schirner, J. Lee, B. Sul-lenger, and K. W. Leong, “Design of therapeutic biomaterials to control inflammation,” *Nature Reviews Materials*, vol. 7, pp. 557–574, feb 2022.
- [10] T. N. Peel, A. C. Cheng, K. L. Busing, and P. F. Choong, “Microbiological aetiology, epidemiology, and clinical profile of prosthetic joint infections: Are current antibiotic prophylaxis guidelines effective?,” *Antimicrobial Agents and Chemotherapy*, vol. 56, pp. 2386–2391, may 2012.
- [11] A. W. Bridges and A. J. García, “Anti-inflammatory polymeric coatings for implantable biomaterials and devices,” *Journal of Diabetes Science and Technology*, vol. 2, pp. 984–994, nov 2008.
- [12] E. Lo, L. E. Nicolle, S. E. Coffin, C. Gould, L. L. Maragakis, J. Meddings, D. A. Pegues, A. M. Pettis, S. Saint, and D. S. Yokoe, “Strategies to Prevent Catheter-Associated Urinary Tract Infections in Acute Care Hospitals: 2014 Update,” *Infection Control Hospital Epidemiology*, vol. 35, pp. 464–479, may 2014.
- [13] S. S. Gupta, P. K. Irukulla, M. A. Shenoy, V. Nyemba, D. Yacoub, and Y. Kupfer, “Successful strategy to decrease indwelling catheter utilization rates in an academic medical intensive care unit,” *American Journal of Infection Control*, vol. 45, pp. 1349–1355, dec 2017.
- [14] J. Chadha, N. Thakur, S. Chhibber, and K. Harjai, “A comprehensive status update on modification of foley catheter to combat catheter-associated urinary tract infections and microbial biofilms,” 2023.

- [15] N. T. Ting and C. J. Della Valle, “Diagnosis of Periprosthetic Joint Infection—An Algorithm-Based Approach,” *Journal of Arthroplasty*, vol. 32, pp. 2047–2050, jul 2017.
- [16] P. R. Kuzyk, H. S. Dhotar, A. Sternheim, A. E. Gross, O. Safir, and D. Backstein, “Two-stage revision arthroplasty for management of chronic periprosthetic hip and knee infection: Techniques, controversies, and outcomes,” *Journal of the American Academy of Orthopaedic Surgeons*, vol. 22, pp. 153–164, mar 2014.
- [17] S. Alshimaysawee, R. Fadhel Obaid, M. E. Al-Gazally, A. Alexis Ramírez-Coronel, and M. S. Bathaei, “Recent Advancements in Metallic Drug-Eluting Implants,” *Pharmaceutics*, vol. 15, p. 223, jan 2023.
- [18] E. Sanchez-Rexach, E. Meaurio, and J.-R. Sarasua, “Recent developments in drug eluting devices with tailored interfacial properties,” *Advances in Colloid and Interface Science*, vol. 249, pp. 181–191, nov 2017.
- [19] Q. Wang, W. Chen, W. Zhu, D. J. McClements, X. Liu, and F. Liu, “A review of multilayer and composite films and coatings for active biodegradable packaging,” *npj Science of Food*, vol. 6, pp. 1–16, mar 2022.
- [20] P. Chichareon, Y. Katagiri, T. Asano, K. Takahashi, N. Kogame, R. Modolo, E. Tenekecioglu, C. C. Chang, M. Tomaniak, N. Kukreja, J. J. Wykrzykowska, J. J. Piek, P. W. Serruys, and Y. Onuma, “Mechanical properties and performances of contemporary drug-eluting stent: focus on the metallic backbone,” *Expert Review of Medical Devices*, vol. 16, pp. 211–228, mar 2019.
- [21] V. J. Suhardi, D. A. Bichara, S. J. Kwok, A. A. Freiberg, H. Rubash, H. Malchau, S. H. Yun, O. K. Muratoglu, and E. Oral, “A fully functional drug-eluting joint implant,” *Nature Biomedical Engineering*, vol. 1, pp. 1–11, jun 2017.

- [22] M. Gatti, S. Barnini, F. Guarracino, E. M. Parisio, M. Spinicci, B. Viaggi, S. D'ariento, S. Forni, A. Galano, and F. Gemmi, "Orthopaedic Implant-Associated Staphylococcal Infections: A Critical Reappraisal of Unmet Clinical Needs Associated with the Implementation of the Best Antibiotic Choice," *Antibiotics*, vol. 11, p. 406, mar 2022.
- [23] W. M. Gibson, "Can personalized medicine survive?," *Canadian family physician Medecin de famille canadien*, vol. 17, pp. 29–88, aug 1971.
- [24] R. Gupta, J. Kim, J. Spiegel, and S. M. Ferguson, "Developing products for personalized medicine: NIH Research Tools Policy applications," *Personalized Medicine*, vol. 1, pp. 115–124, dec 2004.
- [25] W. Burke and B. M. Psaty, "Personalized medicine in the era of genomics," *Jama*, vol. 298, pp. 1682–1684, oct 2007.
- [26] E. Abrahams, G. S. Ginsburg, and M. Silver, "The personalized medicine coalition: Goals and strategies," 2005.
- [27] A. Brand, "Public health genomics and personalized healthcare: A pipeline from cell to society," 2012.
- [28] C. Carlberg, "The need for education in personalized medicine," 2012.
- [29] W. Fierz, "Challenge of personalized health care: To what extent is medicine already individualized and what are the future trends?," 2004.
- [30] D. Zhang, Z. Yu, and C. Y. Chin, "Context-aware infrastructure for personalized healthcare," in *Studies in Health Technology and Informatics*, vol. 117, pp. 154–163, 2005.
- [31] H. Jang, S. Kim, and C. Bae, "Personalized healthcare through intelligent gadgets," in *Proceedings of the 30th Annual International Conference of the IEEE Engineering in Medicine and Biology Society, EMBS'08 - "Personalized Healthcare through Technology"*, pp. 3308–3311, 2008.

- [32] J. K. Nicholson and E. Holmes, “Global systems biology and personalized healthcare solutions.,” *Discovery medicine*, vol. 6, no. 32, pp. 63–70, 2006.
- [33] L. Hood, “A personal journey of discovery: developing technology and changing biology.,” *Annual review of analytical chemistry (Palo Alto, Calif.)*, vol. 1, pp. 1–43, 2008.
- [34] L. A. Simmons, M. A. Dinan, T. J. Robinson, and R. Snyderman, “Personalized medicine is more than genomic medicine: confusion over terminology impedes progress towards personalized healthcare,” *Personalized Medicine*, vol. 9, no. 1, pp. 85–91, 2012.
- [35] H. Park, A. Otte, and K. Park, “Evolution of drug delivery systems: From 1950 to 2020 and beyond,” *Journal of Controlled Release*, vol. 342, pp. 53–65, feb 2022.
- [36] P. Valent, B. Groner, U. Schumacher, G. Superti-Furga, M. Busslinger, R. Kralovics, C. Zielinski, J. M. Penninger, D. Kerjaschki, G. Stingl, J. S. Smolen, R. Valenta, H. Lassmann, H. Kovar, U. Jäger, G. Kornek, M. Müller, and F. Sörgel, “Paul Ehrlich (1854-1915) and His Contributions to the Foundation and Birth of Translational Medicine,” mar 2016.
- [37] J. K. Mills and D. Needham, “Targeted drug delivery,” *Expert Opinion on Therapeutic Patents*, vol. 9, no. 11, pp. 1499–1513, 1999.
- [38] M. Kinoshita, “Targeted Drug Delivery,” *MRI-Guided Focused Ultrasound Surgery*, pp. 147–159, 2007.
- [39] D. Rosenblum, N. Joshi, W. Tao, J. M. Karp, and D. Peer, “Progress and challenges towards targeted delivery of cancer therapeutics,” *Nature Communications*, vol. 9, dec 2018.
- [40] N. Bodor, “Soft drugs: Principles and methods for the design of safe drugs,” *Medicinal Research Reviews*, vol. 4, no. 4, pp. 449–469, 1984.

- [41] T. Hu, S. Lin, R. Du, M. Fu, Q. Rao, T. Yin, Y. Huang, and G. Wang, "Design, preparation and performance of a novel drug-eluting stent with multiple layer coatings," *Biomaterials Science*, vol. 5, no. 9, pp. 1845–1857, 2017.
- [42] B. D. Weinberg, E. Blanco, and J. Gao, "Polymer implants for intratumoral drug delivery and cancer therapy," 2008.
- [43] L. Gao, S. Cai, A. Cai, Y. Zhao, T. Xu, Y. Ma, Y. Xu, Y. Wang, H. Wang, and Y. Hu, "The improved antitumor efficacy of continuous intratumoral chemotherapy with cisplatin-loaded implants for the treatment of sarcoma 180 tumor-bearing mice," *Drug Delivery*, vol. 26, no. 1, pp. 208–215, 2019.
- [44] T. D. Moshood, G. Nawanir, F. Mahmud, F. Mohamad, M. H. Ahmad, and A. AbdulGhani, "Biodegradable plastic applications towards sustainability: A recent innovations in the green product," *Cleaner Engineering and Technology*, vol. 6, p. 100404, feb 2022.
- [45] C. Stettler, S. Wandel, S. Allemann, A. Kastrati, M. C. Morice, A. Schömig, M. E. Pfisterer, G. W. Stone, M. B. Leon, J. S. de Lezo, J. J. Goy, S. J. Park, M. Sabaté, M. J. Suttorp, H. Kelbaek, C. Spaulding, M. Menichelli, P. Vermeersch, M. T. Dirksen, P. Cervinka, A. S. Petronio, A. J. Nordmann, P. Diem, B. Meier, M. Zwahlen, S. Reichenbach, S. Trelle, S. Windecker, and P. Jüni, "Outcomes associated with drug-eluting and bare-metal stents: a collaborative network meta-analysis," *Lancet*, vol. 370, no. 9591, pp. 937–948, 2007.
- [46] R. Pantani and A. Sorrentino, "Influence of crystallinity on the biodegradation rate of injection-moulded poly(lactic acid) samples in controlled composting conditions," *Polymer Degradation and Stability*, vol. 98, pp. 1089–1096, may 2013.

- [47] I. Rykowska, I. Nowak, and R. Nowak, “Drug-eluting stents and balloons-materials, structure designs, and coating techniques: A review,” *Molecules*, vol. 25, no. 20, 2020.
- [48] S. Liparoti, V. Iozzino, V. Speranza, and R. Pantani, “Modulating poly(lactic acid) degradation rate for environmentally sustainable applications,” *Waste Management*, vol. 175, pp. 215–224, mar 2024.
- [49] C. G. Pitt, M. M. Gratzl, A. R. Jeffcoat, R. Zweidinger, and A. Schindler, “Sustained drug delivery systems II: Factors affecting release rates from poly(ϵ -caprolactone) and related biodegradable polyesters,” *Journal of Pharmaceutical Sciences*, vol. 68, no. 12, pp. 1534–1538, 1979.
- [50] T. Iwata and Y. Doi, “Morphology and enzymatic degradation of poly(L-lactic acid) single crystals,” *Macromolecules*, vol. 31, pp. 2461–2467, apr 1998.
- [51] K. Van de Velde and P. Kiekens, “Biopolymers: overview of several properties and consequences on their applications,” *Polymer Testing*, vol. 21, pp. 433–442, jan 2002.
- [52] M. Ajioka, K. Enomoto, K. Suzuki, and A. Yamaguchi, “The basic properties of poly(lactic acid) produced by the direct condensation polymerization of lactic acid,” *Journal of Environmental Polymer Degradation*, vol. 3, pp. 225–234, oct 1995.
- [53] N. A. Weir, F. J. Buchanan, J. F. Orr, D. F. Farrar, and A. Boyd, “Processing, annealing and sterilisation of poly-L-lactide,” *Biomaterials*, vol. 25, pp. 3939–3949, aug 2004.
- [54] G. Li, M. Zhao, F. Xu, B. Yang, X. Li, X. Meng, L. Teng, F. Sun, and Y. Li, “Synthesis and Biological Application of Polylactic Acid,” 2020.

- [55] S. Sato, D. Gondo, T. Wada, S. Kanehashi, and K. Nagai, “Effects of various liquid organic solvents on solvent-induced crystallization of amorphous poly(lactic acid) film,” *Journal of Applied Polymer Science*, vol. 129, pp. 1607–1617, aug 2013.
- [56] K. Madhavan Nampoothiri, N. R. Nair, and R. P. John, “An overview of the recent developments in polylactide (PLA) research,” 2010.
- [57] H. K. Makadia and S. J. Siegel, “Poly Lactic-co-Glycolic Acid (PLGA) as biodegradable controlled drug delivery carrier,” *Polymers*, vol. 3, pp. 1377–1397, sep 2011.
- [58] P. Gentile, V. Chiono, I. Carmagnola, and P. V. Hatton, “An overview of poly(lactic-co-glycolic) Acid (PLGA)-based biomaterials for bone tissue engineering,” *International Journal of Molecular Sciences*, vol. 15, pp. 3640–3659, feb 2014.
- [59] D. N. Kapoor, A. Bhatia, R. Kaur, R. Sharma, G. Kaur, and S. Dhawan, “PLGA: A unique polymer for drug delivery,” *Therapeutic Delivery*, vol. 6, pp. 41–58, jan 2015.
- [60] C. D’Avila Carvalho Erbetta, “Synthesis and Characterization of Poly(D,L-Lactide-co-Glycolide) Copolymer,” *Journal of Biomaterials and Nanobiotechnology*, vol. 03, no. 02, pp. 208–225, 2012.
- [61] M. Labet and W. Thielemans, “Synthesis of polycaprolactone: A review,” *Chemical Society Reviews*, vol. 38, pp. 3484–3504, nov 2009.
- [62] M. Bartnikowski, T. R. Dargaville, S. Ivanovski, and D. W. Hutmacher, “Degradation mechanisms of polycaprolactone in the context of chemistry, geometry and environment,” *Progress in Polymer Science*, vol. 96, pp. 1–20, sep 2019.

- [63] B. D. Ulery, L. S. Nair, and C. T. Laurencin, “Biomedical applications of biodegradable polymers,” *Journal of Polymer Science, Part B: Polymer Physics*, vol. 49, pp. 832–864, jun 2011.
- [64] A. Cipitria, A. Skelton, T. R. Dargaville, P. D. Dalton, and D. W. Huttmacher, “Design, fabrication and characterization of PCL electrospun scaffolds - A review,” *Journal of Materials Chemistry*, vol. 21, pp. 9419–9453, jul 2011.
- [65] A. A. Jose, S. H. Hazeena, N. M. Lakshmi, A. K. B, A. Madhavan, R. Sirohi, A. Tarafdar, R. Sindhu, M. K. Awasthi, A. Pandey, and P. Binod, “Bacterial biopolymers: From production to applications in biomedicine,” *Sustainable Chemistry and Pharmacy*, vol. 25, p. 100582, apr 2022.
- [66] H. Tsuji and K. Suzuyoshi, “Environmental degradation of biodegradable polyesters 1. Poly(ϵ -caprolactone), poly[(R)-3-hydroxybutyrate], and poly(L-lactide) films in controlled static seawater,” *Polymer Degradation and Stability*, vol. 75, no. 2, pp. 347–355, 2002.
- [67] G. Rivera-Hernández, M. Antunes-Ricardo, P. Martínez-Morales, and M. L. Sánchez, “Polyvinyl alcohol based-drug delivery systems for cancer treatment,” *International Journal of Pharmaceutics*, vol. 600, p. 120478, may 2021.
- [68] M. I. Baker, S. P. Walsh, Z. Schwartz, and B. D. Boyan, “A review of polyvinyl alcohol and its uses in cartilage and orthopedic applications,” *Journal of Biomedical Materials Research - Part B Applied Biomaterials*, vol. 100 B, pp. 1451–1457, jul 2012.
- [69] A. Kumar and S. S. Han, “PVA-based hydrogels for tissue engineering: A review,” *International Journal of Polymeric Materials and Polymeric Biomaterials*, vol. 66, pp. 159–182, mar 2017.

- [70] Y. Cai, J. Che, M. Yuan, X. Shi, W. Chen, and W. E. Yuan, "Effect of glycerol on sustained insulin release from PVA hydrogels and its application in diabetes therapy," *Experimental and Therapeutic Medicine*, vol. 12, pp. 2039–2044, oct 2016.
- [71] S. L. Bourke, M. Al-Khalili, T. Briggs, B. B. Michniak, J. Kohn, and L. A. Poole-Warren, "A photo-crosslinked poly(vinyl alcohol) hydrogel growth factor release vehicle for wound healing applications," *AAPS PharmSci*, vol. 5, no. 4, 2003.
- [72] P. K. Panda, K. Sadeghi, and J. Seo, "Recent advances in poly (vinyl alcohol)/natural polymer based films for food packaging applications: A review," *Food Packaging and Shelf Life*, vol. 33, sep 2022.
- [73] A. K. Yontar, S. Çevik, and O. Yontar, "Green production of plant/collagen-based antibacterial polyvinyl alcohol (PVA) nanocomposite films," *Sustainable Chemistry and Pharmacy*, vol. 33, p. 101119, jun 2023.
- [74] V. S. Ghorpade, R. J. Dias, K. K. Mali, and S. I. Mulla, "Citric acid crosslinked carboxymethylcellulose-polyvinyl alcohol hydrogel films for extended release of water soluble basic drugs," *Journal of Drug Delivery Science and Technology*, vol. 52, pp. 421–430, aug 2019.
- [75] R. W. Korsmeyer, R. Gurny, E. Doelker, P. Buri, and N. A. Peppas, "Mechanisms of solute release from porous hydrophilic polymers," *International Journal of Pharmaceutics*, vol. 15, pp. 25–35, may 1983.
- [76] P. L. Ritger and N. A. Peppas, "A simple equation for description of solute release I. Fickian and non-fickian release from non-swellable devices in the form of slabs, spheres, cylinders or discs," *Journal of Controlled Release*, vol. 5, pp. 23–36, jun 1987.

- [77] M. L. Laracuenta, M. H. Yu, and K. J. McHugh, “Zero-order drug delivery: State of the art and future prospects,” *Journal of Controlled Release*, vol. 327, pp. 834–856, nov 2020.
- [78] N. A. Peppas and J. J. Sahlin, “A simple equation for the description of solute release. III. Coupling of diffusion and relaxation,” *International Journal of Pharmaceutics*, vol. 57, pp. 169–172, dec 1989.
- [79] Y. Fu and W. J. Kao, “Drug release kinetics and transport mechanisms of non-degradable and degradable polymeric delivery systems,” *Expert Opinion on Drug Delivery*, vol. 7, pp. 429–444, apr 2010.
- [80] H. J. Haroosh, Y. Dong, S. Jasim, and S. Ramakrishna, “Improvement of drug release and compatibility between hydrophilic drugs and hydrophobic nanofibrous composites,” *Materials*, vol. 14, sep 2021.
- [81] S. Jin, M. A. A. Newton, H. Cheng, Q. Zhang, W. Gao, Y. Zheng, Z. Lu, Z. Dai, and J. Zhu, “Progress of Hydrogel Dressings with Wound Monitoring and Treatment Functions,” *Gels*, vol. 9, p. 694, aug 2023.
- [82] J. Su, J. Li, J. Liang, K. Zhang, and J. Li, “Hydrogel preparation methods and biomaterials for wound dressing,” *Life*, vol. 11, oct 2021.
- [83] S. Mitura, A. Sionkowska, and A. Jaiswal, “Biopolymers for hydrogels in cosmetics: review,” *Journal of Materials Science: Materials in Medicine*, vol. 31, jun 2020.
- [84] Y. Liu, W. Wang, G. Acharya, Y. B. Shim, E. S. Choe, and C. H. Lee, “Advanced stent coating for drug delivery and in vivo biocompatibility,” *Journal of Nanoparticle Research*, vol. 15, p. 1962, oct 2013.
- [85] A. Thakkar, A. Raval, R. Mandal, S. Parmar, A. Jariwala, J. Tailor, and A. Mehta, “Development and Evaluation of Drug Eluting Stent Having Biphasic Release From a Single Layer of Biodegradable Polymer,” *Journal of Medical Devices, Transactions of the ASME*, vol. 7, no. 1, pp. 1–5, 2013.

- [86] D. M. Kim, B. S. Lee, J. H. Kang, J. Choi, K. Park, T. I. Son, M. H. Jeong, and D. K. Han, "Fabrication and controlled release of electrosprayed ReoPro-loaded metal surface for vascular stent," *Macromolecular Research*, vol. 19, pp. 501–506, may 2011.
- [87] H. B. Hopfenberg, "Controlled Release From Erodible Slabs, Cylinders, and Spheres.," *Am Chem Soc Div Org Coat Plast Chem Prepr*, vol. 36, no. 1, pp. 229–234, 1976.
- [88] X. Chen and C. P. Ooi, "Hydrolytic degradation and drug release properties of ganciclovir-loaded biodegradable microspheres," *Acta Biomaterialia*, vol. 4, no. 4, pp. 1046–1056, 2008.
- [89] E. J. Rodriguez, B. Marcos, and M. A. Huneault, "Hydrolysis of polylactide in aqueous media," *Journal of Applied Polymer Science*, vol. 133, no. 44, 2016.
- [90] F. V. Burkersroda, L. Schedl, and A. Göpferich, "Why degradable polymers undergo surface erosion or bulk erosion," *Biomaterials*, vol. 23, no. 21, pp. 4221–4231, 2002.
- [91] H. Sun, L. Mei, C. Song, X. Cui, and P. Wang, "The in vivo degradation, absorption and excretion of PCL-based implant," *Biomaterials*, vol. 27, pp. 1735–1740, mar 2006.
- [92] D. D. Rao, J. S. Vorhies, N. Senzer, and J. Nemunaitis, "siRNA vs. shRNA: Similarities and differences," *Advanced Drug Delivery Reviews*, vol. 61, pp. 746–759, jul 2009.
- [93] S. Kuramitsu, M. Iwabuchi, H. Yokoi, T. Domei, S. Sonoda, T. Hiromasa, T. Morinaga, Y. Kobayashi, K. Ohe, K. Goya, K. Yamaji, M. Hyodo, Y. Soga, K. Kondo, S. Shirai, K. Ando, K. Sakai, and M. Nobuyoshi, "Incidence and clinical impact of stent fracture after the Nobori biolimus-eluting

- stent implantation.,” *Journal of the American Heart Association*, vol. 3, no. 2, 2014.
- [94] G. Lemesle, G. Schurtz, and C. Delhay, “Biolimus-eluting stent with biodegradable polymer (Nobori®): An overview of recent clinical results, SORT OUT V and COMPARE II trials,” *Expert Review of Cardiovascular Therapy*, vol. 11, no. 10, pp. 1293–1296, 2013.
- [95] R. Waksman, R. Pakala, R. Baffour, R. Seabron, D. Hellenga, R. Chan, S. H. Su, F. Kolodgie, and R. Virmani, “In vivo comparison of a polymer-free Biolimus A9-eluting stent with a biodegradable polymer-based Biolimus A9 eluting stent and a bare metal stent in balloon denuded and radiated hypercholesterolemic rabbit iliac arteries,” *Catheterization and Cardiovascular Interventions*, vol. 80, no. 3, pp. 429–436, 2012.
- [96] G. F. Prado, A. A. Abizaid, G. C. Meireles, R. Sarmiento-Leite, M. Prudente, M. Cantarelli, A. D. Dourado, J. M. Jr, M. A. Perin, C. Costantini, R. Costa, J. R. Costa, D. Chamie, C. M. Campos, E. E. Ribeiro, and P. A. Lemos, “Comparative clinical performance of two types of drug-eluting stents with abluminal biodegradable polymer coating: Five-year results of the DESTINY randomized trial,” *Revista Portuguesa de Cardiologia*, vol. 40, no. 2, pp. 71–76, 2021.
- [97] S. Windecker, P. W. Serruys, S. Wandel, P. Buszman, S. Trznadel, A. Linke, K. Lenk, T. Ischinger, V. Klauss, F. Eberli, R. Corti, W. Wijns, M. C. Morice, C. di Mario, S. Davies, R. J. van Geuns, P. Eerdmans, G. A. van Es, B. Meier, and P. Jüni, “Biolimus-eluting stent with biodegradable polymer versus sirolimus-eluting stent with durable polymer for coronary revascularisation (LEADERS): a randomised non-inferiority trial,” *The Lancet*, vol. 372, pp. 1163–1173, sep 2008.

- [98] J. Bennett and C. Dubois, “A novel platinum chromium everolimus-eluting stent for the treatment of coronary artery disease,” *Biologics: Targets and Therapy*, vol. 7, pp. 149–159, jun 2013.
- [99] S. Liu, J. Yu, H. Li, K. Wang, G. Wu, B. Wang, M. Liu, Y. Zhang, P. Wang, J. Zhang, J. Wu, Y. Jing, F. Li, and M. Zhang, “Controllable Drug Release Behavior of Polylactic Acid (PLA) Surgical Suture Coating with Ciprofloxacin (CPFX)—Polycaprolactone (PCL)/Polyglycolide (PGA),” *Polymers 2020, Vol. 12, Page 288*, vol. 12, p. 288, feb 2020.
- [100] R. A. Keraliya, C. Patel, P. Patel, V. Keraliya, T. G. Soni, R. C. Patel, and M. M. Patel, “Osmotic Drug Delivery System as a Part of Modified Release Dosage Form,” *ISRN Pharmaceutics*, vol. 2012, pp. 1–9, jul 2012.
- [101] F. Theeuwes, “Elementary osmotic pump,” *Journal of Pharmaceutical Sciences*, vol. 64, pp. 1987–1991, dec 1975.
- [102] A. Geraili, M. Xing, and K. Mequanint, “Design and fabrication of drug-delivery systems toward adjustable release profiles for personalized treatment,” *View*, vol. 2, p. 20200126, oct 2021.
- [103] T. Ghosh and A. Ghosh, “Drug delivery through osmotic systems - An overview,” *Journal of Applied Pharmaceutical Science*, vol. 1, no. 2, pp. 38–49, 2011.
- [104] R. K. Verma, D. M. Krishna, and S. Garg, “Formulation aspects in the development of osmotically controlled oral drug delivery systems,” *Journal of Controlled Release*, vol. 79, pp. 7–27, feb 2002.
- [105] F. Theeuwes, R. J. Saunders, and W. S. Mefford, “Process for forming outlet passageways in pills using a laser,” feb 1978.
- [106] C.-M. Chen, D.-Y. Lee, and J. Xie, “Controlled release formulation for water insoluble drugs in which a passageway is formed in situ,” apr 1998.

- [107] J. Guan, H. He, L. J. Lee, and D. J. Hansford, “Fabrication of particulate reservoir-containing, capsulelike, and self-folding polymer microstructures for drug delivery,” *Small*, vol. 3, pp. 412–418, mar 2007.
- [108] M. V. Kiryukhin, S. M. Man, S. R. Gorelik, G. S. Subramanian, H. Y. Low, and G. B. Sukhorukov, “Fabrication and mechanical properties of microchambers made of polyelectrolyte multilayers,” *Soft Matter*, vol. 7, pp. 6550–6556, jul 2011.
- [109] M. Gai, J. Frueh, T. Tao, A. V. Petrov, V. V. Petrov, E. V. Shesterikov, S. I. Tverdokhlebov, and G. B. Sukhorukov, “Polylactic acid nano- and microchamber arrays for encapsulation of small hydrophilic molecules featuring drug release via high intensity focused ultrasound,” *Nanoscale*, vol. 9, pp. 7063–7070, jun 2017.
- [110] Y. Y. Huang, W. Zhou, K. J. Hsia, E. Menard, J. U. Park, J. A. Rogers, and A. G. Alleyne, “Stamp collapse in soft lithography,” *Langmuir*, vol. 21, pp. 8058–8068, dec 2005.
- [111] T. S. Vinothkumar, D. Kandaswamy, G. Arathi, and K. Dinesh, “Influence of different organic solvents on degree of swelling of poly (dimethyl siloxane)-based sealer,” *Journal of Conservative Dentistry*, vol. 14, pp. 156–159, apr 2011.
- [112] J. N. Lee, C. Park, and G. M. Whitesides, “Solvent Compatibility of Poly(dimethylsiloxane)-Based Microfluidic Devices,” *Analytical Chemistry*, vol. 75, pp. 6544–6554, dec 2003.
- [113] J. Shin, J. Ko, S. Jeong, P. Won, Y. Lee, J. Kim, S. Hong, N. L. Jeon, and S. H. Ko, “Monolithic digital patterning of polydimethylsiloxane with successive laser pyrolysis,” *Nature Materials*, vol. 20, pp. 100–107, aug 2021.
- [114] Y. Zykova, V. Kudryavtseva, M. Gai, A. Kozelskaya, J. Frueh, G. Sukhorukov, and S. Tverdokhlebov, “Free-standing microchamber arrays as a

- biodegradable drug depot system for implant coatings,” *European Polymer Journal*, vol. 114, pp. 72–80, may 2019.
- [115] E. A. Mordovina, O. A. Sindeeva, A. M. Abramova, D. V. Tsyupka, V. S. Atkin, D. N. Bratashov, I. Y. Goryacheva, and G. B. Sukhorukov, “Controlled release of α -amylase from microchamber arrays containing carbon nanoparticle aggregates,” *Mendeleev Communications*, vol. 31, pp. 869–871, nov 2021.
- [116] M. Gai, M. A. Kurochkin, D. Li, B. N. Khlebtsov, L. Dong, N. Tarakina, R. Poston, D. J. Gould, J. Frueh, and G. B. Sukhorukov, “In-situ NIR-laser mediated bioactive substance delivery to single cell for EGFP expression based on biocompatible microchamber-arrays,” *Journal of Controlled Release*, vol. 276, pp. 84–92, apr 2018.
- [117] M. A. Kurochkin, O. A. Sindeeva, E. P. Brodovskaya, M. Gai, J. Frueh, L. Su, A. Sapelkin, V. V. Tuchin, and G. B. Sukhorukov, “Laser-triggered drug release from polymeric 3-D micro-structured films via optical fibers,” *Materials Science and Engineering C*, vol. 110, p. 110664, may 2020.
- [118] O. A. Sindeeva, O. I. Gusliakova, O. A. Inozemtseva, A. S. Abdurashitov, E. P. Brodovskaya, M. Gai, V. V. Tuchin, D. A. Gorin, and G. B. Sukhorukov, “Effect of a Controlled Release of Epinephrine Hydrochloride from PLGA Microchamber Array: In Vivo Studies,” *ACS Applied Materials and Interfaces*, vol. 10, pp. 37855–37864, nov 2018.
- [119] O. A. Sindeeva, E. S. Prikhodzhenko, D. N. Bratashov, A. M. Vostrikova, V. S. Atkin, A. V. Ermakov, B. N. Khlebtsov, A. V. Sapelkin, I. Y. Goryacheva, and G. B. Sukhorukov, “Carbon dot aggregates as an alternative to gold nanoparticles for the laser-induced opening of microchamber arrays,” *Soft Matter*, vol. 14, pp. 9012–9019, nov 2018.

- [120] A. M. Gañán-Calvo, J. M. López-Herrera, M. A. Herrada, A. Ramos, and J. M. Montanero, “Review on the physics of electrospray: From electrokinetics to the operating conditions of single and coaxial Taylor cone-jets, and AC electrospray,” *Journal of Aerosol Science*, vol. 125, pp. 32–56, nov 2018.
- [121] A. Jaworek, A. T. Sobczyk, and A. Krupa, “Electrospray application to powder production and surface coating,” *Journal of Aerosol Science*, vol. 125, pp. 57–92, nov 2018.
- [122] C. Zhang, Z. C. Yao, Q. Ding, J. J. Choi, Z. Ahmad, M. W. Chang, and J. S. Li, “Tri-Needle Coaxial Electrospray Engineering of Magnetic Polymer Yolk-Shell Particles Possessing Dual-Imaging Modality, Multiagent Compartments, and Trigger Release Potential,” *ACS Applied Materials and Interfaces*, vol. 9, pp. 21485–21495, jun 2017.
- [123] C. Li, F. Wang, P. Ge, Y. Mao, and L. Wang, “Anti-acute thrombogenic surface using coaxial electrospraying coating for vascular graft application,” *Materials Letters*, vol. 205, pp. 15–19, oct 2017.
- [124] D. G. Yu, X. Y. Li, X. Wang, J. H. Yang, S. W. Bligh, and G. R. Williams, “Nanofibers Fabricated Using Triaxial Electrospinning as Zero Order Drug Delivery Systems,” *ACS Applied Materials and Interfaces*, vol. 7, pp. 18891–18897, aug 2015.
- [125] M. Habibi Jouybari, S. Hosseini, K. Mahboobnia, L. A. Boloursaz, M. Moradi, and M. Irani, “Simultaneous controlled release of 5-FU, DOX and PTX from chitosan/PLA/5-FU/g-C₃N₄-DOX/g-C₃N₄-PTX triaxial nanofibers for breast cancer treatment in vitro,” *Colloids and Surfaces B: Biointerfaces*, vol. 179, pp. 495–504, jul 2019.
- [126] J. Tang, R. Schutzman, C. A. Rodríguez, J. Lahann, N. Rodríguez-Hornedo, M. R. Prausnitz, and S. P. Schwendeman, “Coaxial electrospray of uniform

- polylactide core-shell microparticles for long-acting contraceptive,” *Journal of Controlled Release*, vol. 341, pp. 634–645, jan 2022.
- [127] K. Gulati, S. Ramakrishnan, M. S. Aw, G. J. Atkins, D. M. Findlay, and D. Losic, “Biocompatible polymer coating of titania nanotube arrays for improved drug elution and osteoblast adhesion,” *Acta Biomaterialia*, vol. 8, pp. 449–456, jan 2012.
- [128] F. Davoodian, E. Salahinejad, E. Sharifi, Z. Barabadi, and L. Tayebi, “PLGA-coated drug-loaded nanotubes anodically grown on nitinol,” *Materials Science and Engineering C*, vol. 116, p. 111174, nov 2020.
- [129] A. Jadidi, F. Davoodian, and E. Salahinejad, “Effect of poly lactic-co-glycolic acid encapsulation on drug delivery kinetics from vancomycin-impregnated Ca-Mg silicate scaffolds,” *Progress in Organic Coatings*, vol. 149, p. 105970, dec 2020.
- [130] F. K. Aldawood, A. Andar, and S. Desai, “A comprehensive review of microneedles: Types, materials, processes, characterizations and applications,” *Polymers*, vol. 13, p. 2815, aug 2021.
- [131] W. Li, J. Y. Chen, R. N. Terry, J. Tang, A. Romanyuk, S. P. Schwendeman, and M. R. Prausnitz, “Core-shell microneedle patch for six-month controlled-release contraceptive delivery,” *Journal of Controlled Release*, vol. 347, pp. 489–499, jul 2022.
- [132] N. Z. Chamgordani, S. Asiaei, F. Ghorbani-Bidkorpeh, M. B. Foroutan, M. Dahmardehei, and H. R. Moghimi, “A Long-Lasting Triamcinolone-Loaded Microneedle Patch for Prolonged Dermal Delivery,” *Iranian Journal of Pharmaceutical Research 2024 23:1*, vol. 23, p. 138857, dec 2024.
- [133] X. Xu, P. Robles-Martinez, C. M. Madla, F. Joubert, A. Goyanes, A. W. Basit, and S. Gaisford, “Stereolithography (SLA) 3D printing of an anti-

hypertensive polyprintlet: Case study of an unexpected photopolymer-drug reaction,” *Additive Manufacturing*, vol. 33, may 2020.

- [134] C. J. Boyer, D. H. Ballard, J. A. Weisman, S. Hurst, D. J. McGee, D. K. Mills, J. E. Woerner, U. Jammalamadaka, K. Tappa, and J. S. Alexander, “Three-Dimensional Printing Antimicrobial and Radiopaque Constructs,” *3D printing and additive manufacturing*, vol. 5, pp. 29–35, mar 2018.
- [135] J. H. Lee, J. M. Baik, Y. S. Yu, J. H. Kim, C. B. Ahn, K. H. Son, J. H. Kim, E. S. Choi, and J. W. Lee, “Development of a heat labile antibiotic eluting 3D printed scaffold for the treatment of osteomyelitis,” *Scientific Reports 2020 10:1*, vol. 10, pp. 1–8, may 2020.
- [136] K. Tappa, U. Jammalamadaka, J. A. Weisman, D. H. Ballard, D. D. Wolford, C. Pascual-Garrido, L. M. Wolford, P. K. Woodard, and D. K. Mills, “3D Printing Custom Bioactive and Absorbable Surgical Screws, Pins, and Bone Plates for Localized Drug Delivery,” *Journal of Functional Biomaterials 2019, Vol. 10, Page 17*, vol. 10, p. 17, apr 2019.
- [137] M. Sadia, A. Sośnicka, B. Arafat, A. Isreb, W. Ahmed, A. Kelarakis, and M. A. Alhnan, “Adaptation of pharmaceutical excipients to FDM 3D printing for the fabrication of patient-tailored immediate release tablets,” *International Journal of Pharmaceutics*, vol. 513, pp. 659–668, nov 2016.
- [138] P. Robles-Martinez, X. Xu, S. J. Trenfield, A. Awad, A. Goyanes, R. Telford, A. W. Basit, and S. Gaisford, “3D printing of a multi-layered polypill containing six drugs using a novel stereolithographic method,” *Pharmaceutics*, vol. 11, no. 6, 2019.
- [139] R. O. Darouiche, “Device-associated infections: a macroproblem that starts with microadherence,” *Clinical infectious diseases : an official publication of the Infectious Diseases Society of America*, vol. 33, pp. 1567–1572, nov 2001.

- [140] Z. Dai, J. Ronholm, Y. Tian, B. Sethi, and X. Cao, “Sterilization techniques for biodegradable scaffolds in tissue engineering applications,” *Journal of tissue engineering*, vol. 7, feb 2016.
- [141] P. Rychter, N. Śmigiel-Gac, E. Pamuła, A. Smola-Dmochowska, H. Janeczek, W. Prochwicz, and P. Dobrzyński, “Influence of Radiation Sterilization on Properties of Biodegradable Lactide/Glycolide/Trimethylene Carbonate and Lactide/Glycolide/ ϵ -caprolactone Porous Scaffolds with Shape Memory Behavior,” *Materials (Basel, Switzerland)*, vol. 9, no. 1, 2016.
- [142] S. Alavi, F. Asadi, S. H. Raji, and S. Samie, “Effect of steam and dry heat sterilization on the insertion and fracture torque of orthodontic miniscrews,” *Dental Research Journal*, vol. 17, no. 3, p. 219, 2020.
- [143] S. J. Peniston and S. J. Choi, “Effect of sterilization on the physicochemical properties of molded poly(L-lactic acid),” *Journal of biomedical materials research. Part B, Applied biomaterials*, vol. 80, pp. 67–77, jan 2007.
- [144] A. T. Neffe, Q. Zhang, P. J. Hommes-Schattmann, and A. Lendlein, “Ethylene oxide sterilization of electrospun poly(l-lactide)/poly(d-lactide) core/shell nanofibers,” *MRS Advances*, vol. 6, pp. 786–789, oct 2021.
- [145] C. E. Holy, C. Cheng, J. E. Davies, and M. S. Shoichet, “Optimizing the sterilization of PLGA scaffolds for use in tissue engineering,” *Biomaterials*, vol. 22, no. 1, pp. 25–31, 2001.
- [146] M. Haim Zada, A. Kumar, O. Elmalak, G. Mechrez, and A. J. Domb, “Effect of Ethylene Oxide and Gamma (γ -) Sterilization on the Properties of a PLCL Polymer Material in Balloon Implants,” *ACS Omega*, vol. 4, pp. 21319–21326, dec 2019.
- [147] A. J. Berejka and I. M. Kaluska, “Trends in Radiation Sterilization of Health Care Products,” *Trends in Radiation Sterilization of Health Care Products*, no. (February), pp. 1–261, 2008.

- [148] B. McEvoy, A. Maksimovic, D. Howell, P. Reppert, D. Ryan, N. Rowan, and H. Michel, “Studies on the comparative effectiveness of X-rays, gamma rays and electron beams to inactivate microorganisms at different dose rates in industrial sterilization of medical devices,” *Radiation Physics and Chemistry*, vol. 208, p. 110915, jul 2023.
- [149] J. H. Kang, J. Kaneda, J. G. Jang, K. Sakthiabirami, E. Lui, C. Kim, A. Wang, S. W. Park, and Y. P. Yang, “The influence of electron beam sterilization on in vivo degradation of (β -TCP/PCL of different composite ratios for bone tissue engineering,” *Micromachines*, vol. 11, no. 3, 2020.
- [150] P. Benyathiar, S. Selke, and R. Auras, “The Effect of Gamma and Electron Beam Irradiation on the Biodegradability of PLA Films,” *Journal of Polymers and the Environment*, vol. 24, no. 3, 2016.
- [151] K. Nakamura, H. Kiminami, A. Yamashita, Y. Abe, K. Yoshino, and S. Suzuki, “Assessment of the effects of sterilization methods on protein drug stability by elucidating decomposition mechanism and material analysis,” *International Journal of Pharmaceutics*, vol. 484, no. 1-2, 2015.
- [152] J. Wilińska, A. Turek, A. Borecka, J. Rech, and J. Kasperczyk, “Electron beam sterilization of implantable rods with risperidone and with 17- β -estradiol: A structural, thermal and morphology study,” *Acta of Bioengineering and Biomechanics*, vol. 21, no. 3, 2019.
- [153] Y. K. Kim, K. B. Lee, S. Y. Kim, Y. S. Jang, J. H. Kim, and M. H. Lee, “Improvement of osteogenesis by a uniform PCL coating on a magnesium screw for biodegradable applications,” *Scientific Reports*, vol. 8, pp. 1–11, sep 2018.
- [154] I. M. Domańska, A. Zalewska, K. Cieśla, A. Plichta, W. Głuszewski, M. Łyczko, S. Kowalczyk, E. Oledzka, and M. Sobczak, “The influence of electron beam and gamma irradiation on paclitaxel-loaded nanoparticles of

fully randomized copolymers in relation to potential sterilization,” *Journal of Drug Delivery Science and Technology*, vol. 90, 2023.

- [155] H. D. Williams, N. L. Trevaskis, S. A. Charman, R. M. Shanker, W. N. Charman, C. W. Pouton, and C. J. H. Porter, “Strategies to address low drug solubility in discovery and development,” vol. 65, no. 1, pp. 315–499. Publisher: American Society for Pharmacology & Experimental Therapeutics (ASPET).
- [156] B. J. Boyd, C. A. S. Bergström, Z. Vinarov, M. Kuentz, J. Brouwers, P. Augustijns, M. Brandl, A. Bernkop-Schnürch, N. Shrestha, V. Préat, A. Müllertz, A. Bauer-Brandl, and V. Jannin, “Successful oral delivery of poorly water-soluble drugs both depends on the intraluminal behavior of drugs and of appropriate advanced drug delivery systems,” vol. 137, no. 104967, p. 104967. Publisher: Elsevier BV.
- [157] A.-R. Coltescu, M. Butnariu, and I. Sarac, “The importance of solubility for new drug molecules,” vol. 13, no. 2, pp. 577–583. Publisher: Oriental Scientific Publishing Company.
- [158] M. Rashid, M. Y. Malik, S. K. Singh, S. Chaturvedi, J. R. Gayen, and M. Wahajuddin, “Bioavailability enhancement of poorly soluble drugs: The holy grail in pharma industry,” vol. 25, no. 9, pp. 987–1020. Publisher: Bentham Science Publishers Ltd.
- [159] Y. Shi, W. Porter, T. Merdan, and L. C. Li, “Recent advances in intravenous delivery of poorly water-soluble compounds,” vol. 6, no. 12, pp. 1261–1282. Publisher: Informa Healthcare.
- [160] S. Kalepu and V. Nekkanti, “Insoluble drug delivery strategies: review of recent advances and business prospects,” vol. 5, no. 5, pp. 442–453. Publisher: Elsevier BV.

- [161] K. Barakat, “Solubility: A speed-breaker on the drug discovery highway,” vol. 3, no. 3. Publisher: MedCrave Group, LLC.
- [162] Sahu and Gupta, “Exploration of solubilization strategies: Enhancing bioavailability for low solubility drugs,” pp. 96–115. Publisher: Lloyd Institute of Management and Technology.
- [163] A. Chaudhary and S. Shambhakar, “Nanotechnology in drug delivery: Overcoming poor solubility challenges through nanoformulations,” vol. 14, no. 3, pp. 200–211. Publisher: Bentham Science Publishers Ltd.
- [164] K. U. Khan, M. U. Minhas, S. F. Badshah, M. Suhail, A. Ahmad, and S. Ijaz, “Overview of nanoparticulate strategies for solubility enhancement of poorly soluble drugs,” vol. 291, no. 120301, p. 120301. Publisher: Elsevier BV.
- [165] V. Choi, J. L. Rohn, P. Stoodley, D. Carugo, and E. Stride, “Drug delivery strategies for antibiofilm therapy,” *Nature Reviews Microbiology* 2023 21:9, vol. 21, pp. 555–572, may 2023.
- [166] R. Mirghani, T. Saba, H. Khaliq, J. Mitchell, L. Do, L. Chambi, K. Diaz, T. Kennedy, K. Alkassab, T. Huynh, M. Elmi, J. Martinez, S. Sawan, and G. Rijal, “Biofilms: Formation, drug resistance and alternatives to conventional approaches,” *AIMS Microbiology*, vol. 8, no. 3, p. 239, 2022.
- [167] J. G. S. Souza, M. M. Bertolini, R. C. Costa, B. E. Nagay, A. Dongari-Bagtzoglou, and V. A. R. Barão, “Targeting implant-associated infections: titanium surface loaded with antimicrobial,” *iScience*, vol. 24, p. 102008, jan 2021.
- [168] J. Davies, G. B. Spiegelman, and G. Yim, “The world of subinhibitory antibiotic concentrations,” *Current opinion in microbiology*, vol. 9, pp. 445–453, oct 2006.
- [169] E.-B. Goh, G. Yim, W. Tsui, J. McClure, M. G. Surette, and J. Davies, “Transcriptional modulation of bacterial gene expression by subinhibitory

- concentrations of antibiotics,” *Proceedings of the National Academy of Sciences*, vol. 99, pp. 17025–17030, dec 2002.
- [170] L. Keller and M. G. Surette, “Communication in bacteria: an ecological and evolutionary perspective,” *Nature reviews. Microbiology*, vol. 4, pp. 249–258, apr 2006.
- [171] M. E. Hibbing, C. Fuqua, M. R. Parsek, and S. B. Peterson, “Bacterial competition: surviving and thriving in the microbial jungle,” *Nature reviews. Microbiology*, vol. 8, pp. 15–25, jan 2010.
- [172] G. Yim, H. H. Wang, and J. Davies, “Antibiotics as signalling molecules,” *Philosophical transactions of the Royal Society of London. Series B, Biological sciences*, vol. 362, pp. 1195–1200, jul 2007.
- [173] J. F. Linares, I. Gustafsson, F. Baquero, and J. L. Martinez, “Antibiotics as intermicrobiol signaling agents instead of weapons,” *Proceedings of the National Academy of Sciences of the United States of America*, vol. 103, pp. 19484–19489, dec 2006.
- [174] E. Shun-Mei, J. M. Zeng, H. Yuan, Y. Lu, R. X. Cai, and C. Chen, “Sub-inhibitory concentrations of fluoroquinolones increase conjugation frequency,” *Microbial pathogenesis*, vol. 114, pp. 57–62, jan 2018.
- [175] L. W. Goneau, T. J. Hannan, R. A. Macphee, D. J. Schwartz, J. M. Macklaim, G. B. Gloor, H. Razvi, G. Reid, S. J. Hultgren, and J. P. Burton, “Subinhibitory antibiotic therapy alters recurrent urinary tract infection pathogenesis through modulation of bacterial virulence and host immunity,” *mBio*, vol. 6, mar 2015.
- [176] L. W. Goneau, J. Delport, L. Langlois, S. M. Poutanen, H. Razvi, G. Reid, and J. P. Burton, “Issues beyond resistance: inadequate antibiotic therapy and bacterial hypervirulence,” *FEMS Microbes*, vol. 1, p. 4, sep 2020.

- [177] T. Bjarnsholt, O. Ciofu, S. Molin, M. Givskov, and N. Høiby, “Applying insights from biofilm biology to drug development — can a new approach be developed?,” *Nature Reviews Drug Discovery* 2013 12:10, vol. 12, pp. 791–808, oct 2013.
- [178] J. B. Kaplan, E. A. Izano, P. Gopal, M. T. Karwacki, S. Kim, J. L. Bose, K. W. Bayles, and A. R. Horswill, “Low levels of β -lactam antibiotics induce extracellular DNA release and biofilm formation in *Staphylococcus aureus*,” *mBio*, vol. 3, no. 4, 2012.
- [179] B. W. Brunelle, S. M. Bearson, and B. L. Bearson, “Tetracycline accelerates the temporally-regulated invasion response in specific isolates of multidrug-resistant *Salmonella enterica* serovar Typhimurium,” *BMC Microbiology*, vol. 13, no. 1, p. 202, 2013.
- [180] F. C. Krebs, “Fabrication and processing of polymer solar cells: A review of printing and coating techniques,” *Solar Energy Materials and Solar Cells*, vol. 93, no. 4, pp. 394–412, 2009.
- [181] G. N. Howatt, R. G. Breckenridge, and J. M. Brownlow, “Fabrication of Thin Ceramic Sheets for Capacitors,” *Journal of the American Ceramic Society*, vol. 30, pp. 237–242, aug 1947.
- [182] Y. Zhang, M. Huo, J. Zhou, A. Zou, W. Li, C. Yao, and S. Xie, “DDSolver: An Add-In Program for Modeling and Comparison of Drug Dissolution Profiles,” *The AAPS Journal*, vol. 12, p. 263, sep 2010.
- [183] G. C. Patil, “Doctor Blade: A Promising Technique for Thin Film Coating,” *Simple Chemical Methods for Thin Film Deposition*, pp. 509–530, 2023.
- [184] Bindu Nair, “Final Report On the Safety Assessment of Polyvinyl Alcohol,” *International Journal of Toxicology*, vol. 17, pp. 67–92, dec 1998.
- [185] X. P. Zhang, B. B. Wang, W. X. Li, W. M. Fei, Y. Cui, and X. D. Guo, “In vivo safety assessment, biodistribution and toxicology of polyvinyl alcohol

- microneedles with 160-day uninterruptedly applications in mice,” *European Journal of Pharmaceutics and Biopharmaceutics*, vol. 160, pp. 1–8, mar 2021.
- [186] G. Paradossi, F. Cavalieri, E. Chiessi, C. Spagnoli, and M. K. Cowman, “Poly(vinyl alcohol) as versatile biomaterial for potential biomedical applications,” *Journal of Materials Science: Materials in Medicine*, vol. 14, pp. 687–691, aug 2003.
- [187] C. C. DeMerlis and D. R. Schoneker, “Review of the oral toxicity of polyvinyl alcohol (PVA),” *Food and Chemical Toxicology*, vol. 41, pp. 319–326, mar 2003.
- [188] T. Yamaoka, Y. Tabata, and Y. Ikada, “Comparison of body distribution of poly(vinyl alcohol) with other water-soluble polymers after intravenous administration,” vol. 47, no. 6, pp. 479–486.
- [189] Q. Liu, X. Li, B. Liu, J. Kong, Q. Wang, and Z. Gao, “Using polymers as crystal inhibitors to prevent the crystallization of the rotigotine patch,” vol. 16, no. 5, p. 630.
- [190] G. Michailidou, N. M. Ainali, E. Xanthopoulou, S. Nanaki, M. Kostoglou, E. N. Koukaras, and D. N. Bikiaris, “Effect of poly(vinyl alcohol) on nanoencapsulation of budesonide in chitosan nanoparticles via ionic gelation and its improved bioavailability,” vol. 12, no. 5, p. 1101.
- [191] B. Van Eerdenbrugh and L. S. Taylor, “Small scale screening to determine the ability of different polymers to inhibit drug crystallization upon rapid solvent evaporation,” vol. 7, no. 4, pp. 1328–1337.
- [192] D. Campoccia, L. Montanaro, P. Speziale, and C. R. Arciola, “Antibiotic-loaded biomaterials and the risks for the spread of antibiotic resistance following their prophylactic and therapeutic clinical use,” *Biomaterials*, vol. 31, pp. 6363–6377, sep 2010.

- [193] A. Kodym, P. Bilski, A. Domańska, Ł. Helminiak, M. Jabłońska, and A. Jachymska, “Physical and chemical properties and stability of sodium cefazolin in buffered eye drops determined with HPLC method,” *Acta polonae pharmaceutica*, vol. 69, no. 1, pp. 95–105, 2012.
- [194] A. Ilyas, M. Islam, W. Asghar, J. U. Menon, A. S. Wadajkar, K. T. Nguyen, and S. M. Iqbal, “Salt-leaching synthesis of porous PLGA nanoparticles,” vol. 12, no. 6, pp. 1082–1088.
- [195] G. Tang, H. Zhang, Y. Zhao, Y. Zhang, X. Li, and X. Yuan, “Preparation of PLGA scaffolds with graded pores by using a gelatin-microsphere template as porogen,” vol. 23, no. 17, pp. 2241–2257.
- [196] F. Huang, S. Yang, H. Wang, P. Zhao, B. Zhou, B. Cheng, S. Dong, J. Yang, B. Li, and X. Wang, “pH-responsive PLGA/gelatin porous microspheres containing paclitaxel used for inhibition of cancer cell proliferation,” vol. 86, p. 104735.
- [197] C. Zhang and R. Bodmeier, “Porous PLGA microparticles prepared with nanosized/micronized sugar particles as porogens,” vol. 660, p. 124329.